JPRS L/8928

15 February 1980

USSR Report

ELECTRONICS AND ELECTRICAL ENGINEERING

(FOUO 2/80)

FBIS FOREIGN BROADCAST INFORMATION SERVICE

NOTE

JPRS publications contain information primarily from foreign newspapers, periodicals and books, but also from news agency transmissions and broadcasts. Materials from foreign-language sources are translated; those from English-language sources are transcribed or reprinted, with the original phrasing and other characteristics retained.

Headlines, editorial reports, and material enclosed in brackets [] are supplied by JPRS. Processing indicators such as [Text] or [Excerpt] in the first line of each item, or following the last line of a brief, indicate how the original information was processed. Where no processing indicator is given, the information was summarized or extracted.

Unfamiliar names rendered phonetically or transliterated are enclosed in parentheses. Words or names preceded by a question mark and enclosed in parentheses were not clear in the original but have been supplied as appropriate in context. Other unattributed parenthetical notes within the body of an item originate with the source. Times within items are as given by source.

The contents of this publication in no way represent the policies, views or attitudes of the U.S. Government.

For further information on report content call (703) 351-2938 (economic); 3468 (political, sociological, military); 2726 (life sciences); 2725 (physical sciences).

APPROVED FOR RELEASE: 2007/02/08: CIA-RDP82-00850R000200050030-1

JPRS L/8928

15 February 1980

USSR REPORT

ELECTRONICS AND ELECTRICAL ENGINEERING

(FOUO 2/80)

This serial publication contains articles, abstracts of articles and news items from USSR scientific and technical journals on the specific subjects reflected in the table of contents.

Photoduplications of foreign-language sources may be obtained from the Photoduplication Service, Library of Congress, Washington, D. C. 20540. Requests should provide adequate identification both as to the source and the individual article(s) desired.

CONTENTS PAGE

CONTENTS (Continued) Page

CONTENTS (Continued) Page

Antennas

UDC 621.396.677

ANTENNAS (PRESENT STATE AND PROBLEMS)

Moscow ANTENNY (Sovremennoye sostoyaniye i problemy) [Antennas (Present State and Problems)] in Russian 1979 signed to press 19 Apr 79 p 2, 206-207

[Annotation and table of contents from book by D. I. Voskresenkiy, V. L. Gostyukhin, K. I. Grineva, A. Yu. Grinev, B. Ya. Myakishev, L. I. Ponomarev, and V. S. Filippov, edited by L. D. Bakhrakh, Associate member of the USSR Academy of Sciences, and Professor D. I. Voskresenskiy, Sovetskoye radio, 30,000 copies 208 pages]

[Text] This book familiarizes radio engineers with main achievements in the theory and the technology of antennas, as well as with the problems existing in this area. It describes the main tendencies in the development and the role of antenna devices in modern foreign radio engineering complexes. Special attention is given to the types of antennas which are most developed and used (phased antenna arrays, active antenna arrays, signal-processing antenna arrays). It gives the main relations necessary for the analysis of antennas and describes main achievements in the area of the synthesis of antennas and automation in designing antenna devices.

The authors used materials of domestic and foreign publications.

The book is intended for a broad section of radio specialists and senior students of vuzes.

Figures 88; tables 5; bibliography 82 items.

Contents

10,233
CSO: 1860

UDC 621.396.677.833.2

CERTAIN FEATURES OF DESIGNING TYPE ADE ANTENNA EXCITERS

Moscow RADIOTEKHNIKA in Russian No 9, 1979, signed to press 9 Jan 79 pp 35-39

[Article by Yu. B. Buzuyev, Yu. A. Yerukhimovich, A. A. Timofeyeva]

[Text] The type ADE (Fig. 1) antenna consists of a basic reflecting mirror (OZ) -- a paraboloid with a shifted focal axis, a primary horn radiator (PI), an auxiliary mirror (VZ) with an elliptical generatrix and a supporting system for the auxiliary mirror made, in the case being considered, of radio-transparent material in the shape of a flat toroid (PT) with a special profile. We will call the unit consisting of a primary radiator, auxiliary mirror and toroid, the exciter. The theoretical analysis and detailed description of the antenna were given in a number of papers [1-4]. Below we consider some features of optimization of an ADE type antenna with $\psi = 105^{\circ}$ with respect to the coefficient of utilization of the aperture surface (KIP) and matching.

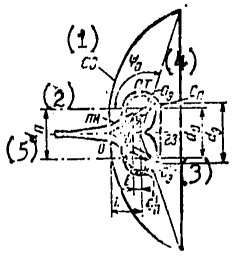

Fig. 1

1. OZ
2. PI
3. VZ
4. PT
5. d_n
6. $d_э$

When designing an exciter for a type ADE antenna, it is necessary to take into account one of its basic features -- the close location of the primary radiator to the auxiliary mirror, which causes a considerable change in the amplitude and phase characteristics of the radiator within the radiation zone of the auxiliary mirror which is different in the frequency range. Therefore, one of the basic problems is to obtain, as far as possible, unchanging characteristics of the primary radiation within the limits of the working range.

One way of reaching the goal is to use practically synphase horn antennas with an aperature diameter 2R and a distance from the aperture plane to the point of the auxiliary mirror selected so that total dephasing $\Delta\varphi_{\Sigma}$ (of the horn itself and spatial) within the working range limits does not exceed $0,2\pi$ i.e., that the following condition is met:

$$(R^2+H^2)^{1/2}-H+(R^2+l^2)^{1/2}-l\leqslant 0,1\lambda, \qquad (1)$$

where H -- distance from horn aperture to its geometrical apex, λ -- wavelength. According to (1), the horn radiator is practically synphase, i.e., it has a phase center located near the horn aperature [5] and has all the advantages inherent in such a radiator (small size) and shortcomings (poor match to the feed channel and a comparatively narrow frequency range).

Another way is to use various modifications of strongly dephased horn antennas, for example [6-8], etc. Dephased horn radiators are better matched than synphased to the feed channel and their phase center is located near the apex. When using dephased horn antennas, it is necessary to select a horn geometry, that within the working range $\Delta\varphi_{\Sigma}>2\pi$, i.e., fulfills condition:

$$(R^2+H^2)^{1/2}-H+(R^2+S^2)^{1/2}-S\geqslant\lambda, \qquad (2)$$

where S -- distance along axis of horn aperture to the circle with a center at focus "0" (Fig. 1), passing through the edge of the auxiliary mirror. Fulfilling condition (2) makes it possible to obtain comparatively stable amplitude and phase characteristics in a fairly wide frequency range. For horns with a break in the generatrix (Fig. 2), it is necessary, moreoever, that waveguide transition from the waveguide cross section to the cross section of the break have low dephasing i.e., the following condition be met:

$$(r^2+h^2)^{1/2}-h+[r^2+(H_0+l)^2]^{1/2}-(H_0+l)\leqslant 0,1\lambda, \qquad (3)$$

where r -- radius of break cross section, h -- distance from the break cross section to the geometrical apex of the cone forming the waveguide transition, H_0 -- distance from horn aperture to the break cross section. In a usual dephased horn with a matched transition, condition (3) must be fulfilled for the matching transition. This makes it possible to obtain a stable position of the phase center in a wider range of frequencies.

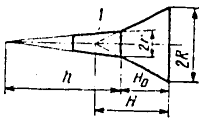

Fig. 2

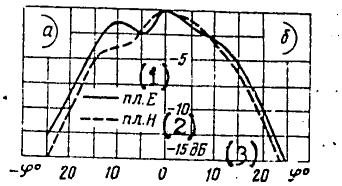

Fig. 3.

1. plane E
2. plane H
3. db

In optimizing the antenna for KIP, it is necessary that the phase center of the horn be superposed on the focus of the auxiliary mirror for an optimal amplitude characteristic.

The relationship between the amplitude characteristics of the primary radiator and the distance to the near zone is great; therefore, it is necessary to know the position of the phase center of the horn very accurately. Moreoever, moving the horn closer to the auxiliary mirror in order to superpose its phase center on focus "0" is limited due to the effect on the horn of the radiation field of the basic mirror by the auxiliary one. Therefore, it is found in practice when designing the exciter, that it is necessary to select $l \geq \lambda/4$ and $2R < d$. When using strongly dephased horn antennas, an effort should be made to use horns with large aperture angles (45 to 90°) which makes it possible to reduce their size considerably.

Fulfilling the above-enumerated requirements makes it possible to obtain a fairly high total KIP (0.65 to 0.7) in ADE type antennas.

A further increase in the KIP is possible by optimizing the characteristics of the primary radiator taking into account the near zone effect. Thus, for example, it is well known that a change in dephasing horn

antennas changes the shape of the main lope apex [9] . For dephased horns with a break in the generatrix, this change in planes E and H is about the same. The main lobe apex DH is dome-shaped, flat or funnel-shaped depending upon the multiplicity of the total dephasing of 0.5π [10]. This relationship between the characteristics of the primary radiator and the total dephasing leads to the fact that in type ADE antennas there appear in the radiation zone of the auxiliary mirror (due to the small distance between the exciter components) amplitude and phase oscillations which cause some amplification losses. The practice of designing exciters for type ADE antennas indicated that it is good practice to select the exciter geometry so that for the distance, corresponding to the edge of the auxiliary mirror, $\Delta\varphi_\Sigma \approx 2\pi$, and for the distance corresponding to the point, $\Delta\varphi_\Sigma \approx 3\pi$. This makes it possible to obtain at minimal horn size a field amplitude distribution on the surface of the auxiliary mirror without noticeable oscillations. Fig. 3a shows the field amplitude distribution on the surface of the auxiliary mirror for the case when $\Delta\varphi_\Sigma$ changes within the zone of excitation of the auxiliary mirror from 2π to 4π and in Fig. 3b -- from 2π to 3π . In the second case, there are practically no oscillations in the field amplitude distribution and the nature of the distribution is closer to the optimal one. Oscillations may also be reduced by increasing considerably the dephasing of the horn within the excitation zone of the auxiliary mirror ($\Delta\varphi_\Sigma > 4\pi$), but this involves increasing the size of the horn or reducing the distance between it and the auxiliary mirror, which is not always possible. Optimizing the amplitude characteristics and taking into account the effect of the near zone produces an additional gain by 5 to 10% in amplification, but in a limited frequency range.

Matching type ADE antennas is determined basically by the same factors as of other two-mirror antennas [11] : internal matching of the primary radiator to the feed waveguide, diffraction by the edge of the auxiliary mirror, deflection by the point, reflection from the central part of the basic mirror and diffraction by its edge.

Matching the primary horn radiator depends on the arrangement of the horn. The reflection coefficient of dephased horns with matching transitions and horns with a break in the generatrix is very small. It increases with an increase in the aperture angle and with a reduction in the size of the horn aperture and, as a rule, does not exceed 1 to 2%.

The effect of the reflection coefficient of the signal, diffracted from the edge of the auxiliary mirror, depends on the excitation level of the edge, and on the value of the angle at which the horn is seen from the edge. The optimum (with respect to KIP) of excitation of the edge of the auxiliary mirror depending upon the antenna arrangement varies within -(10 to 20db). With the reduction in the excitation of

the auxiliary mirror edge antenna matching is improved, but amplification losses become apparent if this level is lower than the optimal one. Therefore, in some cases, it is better practice to increase angle $\gamma_к$ (Fig. 4) between reflected beam I and diffracted beam II. In this case, the excitation sector of the horn and the level of the radiated field and its direction are reduced. Angle $\gamma_к$ may be increased, decreasing the horn aperture or (for a given horn geometry) increasing the diameter of the focal ring of auxiliary mirror $d_э$ so that it is greater than the diameter of the focal ring of basic mirror $d_п$. However, if there is an essential difference between these diameters, there is an underexcitation in the central part of the basic mirror, i.e., as if the darkening of the antenna aperture increases. This may lead to considerable amplification losses and an increase in the near side lobes. The correct selection of $d_э$ and $d_п$ improves the antenna matching without noticeable amplification losses and even with some gain [12] , which is due to some (favorable) redistribution of field amplitudes due to the differences in $d_э$ and $d_п$.

The effect of the auxiliary mirror point on the antenna matching is related to the shape of the diffraction DN [radiation pattern] of the point and the value of the angular sector within whose limits beams diffracted by the point are intercepted by the horn. For a given cone angle $\gamma = \pi - \gamma_0$, the effect of the effective field of the point is weakened by the reduction in the excitation sector of the horn aperture by this field, i.e., by increasing angle γ_0 between beam III, reflected from point, and diffraction beam IV (Fig. 4). This is achieved by increasing distance l between the horn aperture and the point of the auxiliary mirror or by reducing the horn aperture.

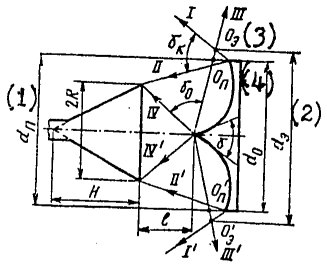

Fig. 4

1. $d_п$
2. $d_э$
3. $O_э$
4. $O_п$

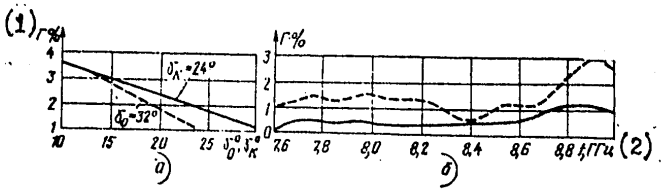

Fig. 5

1. G

2. GigaHz

Fig. 5a shows curves given the relationships between the value of the reflection coefficient of exciter G and the change in angle for a fixed value of $\gamma_к$ (solid line) and the changes in angle $\gamma_к$ for a fixed γ_0 (broken line). These curves were plotted on the basis of experimental results obtained in investigating one of the exciters of the type ADE antenna with auxiliary mirrors which have different diameters of the focal rings. They determine the nature of the relationship, but not the absolute value of the reflection coefficient which is different for different exciters.

The effect of the central part of the basic mirror on antenna matching (for a fixed level of excitation of the auxiliary mirror) weakens for $d_э > d_п$ and $d_э > d_0$. For example, for a 1m diameter of the antenna with an aperture angle of the parabolic generatrix 2 γ_0 = 210° at

$$d_п = 200 \text{ мм}, \; d_э = 210 \text{ мм}, \; d_0 = 200 \text{ мм}$$

and at edge excitation level of about -15db this effect is practically absent in the 8 gigaHz range.

The close disposition of the exciter components in the ADE arrangement makes it possible (with the proper selection of the distance between the basic nonuniformities) to obtain, in a comparatively broad but limited frequency range, close to an antiphase addition of reflected signals. Fig. 5b shows by solid and broken lines respectively the frequency relationships between the reflection coefficient of the primary exciter and the ADE antenna (their design dimensions are given below). In the frequency passband 7.6 to 8.6 gigaHz, where signals reflected by nonuniformities are added close to antiphase, the reflection coefficient of the horn does not exceed 0.5% and of the antenna -- 1.5%. The width of this band depends on the distance between the nonuniformities and increases with its decrease. It is possible to improve matching in a given frequency range, due to compensating reflection coefficients, by changing the distances between the horn aperture and the auxiliary mirror, i.e., by selecting 1 optimal from the matching standpoint.

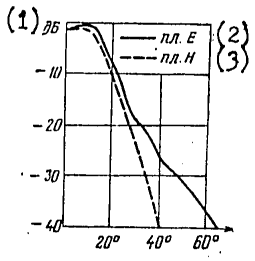

Fig. 6

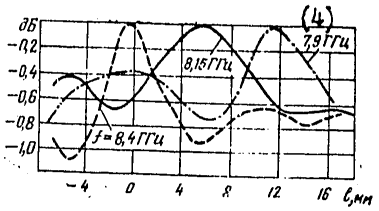

Fig. 7

1. db
2. plane E
3. plane H
4. gigaHz

In conclusion, we will show the results of an experimental investigation of the primary radiator and the type ADE antenna, intended to operate in the 7.9 to 8.4 gigaHz range. In an antenna with basic design parameters

$$2\psi_0=210^\circ,\ d_0=200\text{ мм},\ d_\text{п}=200\text{ мм},\ d_\text{э}=210\text{ мм},\ L=153{,}7\text{ мм},\ \varphi_1=30^\circ,\ \varphi_2=25^\circ,\ D=1000\text{ мм},$$

a dephased horn, with a break in the generatrix that has an aperture diameter 2R = 137mm, aperture angle $2\alpha = 48^\circ$ and a diameter of the break section 2r = 70mm, was used as a primary radiator. The transition from the cross section of the break to the cross section of the waveguide was made in the form of a parabolic transition 150mm long. The axial symmetry of the main lobe DN of the horn with parabolic transition is somewhat worse than with a DN of the horn with conical transition, but the match is better. DN of horns, measured on the circumference, that pass through the edge of the auxiliary mirror when the horn is installed in a position optimal with respect to the KIP of antenna tuning at frequency 8.15 gigaHz, are shown in Fig. 6 (solid line -- in plane E, broken line -- in plane H). The total horn dephasing for this case is about 2.5π .

Tuning curves of the antenna for maximum amplification, measured at frequencies 7.9, 8.15 and 8.4 gigaHz, are shown in Fig. 7 by dash-dot, solid and broken lines respectively. The distance between the horn and the auxiliary mirror l = 5mm corresponds to the signal maximum at a frequency of 8.15 gigaHz. A shift in the tuning frequencies, may be explained by the fact that the synphase condition of the waveguide parabolic transition was not fulfilled. In the following designs where the transition from the cross section of the break to the cross section

of the waveguide was made in the shape of a conical transition (the horn coefficient of reflection was increased in this case by a fraction of a percent) and condition (3) was fulfilled, tuning maxima at all frequencies of the range practically coincided.

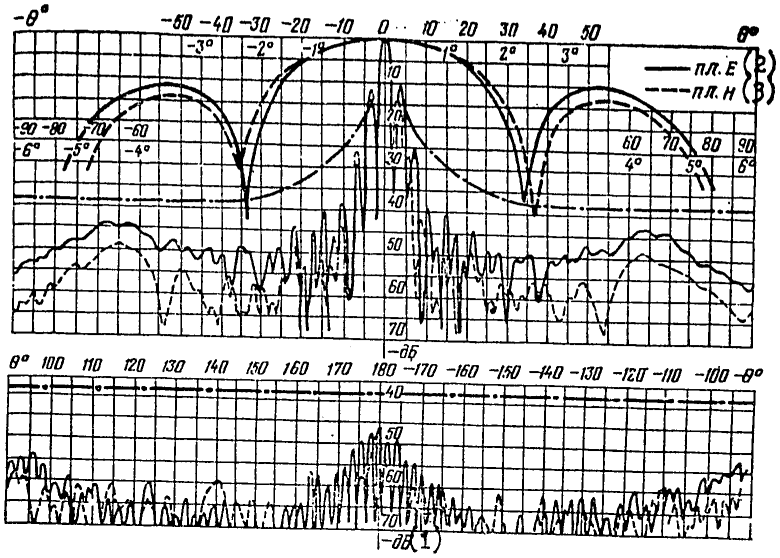

Fig. 8

1. db
2. plane E
3. plane H

Antenna radiation patterns without shields for increasing the protective action [4] in planes E and H, measured at the average working range frequency (8.15 gigaHz) when the antenna is tuned to this frequency for maximum amplification, are shown in Fig. 8 by solid and broken lines respectively; DN recommended by the MKKR [International Consultation Committee for Radio Communications] for RRL [Radio relay line antennas] [13] . A comparison shows that the DN of the designed antenna satisfies the DN cited in the MKKR report in all sectors of angles except the sector of the first side lobes whose greater level is explained by the underexcitation of the central part of the antenna mirror.

The coefficient of the reflection from the input antenna (see Fig. 5b) within the working limits does not exceed 1.5% and of the horn -- 0.5%.

The antenna amplification coefficient at the middle part of the working range, calculated from experimental DN of the antenna, is equal to 37.9db while, when measured by comparing it to a standard antenna was 37.8db (total KIP equal to 0.85 and 0.83 respectively). At the extreme frequencies of the range (at optimal antenna tuning at an average frequency), the amplification coefficient is equal to 37.0 and 36.3db respectively; at frequencies of 8.4 and 7.9 gigaHz (KIP 0.64 and 0.69). The reduction in the KIP is due to the fact that 1 = 5mm corresponds to a minimum signal at these frequencies (see Fig. 7).

Thus, the described antenna makes it possible to obtain a high KIP and a good match. This requires a comprehensive solution of problems related to the exciter design. The proper selection of the exciter geometry, taking into account the enumerated-above and frequently contradictory requirements, makes it possible to optimize simultaneously the KIP and the matching of the antenna (up to 0.8 with respect to the KIP and 1.5% with respect to the reflection coefficient) in a narrow frequency range.

BIBLIOGRAPHY

1. Yerukhimovich, Yu. A. "Parameter Analysis of a Two-Mirror Antenna with a Shifted Focal Axis." Trudy NII Radio, 1968, No 4.

2. Yerukhimovich, Yu. A. RADIOTEKHNIKA, 1972, v. 27, No 11.

3. Yerukhimovich, Yu. A.; Miroshnichenko, A. Ya. RADIOTEKHNIKA, 1972, v. 30, No 9.

4. Ayzenberg, G. Z.; Yampol'skiy, V. G.; Tereshin, O. N. "Ultra-shortwave Antennas," Part 2, Moscow, SVYAZ', 1977.

5. Yampol'skiy, V. G. In book "Antennas," 1972, issue 16.

6. Patent No 237934, cl. MPK No I q 13/00 (USSR) "Horn Antenna." Yerukhimovich, Yu. A.

7. Timofeyeva, A. A. RADIOTEKHNIKA, 1975, v. 30, No 8.

8. Yerukhimovich, Yu. A.; Timofeyeva, A. A. Trudy NII Radio, 1979, No 1.

9. Yerukhimovich, Yu. A.; Kobrina, G. A. "Radiation of Nonsynphase Round Aperture," Trudy NII Radio, 1967, issue 4 (49).

10. Timofeyeva, A. A. ELEKTROSVYAZ", 1977, No 5.

11. Yerukhimovich, Yu. A.; Yampol'skiy, V. G. RADIOTEKHNIKA, 1978, v. 33, No 8.

12. Yerukhimovich, Yu. A. In book "Antennas," 1974, issue 19.

13. C.C.I.R. XIII Assemblee pleniere Geneve, 1974, ITU, 1975

[35-2291]

2291
CSO: 1860

UDC 621.396.67

IMPROVING THE DECOUPLING BETWEEN ANTENNAS LOCATED ON A CONVEX OBJECT

Moscow RADIOTEKHNIKA I ELEKTRONIKA in Russian Vol 24 No 10, Oct 79
pp 1989-1995 manuscript received 14 Mar 78

[Article by Yu.L. Lomukhin and N.B. Chimitdorzhiyev]

[Text] Results are given for a theoretical and experimental study of the possibility of attenuating a microwave field which envelopes a convex cylindrical surface by means of diffracting elements: compensators installed on the given surface. Expressions are derived which permit the determination of the optimal dimensions of a decoupling, rectangular attachment, with which the maximum suppression of the shadow field is observed. The experimental results cited are in good agreement with calculated data.

An analysis of the results obtained indicates the possibility of effective additional decoupling using small, planar diffracting elements.

Introduction

When several antennas are placed close to or directly on a convex object, the problem of decoupling between them is of considerable importance, especially if the antennas operate on adjacent frequencies. Usually, the shielding effect of the object itself is utilized to eliminate the mutual coupling of the antennas, by means of optimal positioning of the antennas. Through the choice of the position of the antennas, one cannot always successfully assure the requisite decoupling. In such cases, diverse additional methods are employed, which increase the attenuation of the field, where these methods include the use of impedance, ribbed structures, dielectric plates, etc. [1 - 6].

This article is devoted to a study of the possibility of supplemental attenuation of a microwave field which envelops a convex conducting body, by means of a plane diffracting screen: a compensator, installed on the surface of the object, or by using already existing protruding elements of the structure for this purpose. In contrast to the well-known decoupling methods, where the

field attenuation is accomplished by changing the electrical properties of the surface, in the method we propose, the reduction in the shadow field is due to a diffracting element, which splits the initial field of the interference into components, which cancel each other out.

Diffraction screens were previously studied as applied to the amplification of the field of convex ground obstacles [7 - 8] and to the suppression of interfering radio fields on closed paths near the Earth [9 - 10].

1. The Calculation of the Attenuation of the Field of a Convex Cylindrical Surface with a Rectangular Screen

The arrangement of the mutually influencing antennas, A and B, and the additional diffracting element on a cylindrical surface of radius a is shown schematically in Figure 1. The antennas A and B can be elementary dipoles,

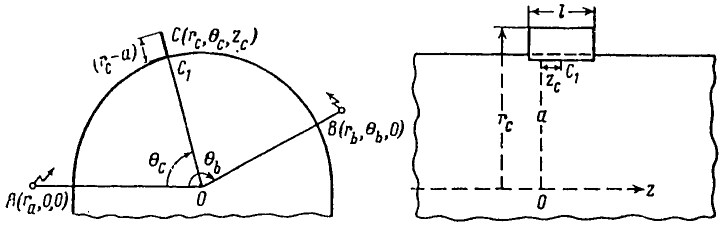

Figure 1.

the open ends of waveguides, slot antennas and other poorly directional microwave systems. Moreover, A and B can be understood to be the bounds (edges) of reflector antennas, through which the parasitic coupling of highly directional antennas passes, where these antennas are shielded by conducting objects. For convenience, the convex object is treated in the form of a half-cylinder, where the electromagnetic coupling between the antennas is realized in one direction. The spacings of the mutually influencing points on the surface of the cylinder are $h_a = (r_a - a)$ and $h_b = (r_b - a)$ and satisfy the conditions $h_a < a$ and $h_b < a$. The inequality $ka > 1$ should also be observed, where $k = 2\pi/\lambda$ is the wave number, and λ is the wavelength.

We determine the field at point B which is due to the source at A by working from Kirchoff's formula:

$$E=-\frac{1}{4\pi}\iint_s\left(G\frac{\partial E_1}{\partial\mu}-E_1\frac{\partial G}{\partial\mu}\right)ds. \tag{1}$$

We shall use the well-known expressions of [11 - 13] as the source function E_1 and Green's function G:

(2)
$$E_1=M\frac{e^{ikR_1}}{R_1}e^{in/4}2\sqrt{\pi x_c}\sum_m\frac{e^{ix_ct_m}}{t_m-q^2}\frac{w(t_m-y_a)}{w(t_m)}\frac{w(t_m-y)}{w(t_m)},$$

$$G=\frac{e^{ikR_2}}{R_2}e^{in/4}2\sqrt{\pi(x_b-x_c)}\sum_n\frac{e^{i(x_b-x_c)t_n}}{t_n-q^2}\times$$

$$\times\frac{w(t_n-y_b)}{w(t_n)}\frac{w(t_n-y)}{w(t_n)},$$

where

$$R_1=a\theta_c\sqrt{1+\left(\frac{z}{a\theta}\right)^2};\quad R_2=a(\theta_b-\theta_c)\sqrt{1+\left[\frac{z}{a(\theta_b-\theta_c)}\right]^2}$$

are the distances along the geodesic (helical) line from points A and B to the plane S where the additional diffracting screen is located; $x_c = (ka/2)^{1/3}\theta_c$, $x_b - x_c = (ka/2)^{1/3}(\theta_b - \theta_c)$ are the distances from points A and B in referenced coordinates; $y_a = (2/ka)^{1/3}k(r_a - a)$, $y_b = (2/ka)^{1/3}k\cdot(r_b - a)$ and $y = (2/ka)^{1/3}k(r_c - a)$ are the referenced heights of the cross coupling antennas A and B, and the diffracting screen; w(t) is an Airy function, which satisfies the equation $w''(t) - tw(t) = 0$; t_m and t_n are the roots of the equations $w'(t_m) - qw(t_m) = 0$ and $w'(t_n) - qw(t_n) = 0$ respectively; q is a parameter which takes into account the electrical properties of the surface, and for horizontal and vertical polarizations, is equal to $i(ka/2)^{1/3}\sqrt{\varepsilon_k - 1}$ and $i(ka/2)^{1/3}\frac{1}{\sqrt{\varepsilon_k+1}}$ respectively; ε_k is the complex dielectric constant of the diffracting surface; M is a constant which characterizes the source A.

Having substituted expression (2) in (1), we carry out the integration in Kirchoff's approximation over the surface S (the half-plane $z\theta_c$), located above the cylindrical body, excluding the portion occupied by the rectangular shield of length l and height $h = (r_c - a)$. In formula (1), μ is the normal to the given surface. We carry out the integration with respect to the variable z using the steady-state phase method, while integration with respect to y is accomplished in accordance with papers [12 - 13]. Without giving the voluminous intermediate mathematical derivations, we write the final expression for the field of the cylindrical body with a flat rectangular diffractor in the following form:

(3)
$$E=M\sum_m\sum_n\frac{w(t_m-y_a)}{w(t_m)}\frac{w(t_n-y_b)}{w(t_n)}e^{i[x_ct_m+(x_b-x_c)t_n]}\times$$

$$\times\left[\frac{w(t_m)w(t_n)}{(N_mN_n)^{1/2}}S_{n,m}\{F(v_1)-F(v_2)\}+\right.$$

$$\left.+\frac{\delta_{n,m}}{t_m-q^2}\{F(-v_1)+F(v_2)\},\right.$$

and when $m \neq n$:

$$S_{n,m}=\frac{1}{(N_nN_m)^{1/4}}\frac{w(t_m-y_c)w'(t_n-y_c)-w(t_n-y_a)w'(t_m-y_c)}{t_n-t_m}$$

is a conversion factor which shows how the incident mode of order m of the left side is transformed by the obstacle to a mode of order n, which propagates from the screen, and when $m = n$:

$$S_{m,m}=\frac{1}{N_m}\{(t_m-y_c)[w(t_m-y_c)]^2-[w'(t_m-y_c)]^2\},$$
$$N_m=(t_m-q^2)[w(t_m)]^2,$$
$$N_n=(t_n-q^2)[w(t_n)]^2,$$

$\delta_{m,n} = 1$ when $m = n$ and $\delta_{m,n} = 0$ when $m \neq n$. The field is expressed as a function of the length and the displacement of the compensator from the geodesic line connecting the interacting points in terms of the Fresnel integrals $F(v_1)$ and $F(v_2)$ in (3), and:

$$F(v_j)=\frac{e^{-i\pi/4}}{\sqrt{2}}\int_{v_j}^{\infty}e^{i(\pi/2)t^2}dt, \quad F(-v_j)=\frac{e^{-i\pi/4}}{\sqrt{2}}\times$$
$$\times\int_{-\infty}^{v_j}e^{i(\pi/2)t^2}dt\,(j=1,2), \quad v_1=\frac{\sqrt{2}}{b}\left(z_c-\frac{l}{2}\right),$$
$$v_2=\frac{\sqrt{2}}{b}\left(z_c+\frac{l}{2}\right), \quad b=\sqrt{\frac{\lambda d_c(d_b-d_c)}{d_b}},$$

l is the length of the compensator, and d_c and $(d_b - d_c)$ are the lengths of the segments AC_1 and C_1B along the arc respectively.

In the absence of the compensating screen, i.e., when $(r_c - a) = 0$, we obtain a formula from expression (3) which defines the diffraction field of the convex surface:

$$E_0=M\sum_m\frac{e^{ix_bt_m}}{t_m-q^2}\frac{w(t_m-y_a)}{w(t_m)}\frac{w(t_m-y_b)}{w(t_m)}.$$

The ratio of E to E_0 will determine the change in the shadow field with the installation of the rectangular diffractor:

(4)
$$B=\frac{\sum_m\sum_n \frac{w(t_m-y_a)}{w(t_m)}\frac{w(t_n-y_b)}{w(t_n)}e^{i[x_c t_m+(x_b-x_c)t_n]}}{\sum_m \frac{e^{ix t_m}}{t_m-q^2}\frac{w(t_m-y_a)}{w(t_m)}\frac{w(t_m-y_b)}{w(t_m)}}\times$$
$$\times\left[\frac{w(t_m)w(t_n)}{(N_mN_n)^{1/4}}S_{n,m}\{[F(v_1)-F(v_2)]\}+\right.$$
$$\left.+\frac{\delta_{m,n}}{t_m-q^2}\{F(-v_1)+F(v_2)\}\right].$$

In the case of an absolutely conducting body and vertical polarization (q = = 0) for antennas located in deep shadow with respect to the decoupling element, for $y_a = y_b = 0$, expression (4) assumes a simple form:

(5)
$$B=S_{1,1}[F(v_1)-F(v_2)]+F(-v_1)+F(v_2),$$

where
$$S_{1,1}=\frac{1}{t_1}\left\{(t_1-y_c)\left[\frac{w(t_1-y_c)}{w(t_1)}\right]^2-\left[\frac{w'(t_1-y_c)}{w(t_1)}\right]^2\right\}.$$

The first term in (5) depends on the height of the upper edge of the rectangular shield above the surface of the cylinder in terms of the function $S_{1,1}$ and its length in terms of $[F(v_1) - F(v_2)]$, and the remaining terms are determined only by the length of the shield. Physically, this means that the diffraction field which envelopes the cyclinder, by virtue of the additional element, is split into components, the amplitudes and phases of which depend on the geometric parameters of the diffractor. Thus, by varying the dimensions of the screen, one can vary the amplitude-phase relationships of the terms in expression (5) and thereby control the resulting field at the receive point. The numerical analysis of formula (5) shows that there exist definite parameters of the shield - the compensator - for which the function B has the deepest minimum and the maximum supplemental decoupling will be observed. As the analysis shows, this occurs when:

(6)
$$h_c=1{,}9\left(\frac{a}{k^2}\right)^{1/3},\quad l=0{,}8b.$$

Formulas (6) were derived for the case where the center of the compensator is located on the geodesic line joining the corresponding points on the surface of the cylinder.

The calculated graphs (the solid curves) for B as a function of the geometric parameters of the compensator, obtained from formula (5), are shown in Figures 2 - 4. A discussion of the calculated results is given below in a comparison of the latter with experimental data.

2. Experimental Results and a Comparison of Them with the Calculated Values

Experimental studies of the supplemental attenuation of a diffraction field were performed under test conditions in an open space using convex

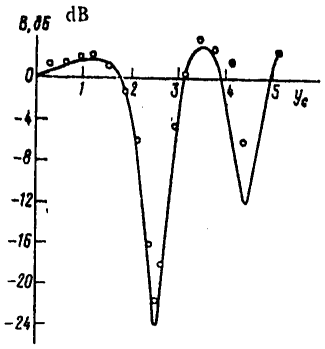

Figure 2.

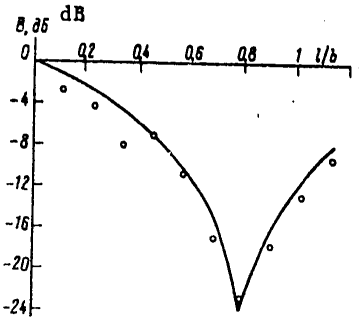

Figure 3.

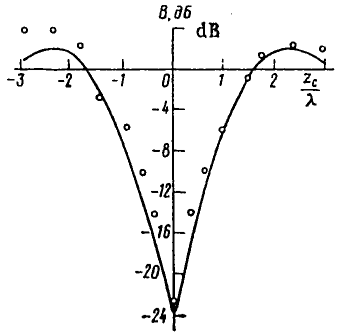

Figure 4.

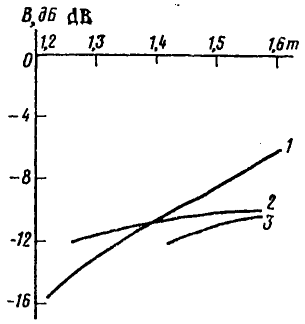

Figure 5.

conducting bodies where λ = 3.3 cm. Used as the cross coupling antennas were the open ends of rectangular waveguides (10 x 23 mm), which were mounted in the shadow zone with respect to each other. The measurement set-up allowed for continuously changing the position and geometric parameters of the compensating elements. A GK4-19A generator served as the source of electromagnetic radiations, while a P5-10 receiver measured the diffraction field.

The experimental curves for the change in the diffraction field of B (the small circles) as a function of the dimensions and position of the diffractor are shown in Figures 2 - 4 along with the the theoretical curves, where the electrical field E of the radiator was directed along the radius of the cylindrical body, while the magnetic field vector was parallel to the axis of cylinder and the mutually influencing antennas were positioned directly on the surface of the object where $\theta_b = \pi$. The results cited here apply to a cylindrical surface with a radius a = 10 λ.

From the graph for the field attenuation as a function of the referenced height y_c (Figure 2), we see that for a length of $\ell = 2.1\lambda$, for the case of small values of the height of the screen-compensator, a slight amplification of the field is observed, after which a deep minimum of the signal is revealed. Such a sharp drop in the radio signal level was caused by the out-of-phase addition of the field from the side sections of the shield to the field produced by the upper edge of the compensator, having approximately equal values of the amplitudes of these signals. A further increase in the height leads to oscillations of the shadow field, which are caused by the change in the amplitude and phase of the field due to the variation in the shield height for the case of constant side fields. It is easy to determine the height of a shield at which the maximum reduction of the field is observed from the graph of B as a function of y_c. We find from $y_c = (2/ka)^{1/3}kh = 2.5$ that $h = 1.9\ (a/k^2)^{1/3}$. For the given geometry, $h = 1.2\lambda$. A comparison of the theoretical curve with the measurement data throughout the entire range of measurement of y_c shows their completely satisfactory agreement.

The nature of the attenuation as a function of the diffractor length is shown by the results presented in Figure 3, where plotted along the abscissa is the ratio of the length of the rectangular attachment to the dimension of the first Fresnel zone, b. This curve, just as the graph of Figure 2, was obtained for the case where the center of the compensator is located on the geodesic line joining the mutually influencing antennas. As can be seen from the calculated and experimental results cited here, where a screen with a height of $h = 1.2\lambda$, when its length is increased, a substantial reduction is observed in the field, which reaches a minimum value (-22 dB) for the given configuration of the antennas and the obstacle, where $\ell = 0.8$ b. With a further increase in the width, the degree of decoupling falls off markedly. Just as in the case of B as a function of h, the change in the supplemental attenuation with a variation in the length of the rectangular element is explained by the interference of the fields produced by the upper and side edges of the diffractor.

The level of signal suppression falls off rather rapidly when the compensator is shifted from the geodesic line joining the antennas. This is illustrated in Figure 4, which shows the change in the supplemental decoupling as a function of the displacement z_c/λ for the case of optimum dimensions of the compensating screen, determined from formulas (6) in the form $h_c = 1.2\lambda$ and $\ell = 2.1\lambda$. When the element is shifted by even about 1.5 λ, the level of the diffraction field of the convex surface approaches its own initial value. The maximum supplemental decoupling is achieved when the center of the rectangular attachement is located on the line joining the antennas.

An important characteristic of decoupling devices is their band coverage properties. Curve 1, shown in Figure 5, was derived from formula (5) and shows the decoupling effectiveness when a rectangular attachment of $1.2\lambda \times 2.1\lambda$ is used in various ranges of change in the working frequency. The value $m = f_{max}/f_{min}\big|_{B = const}$ is plotted along the abscissa in this figure,

where f_{max} and f_{min} are the upper and lower frequencies of the band, while while the supplemental decoupling of B is plotted along the ordinate. Curves 2 and 3, taken from paper [6], which illustrate the frequency characteristics of ribbed structures consisting of 8 and 10 grooves respectively, are also shown there for comparison. It can be seen from this that the band coverage properties of ribbed decoupling devices, the parameters of which are determined from the condition of maximum bandwidth, are somewhat better than similar characteristics of a rectangular compensator. We will note that greater wideband suppression of the field using diffracting elements can be achieved by means of specially profiled compensators, for example, a stepped flat attachment with a height on the order of the wavelength makes it possible to obtain a supplemental attenuation of about 20 dB in a band with a coverage of 1.5. The structural design and the results of studying wideband decoupling devices of this type deserve a separate treatment.

The calculated and experimental results obtained in this paper demonstrate the possibility of the diffractor attenuation of a field for the purpose of improving the decoupling between antennas, separated by a convex object. The use of compensators of a simple structural design and small dimensions can preclude the necessity of experimentally selecting the position of the antennas, as well as the utilization of complex decoupling devices. The presence of a protrubance, which is extremely insignificant in the centimeter band, cannot substantially limit the practical application of the proposed method.

The authors would like to express their deep gratitude to B.Ye. Kinber and G.A. Postnov for much valuable advice in the performance of this work.

BIBLIOGRAPHY

1. O.N. Tereshin, RADIOTEKHNIKA I ELEKTRONIKA, 1960, 5, 12, p 1944.

2. O.N. Tereshin, A.S. Belov, IZV. VUZOV MVO SSSR (RADIOTEKHNIKA) [PROCEEDINGS OF THE HIGHER EDUCATIONAL INSTITUTES OF THE USSR MINISTRY OF HIGHER EDUCATION (RADIO ENGINEERING)], 1960, 3, p 359.

3. A.G. Dmitriyenko, IZV. VUZOV MVSSO SSSR (RADIOELEKTRONIKA) [PROCEEDINGS OF THE HIGHER EDUCATIONAL INSTITUTES OF THE USSR MINISTRY OF HIGHER AND SPECIAL EDUCATION (RADIOELECTRONICS)], 1976, 19, 2, p 123.

4. J.G. Hoffman, "Antenna Decoupling by Means of a Lossy Dielectric Slab" US Patent Class 343-771, No 3, 277488, 1966.

5. A.G. Kyurkchan, RADIOTEKHNIKA I ELEKTRONIKA, 1977, 22, 7, p 1362.

6. Kh.S. Baksht, V.A. Zamotrinskiy, Ye.S. Kovalenko, G.G. Kretov, Zh.M. Sokolova, IZV. VUZOV MVSSO SSSR (RADIOELEKTRONIKA), 1969, 12, 6, p 571.

7. V.N. Troitskiy, ELEKTROSVYAZ' [ELECTRICAL COMMUNICATIONS], 1964, 12.

8. N.B. Chimitdorzhiyev, RADIOTEKHNIKA I ELEKTRONIKA, 1969, 14, 5, p 896.

9. N.B. Chimitdorzhiyev, Yu.L. Lomukhin, "Difraktornyy metod kompensatsii SVCh polya meshayushchikh radiosignalov" ["A Diffractor Method of Compensating for the Microwave Field of Interfering Radio Signals"], in the collection, "X Vsesoyuznaya konferentsiya po rasprostraneniyu radiovoln, sektsiya 3" ["Tenth All-Union Conference on Radio Wave Propagation, Section 3"], 91, Nauka Publishers, 1975.

10. N.B. Chimitdorzhiyev, Yu.L. Lomukhin, ELEKTROSVYAZ', 1979, 1, p 54.

11. V.A. Fok, "Problemy difraktsii i rasprostraneniya elektromagnitnykh voln" ["Problems in Electromagnetic Wave Diffraction and Propagation"], Sovetskoye Radio Publishers, 1970.

12. J.R. Wait, CANAD. J. PHYS., 1962, 40, 8, p 1010.

13. J.R. Wait, RADIO SCIENCE, 1968, 3 (New Series), 10, p 995.

[40-8225]
8225
CSO: 1860

Certain Aspects of Computer Hard and Soft Ware;
Control, Automation, Telemechanics and Machine Planning

UDC 621.318:681.327

PHYSICS OF CYLINDRICAL MAGNETIC DOMAINS

Moscow KIZIKA TSILINDRICHESKIKH MAGNITNYKH DOMENOV in Russian 1979 signed to press 1 Jan 79 p 2, 191-192

[Annotation and table of contents from book by Fedor Vikturovich Lisovskiy, Sovetskoye radio, 3000 copies, 192 pages]

[Text] The author examines the physical properties and principles of practical applications of cylindrical magnetic domains (TsMD). He gives a theoretical analysis of statistical and dynamic properties of domain boundaries, isolated domains, and domain lattices. Information is given on the methods of obtaining, characteristics, and methods of measuring the parameters of materials with TsMD. The author analyses the methods of controlling the movement, generation, and readout of TsMD, as well as the principles of constructing memory devices based on TsMD.

The book is intended for scientists and specialists engaged in the problems of magnetoelectronics, computing technology, and the physics of magnetic phenomena, as well as for undergraduate and graduate students of higher educational institutes of these fields.

Contents

10,233
CSO: 1860

Communication,s Communication Equipment;
Data Transmission and Processing

UDC 621.395.664.12

ECHO SUPPRESSORS IN COMMUNICATION LINES

Moscow EKHOZAGRADITEL'NYYE USTROYSTVA NA SETYAKH SVYAZI (Echo Suppressors in Communication Lines) in Russian 1979 signed to press 30 Oct 78 p 2, 88

[Annotation and table of contents from book by Mikhail Kronidovich Tsybulin, Svyaz', 4400 copies, 88 pages]

[Text] The author describes the phenomena of electric echo in long audio frequency channels, examines the methods of controlling the interfering action of echo currents during telephone calls, and surveys the existing domestic and foreign echo suppressors. Special attention is given to the operation of channels equipped with echo suppressors.

The book is intended for engineers and technicians engaged in the designing, tuning, and operation of telephone communication channels.

Contents

[49-10,233]

10,233
CSO: 1860

USSR UDC 621.396.946:629.783:525

A SPACE COMMUNICATION GROUND STATION IN BULGARIA

RADIO. TELEVIZIYA ELEKTRON in Bulgarian Vol 27 No 7, 1978 pp 2-3

STOYKOV, S.

[From REFERATIVNYY ZHURNAL RADIOTEKHNIKA, No 1, 1979, Abstract No. 1A273 by N. Ye. Sirotina]

[Text] A brief description is presented of a station constructed with the assistance of the USSR and intended for operation in the "Intersputnik" system. A two-reflector antenna with a counter reflector is used for reception and transmission. The antenna rotation system is controlled by a programmed device which coordinates the rotation of the antenna with the trajectory of the satellite. The receiver has a low-noise 4-stage parametric amplifier at its imput, with the first 2 stages cooled by liquid nitrogen. The specific features of the telephone equipment are noted. Figures 1.

6508
CSO: 1860

UDC 621.396

LONG-RANGE PROPAGATION OF RADIO WAVES IN THE IONOSPHERE

Moscow DAL'NEYE RASPROSTRANENIYE RADIOVOLN V. IONOSFERE (Long-Range Propagation of Radio Waves in the Ionosphere) in Russian 1979 signed to press 27 Apr 79 p 2, 151-152

[Annotation and table of contents from book by Aleksandr Grigor'yevich Shlionskiy, Institute of Terrestrial Magnetism, the Ionosphere and Radio Wave Propagation of the USSR Academy of Sciences, Nauka, 850 copies, 152 pages]

[Text] The author examines the conditions and characteristics of superlong range (round-the-world, backward, antipodal) and long-range propagation of short radio waves in ionospheric channels when the radiators are on the surface of the earth and in the ionosphere.

The book gives the results of the analysis and interpretation of experimental data and theoretical examination of the dependence of the characteristics of ionospheric radio waveguides on the main parameters of the ionosphere.

The book is of interest to radio physicists, radio engineers, and graduate and undergraduate students specializing in the area of long-range ionospheric propagation of radio waves.

Tables 2; Figures 66; Bibliography 118 items.

Contents

[45-10,233]

10,233
CSO: 1860

Components and Circuit Elements; Including Waveguides and Cavity Resonators

UDC 621.372.8

OPTICAL BAND DIELECTRIC WAVEGUIDES BASED ON ORGANOSILICON COMPOUNDS

Kiev IZV. VUZ: RADIOELEKTRONIKA in Russian Vol 22 No 8, 1979 pp 96-98
manuscript received 12 Jan 78; after completion 16 Feb 78

[Article by L.M. Andrushko, V.A. Voznesenskiy, L.G. Gassanov, Ye.P. Krivokoby1'skiy and B.V. Tkachuk]

[Text] It is well known that thin polysiloxane films, obtained in a decaying discharge, can be used to produce planar dielectric waveguides. They are distinguished by low optical losses and high stability with aging [1]. However, despite the obvious promise of the application of thin polymer films, the data on the structure and their properties in the literature is inadequate.

The purpose of this paper is to study the structure of waveguide and optical properties of thin polysiloxane films, derived by means of the polymerization of organosilicon compounds in a decaying discharge plasma. The influence of the derivation conditions on the structure and properties of the films are also studied.

The organosilicon compounds octamethatrisiloxane (OMTS) and hectamethadisiloxane (GMDSZ) were chosen as the original substances. The polymer films were obtained in a series produced UVN2M-1 vacuum installation using the procedure of [2]. To perform the polymerization, the reaction chamber was pumped out down to a pressure of $1 \cdot 10^{-3}$ Pa, and then the monomer was admitted up to the requisite pressure. The polymer films were obtained both at the electrodes and in the interelectrode space under the following conditions: the vapor pressure of the original compounds in the reaction chamber was 1--40 Pa, the current density at the electrodes was 0.2--0.8 ma/cm^2, the discharge burn voltage was 300--1,500 volts and the generator frequency was 1,000 Hz.

The polymerization process was carried out under dynamic conditions of a pump down rate of 5 l/s. The polymer films were applied to a substrate of type KV fused quartz ($n' = 1.45$). The waveguides were excited by a He-Ne laser ($\lambda = 0.63$ μm) by means of a prism coupler. The refraction indices and the film thicknesses were determined from measurements of the resonance excitation angles and the calculation of the dispersion equations

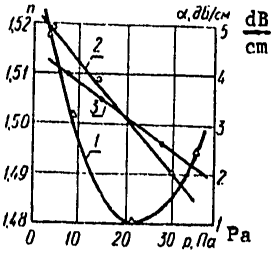

Figure 1. The variation in the index of refraction (n) and the losses (α) of polymer films, obtained at different monomer vapor pressures in the reaction chamber.

of [3]. The optical attenuation was measured by means of moving the extraction prism, as well as by photodiode scanning along the track. The structure of the films was studied using infrared spectroscopy with the IKS-22 spectral photometer in a range of 650-4,000 cm^{-1}.

Polymer films of OMTS and GMDSZ were made with a thickness of from 0.3 to 3 μm (Figure 1, curves 2 and 3). It was found that polymer OMPS films, obtained at low monomer vapor pressures (p = 1 Pa), had a yellowish color, and the waveguide properties of such structures were unsatisfactory (α = 10 dB/cm). The index of refraction for films based on OMTS was 1.53. The values obtained for the refraction index are not typical for organosilicon polymer films, and are apparently due to the considerable increase in the carbon content in the polymer composition, as well as to the mechanical stress in the film.

With an increase in the pressure in the reaction chamber, polymer films were obtained with a somewhat lower value of the refraction index. At a pressure of 25 Pa, polymer films of OMTS had an attenuation not exceeding 1 dB/cm (Figure 1, curve 1). The refractive index in this case was 1.485, the film thickness was 2.7 micrometers and the moderation ratio was γ = = 1.469. The films had good adhesive and mechanical properties.

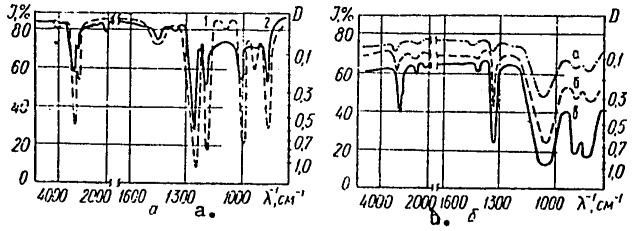

Figure 2. Infrared spectra: a. Of the original monomer (a) and the polymer GMDSZ (b) at p = 20 Pa and j = 0.4 ma/cm^2; b. Of the OMTS polymer films at p = 20 Pa, j = 0.5 ma/cm^2 (a - 0.76; b - 1.1; c - 1.76 micrometers).

It should be noted that increasing the vapor pressure of the monomer in the reaction chamber lead to a significant increase in the rate of polymer film formation and at a pressure of more than 35 Pa, the process of polymerization from the gaseous phase began. Apparently, simultaneously with the process of forming the polymer film on the substrate surface,

polymerization occurred in the volume of the discharge, as a result of which, the resulting film had spotting of the polymer, where the spots reached a diameter of 1 to 3 micrometers and more. With a further increase in the pressure, the polymerization process in the volume of the dishcarge developed even more intensely. The waveguide properties of such structures were considerably degraded.

The structure of the thin polymer films was studied by infrared spectroscopy. The spectra of the original GMDSZ and the polymer films based on it are shown in Figure 2a. The presence of absorption bands at 940 cm^{-1}, which correspond to the valence antisymmetrical vibrations of the Si-N-Si bond, is characteristic of the IR spectrum of the original GMDSZ. Absorption bands at 3,380 and 1,190 cm^{-1} belong to the valence and deformation vibrations of the N-H groups. Absorption in other regions of the spectrum is due to valence deformation and pendulum vibrations of the carbon-hydrogen bond in the methyl groups and the Si-C bond [4].

In a comparison of the spectra of the polymer film (1) and the original monomer (2), it was found that the redistribution of the intensity of the absorption bands is substantial in a range of 650--1,200 cm^{-1}. Moreover, the absorption bands which correspond to the deformational and valence vibrations of the N-H bond (3,380, 1,560 and 1,190 cm^{-1}) and the valence vibrations of the Si-C bond (692 cm^{-1}), are reduced in the spectrum of the polymer. This is evidence of the fact that the polymerization process occurs both by virtue of the rupture of the Si-C and C-H bonds, and by means of the rupture of the N-H bonds and the compounds of the fragments formed via free bonds [5].

The IR spectra for polymer films of differing thicknesses based on OMTS are shown in Figure 2b. The 1.035 cm^{-1} absorption band corresponds to valence antisymmetrical vibrations of the Si-O-Si siloxane group. Bands corresponding to vibrations of methyl groups (1,255, 1,420, 1,460, 2,915 and 2,950 cm^{-1}) are intensively manifest in the spectrum of the polymer. As can be seen from the figure, the ratios of the optical densities of the bands of the valence vibrations of the Si-O-Si groups to the bands of methyl group vibrations ($D_{Si-O-Si}/D_{CH2}$) for all the polymer films remains constant, and is equal to 1.5. This allows the conclusion that the structure of the polymer formed does not depend on the film thickness or the duration of the polymerization process.

Thus, through the choice of the appropriate discharge conditions and the original monomers, inhomogeneous planar dielectric waveguides can be fabricated using the given technology with a specified law governing the change in the index of refraction with respect to film thickness. The inhomogeneous dielectric waveguides have great possibilities as compared to homogeneous ones. They allow for an expansion of the single mode band

of frequencies, the transmission of pulse signals with little distortion, the compensation for the dispersion of the material, etc. [6].

BIBLIOGRAPHY

1. Tien, P.K., Smolinsky, G., Martin, "Thin Organosilicon Films for Integrated Optics", APPLIED OPTICS, 1972, 11, p 637.

2. Tkachuk, B.V., "Polimerizatsiya kremniyorganicheskikh soyedineniy na poverkhnosti tverdogo tela pod deystviyem tleyushchego razryada" ["The Polymerization of Organosilicon Compounds at the Surface of a Solid Subject to the Action of a Decaying Discharge"], VYSOKOMOLEKULYARNYYE SOYEDNINENIYA [HIGH MOLECULAR WEIGHT COMPOUNDS], 1967, 9A, No 9, p 2018.

3. Deryugin, L.N., Marchuk, A.I., Sotin, V.Ye., "Svoystva ploskikh nesimmetrichnykh dielektricheskikh volnovodov na podlozhke iz dielektrika" ["The Properties of Planar Asymmetrical Dielectric Waveguides on a Dielectric Substrate"], IZVESTIYA VUZOV - RADIOELEKTRONIKA [PROCEEDINGS OF THE HIGHER EDUCATIONAL INSTITUTES - RADIO ELECTRONICS], 1967, 10, No 2, p 134.

4. Bellami, L. "Infrakrasnyye spektry slozhnykh molekul" ["Infrared Spectra of Complex Molecules"], Moscow, IIL Publishers, 1963.

5. Tkachuk, B.V., Kolotyrkin, V.M., "Polucheniye tonkikh polimernykh plenok iz gazovoy fazy" ["The Derivation of Thin Polymer Films from the Gaseous Phase"], Moscow, Khimiya Publishers, 1977, 101 pp.

6. Andrushko, L.M., Litvinenko, O.N., "Metod sinteza ploskikh dielektricheskikh svetovodov, osnovannyy na reshenii obratnoy zadachi Shturma-Liuvillya" ["A Method of Synthesizing Planar Dielectric Lightguides, Based on the Solution of the Inverse Sturm--Louiville Problem"], RADIOTEKHNIKA I ELEKTRONIKA, 1967, 22, No 11, p 2272.

[16-8225]

8225
CSO: 1860

Electromagnetic Wave Propagation;
Ionosphere; Troposphere; Electrodynamics

UDC 537.867:621.3.018.2

THE ACTIVE CANCELLATION OF ELECTROMAGNETIC WAVES

Moscow RADIOTEKHNIKA I ELEKTRONIKA in Russian Vol 24 No 10, Oct 79 pp 1982-1988
manuscript received 2 Jan 78

[Article by V.V. Tyutekin, A.T. Ukolov and M.V. Fedoryuk]

[Text] The problems of the active cancellation of a steady-state electromagnetic field in free space and in a waveguide are treated. It is shown that in a region outside the source, the electromagnetic wave can be completely cancelled by using receiving and radiating surfaces on which point dipole receivers and radiators of both electrical and magnetic types are continuously distributed.

The problem of cancellation with a precision of down to the inhomogeneous modes is treated for a waveguide which is uniform over the path. It is shown that this problem can be solved with the use of a finite number of receivers and sources, equal to twice the number of propagating modes.

So called active methods of cancelling acoustical fields have undergone rapid development in recent years in acoustics. The essence of these methods consists in the fact that by receiving information on the initial field by a system of receivers, processing it in the requisite manner and radiating a secondary (cancelling) field by a system of secondary radiators, reductions in the levels of the original field are achieved in a specified region of space. Although the problem of developing and applying active methods to changing the levels of sound fields was studied comparatively long ago, its solution did not have a strictly theoretical substantiation until recently. The most complete and exhaustive substantiation of the problem of active methods of cancelling acoustical fields was set forth in [1, 2, 3], as well as in the paper [4] which was close to the idea of these. The possibility of total cancellation of an original field of any kind inside (or outside) a closed surface by means of creating receiving and radiating systems around it consisting of monopole and dipole type elements which physically realize

closed Huygens wave surfaces, was theoretically demonstrated for the first time in the papers cited here. The essential feature of such systems is the fact that their structure does not depend on the kind of incident field.

Later, a number of experimental works appeared in which active systems designed around this principle were studied, where the systems cancelled acoustical waves for a single mode waveguide [5, 6, 7], a multimode waveguide [8], for free space [9], etc. Moreover, this principle was extended to the case of elastic waves [10], and flexure waves in rods and plates [11].

Active cacellation of wave fields, based on the construction of receiving and radiating Huygens surfaces, is treated in this paper for the case of the cancellation of steady-state electromagnetic fields.

1. *The formulation of the problem.* We shall consider an electromagnetic field in a space R^3, filled with an isotropic medium, with smooth real $\varepsilon(x)$ and $\mu(x)$. The fields U satisfies the system of Maxwell's equations:

$$LU \equiv (\operatorname{rot}\mathbf{H} + ik\varepsilon\mathbf{E},\ \operatorname{rot}\mathbf{E} - ik\mu\mathbf{H}) = \mathbf{J}. \tag{1}$$

The time dependence is given by the factor $\exp(-i\omega t)$, $x = (x_1, x_2, x_3)$, $U(x) = (E(x), H(x))$, $J(x)$ are the 6-vectors (all column vectors).

It is assumed that ε and μ tend sufficiently quickly to the positive constants when $|x| \to \infty$ and that the field U satisfies the radiation condition.

Let S be a smooth closed surface, D^- be its interior, D^+ be exterior, and the sources J which produce the field U are located at D^+, i.e., $J(x) \equiv 0$, $x \in D^-$. Let $\overset{\circ}{S}$ be a smooth closed surface which contains S within itself, and $J(x) \equiv 0$ within $\overset{\circ}{S}$. We shall position electrical and magnetic and dipole radiators (receivers) continuously on $S(\overset{\circ}{S})$, and pose the problem: the generation of a compensating field U^* such that the total field in the region D^- becomes 0, while in the region D^+, it remains equal to the incident field; moreover, we shall require that the receiving surface does not react to the field incident to the system from without. This problem is broken down into two parts:

I. The Radiation Problem. Find those densities of the radiators on S so that the compensating field $U^*(x)$ generated by them has the form:

$$\mathbf{U}^*(x) = \begin{cases} -\mathbf{U}(x), & x \in D^-, \\ 0 & x \in D^+. \end{cases} \tag{2}$$

then the overall field $\tilde{U}$ will be equal to:

$$\tilde{\mathbf{U}}(x) = \begin{cases} 0, & x \in D^-, \\ \mathbf{U}(x), & x \in D^+. \end{cases}$$

II. The Receive Problem. Obtain all of the information needed for the operation of the radiators, from the readings of the receivers which measure the field U on $\tilde{S}$.

We will note that the second part of condition (2) assures the absence of undesirable feedback between the receivers and the secondary radiators.

To solve the active cancellation problem, we need certain properties of Green's operator, and we shall now move on to a consideration of this.

2. *Green's Operator.* Let G(x, x') be a Green's matrix of the system of Maxwell's equations (1), i.e., the solution of the equation:

$$L_x G(x, x') = \frac{4\pi}{c}\delta(x-x') I_6,$$

which satisfies the radiation condition (I_6 is a unit 6 x 6 matrix), and U (x) = (E(x), H(x)) is an arbitrary smooth vector.

We shall introduce Green's operator $(\Gamma_S U)(x)$ using the formula:

$$(\Gamma_S U)(x) = \frac{c}{4\pi}\int_S G(x, x') U_n(x)\, dS', \tag{3}$$

$$U_n(x) = ([H(x), n_x], \quad [E(x), n_x]).$$

Here S is the smooth closed surface, n_x is the exterior normal to S at the point x, and [a, b] is a vector product.

It follows from definition (3) that Green's operator describes the field generated by the radiating surface on which electrical and magnetic dipoles with vectors densities of $p(x) = (c/4\pi)\,[H(x), n_x]$ and $m(x) = (c/4\pi)[E(x), n_x]$ respectively are continuously distributed. There is an arbitrary aspect to the selection of the number of dipoles and the orientation of their axes, located at one point. For example, the surface can be constructed so that there are two electrical and two magnetic dipoles at each point with axes tangential to the S plane. The axes of the electrical (or magnetic) dipoles do not fall on one straight line, while their vector densities p_1 and p_2 (m_1, m_2) are such that $p_1(x) + p_2(x) = p(x)$ ($m_1(x) + m_2(x) = m(x)$). The surface which is constructed in this manner possesses the following property: in the case of a change in the vector U, it is not necessary to change the orientation of the axes of the dipoles; it is sufficient to change in an appropriate manner the absolute values $|p_1|$ and $|p_2|$ ($|m_1|$, $|m_2|$). In this case, the selected number of radiators at each point is minimal. The basic property of Green's operator is the following:

$$(\Gamma_S U)(x) = \Theta_S(x) U(x), \tag{4}$$

$$LU(x) = 0, \quad x \text{ внутри } S,$$

(inside S),

where $\Theta_S(x) \equiv 1$, when x is inside S, and $\Theta_S(x) \equiv 0$, when x is outside S. The proof of the well known formula (4) follows from the lemma of Lorentz. In fact, let D be a limited region with a smooth boundary S, and then:

$$\int_D \{(U(x'), L_{x'}G(x', x)) - (G(x', x), L_{x'}U(x'))\}dx' = \frac{4\pi}{c}\Theta_S(x)U(x). \tag{5}$$

We shall make use of the lemma of Lorentz:

$$\int_D \{(L_x\tilde{U}(x), U(x)) - (\tilde{U}(x), L_xU(x))\}dx =$$

$$= \int_S \{(\tilde{E}, H, n) - (E, \tilde{H}, n)\}dS.$$

Here (a, b, c) is a mixed 3-vector product, (a, b) = $\Sigma a_j b_j$ is the scalar product of the 6-vectors or 3-vectors. By applying this lemma to the left side of formula (5), and taking into account the equality G(x, x') = $= G^T(x', x)$ (the reciprocity principle), we obtain formula (4).

In comparing expressions (2) and (4), we find that:

$$U(x) = (\Gamma_S(-U))(x). \tag{6}$$

It follows from (6) that the solution of problem I is realized by the radiating surface described above, in which case:

$$p_1(x) + p_2(x) = p(x) = -\frac{c}{4\pi}[H(x), n_x],$$
$$m_1(x) + m_2(x) = m(x) = -\frac{c}{4\pi}[E(x), n_x];\ x \in S. \tag{7}$$

Applying formula (4), we find that the solution of the receive problem is given by the formula:

$$U(x) = (\Gamma_{\tilde{S}}U)(x),\ x \in S. \tag{8}$$

Finally, the active cancellation scheme looks like this: By means of receivers arranged on $\tilde{S}$, we measure the components of the electromagnetic field tangential to $\tilde{S}$. Then, by computing the integral $\Gamma_{\tilde{S}}U$, we find the amplitudes of the electrical and magnetic dipoles on S, which must be specified in order to obtain the compensating field.

In order to compensate for the field U outside of S, it is sufficient, of course, to position only electrical dipole radiators on S (correspondingly, in the acoustical problem, one can place only monopole radiators on S).

But then the radiation will not be unidirectional -- the compensating field will not be zero outside S, i.e., feedback will appear between the radiators and the receivers.

The integral $\Gamma_{\tilde{S}}U$ can be approximately replaced by an integral Riemannian sum. This means that one must place a discrete system on $\tilde{S}$ consisting of a sufficiently large number of receivers. Correspondingly, we shall place a discrete system of radiators on S. Then the calculation of the amplitudes of the radiators on S reduces to a radio engineering problem. Each receiver must be coupled to each radiator, including in each such coupling an amplifier and a phase shifter.

The cancelling system treated here differs from the analogous acoustical system in having twice the number of both receivers and radiators (in the acoustic case, located at each point of the receiving and radiating surfaces were one monopole and dipole each, and in the electromagnetic case, two electrical and magnetic dipoles each). This circumstance is due to the fact that it is necessary in the electromagnetic case, in contrast to the acoustic one, both when receiving the original field and when radiating the secondary field, to take their polarization into account.

We will note that the processing of the readings of the receivers based on formula (7) makes the receive surface unidirectional. In fact, let a field U^-, generated by a source J^- which is located in D^- fall on $\tilde{S}$ in addition to the field U. Then:

$$(\Gamma_{\tilde{S}}(U+U^-))(x)=(\Gamma_{\tilde{S}}U)(x)+(\Gamma_{\tilde{S}}U^-)(x)=U(x),\ x\in S. \tag{9}$$

The latter equality obtains by virtue of a formula similar to (4):

$$(\Gamma_s\tilde{U})(x)=(\Theta_s(x)-1)\tilde{U}(x). \tag{4'}$$

Here, $\tilde{U}$ satisfies the homogeneous system of Maxwell's equations outside of S and the condition for cancellation feasibility.

Other variants of the active cancellation problem have also been studied in a similar manner. For example, let it be necessary, as before, to cancel a field U in the region D^-, but let there be a source J^- such that $J^-(x) \equiv 0$, x D^+. Then formulas (6) remain unchanged, while (9) obtains instead of (8).

3. *The waveguide problem.* Let W be a waveguide with an axis x_3, with a smooth boundary and with ideally conducting walls, and the field U satisfies equation (1). Here, $J(x) = J^+(x) + J^-(x)$, $J^\pm$ are smooth finite vector functions of $J^+(x) \equiv 0$ when $x_3 \geq l_1$, $J^-(x) \equiv 0$ when $x_3 \leq l_2$, $l_1 < l_2$. It is required that the right half, W^+, of the waveguide be insulated: $x_3 > l_2$ from the sources J^+ located to the left, i.e., it is required that the following field be generated: $U'(x)=-U^+(x)\Theta(x_3-l_2)$.

We shall take the sections $x_3 = l_1$ and $x_3 = l_2$ respectively as the receiving and radiating S surfaces. Then, formulas (6) and (8) are preserved, but instead of Green's matrix G, the Green's matrix G_W must be taken for the waveguide W, while the normal n will be directed along the x_3 axis. It follows from this that the axes of the electrical and magnetic dipole radiators, located on S, fall in the plane of the cross-section. It is sufficient for the proof to apply formula (4) to the region $x \in W$, $a < x_3 < N$. By virtue of the boundary conditions, the integral over the surface of the waveguide goes to zero, while the integral over the cross-section $x_3 = N$ tends to zero when $N \to +\infty$ because of the radiation conditions.

We shall consider a regular waveguide W with a constant cross-section D. Let ε and μ be smooth real functions which do not depend on x_3. The problem is treated with the assumption that the receivers and radiators, and the external sources, are spaced sufficiently far apart. Then, one can neglect inhomogeneous modes and limit oneself to the cancellation of only the propagating modes. The normal modes have the form $U^\alpha(x_1, x_2)\exp(i\gamma_\alpha x_3)$, where U^α is an eigen function; the spectrum of the corresponding boundary problem in the cross-section, as is well-known, is symmetrical with respect to the point $\alpha = 0$. Let the frequency ω be noncritical; then:

$$G_w(x, x') = \sum_\alpha C_{\pm\alpha} \exp(i\gamma_{\pm\alpha}(x_3 - x_3'))\times \times (U^{\mp\alpha}(x_1', x_2'))^T U^{\pm\alpha}(x_1, x_2). \tag{10}$$

The summing is carried out with respect to those γ_α, such that $\gamma_\alpha > 0$ or $\operatorname{Im}\gamma_\alpha > 0$.

The plus or minus signs are chosen when $x_3 > x_3'$ and $x_3 < x_3'$ respectively.

$$C_{\pm\alpha} = \mp\{U^\alpha, U^{-\alpha}\}^{-1}, \tag{11}$$

where we designate: $\{U^\alpha, U^\beta\} = \int_D ([H^\beta, E^\alpha]_{x_3} - [E^\beta, H^\alpha]_{x_3})\,dx_1\,dx_2$. The orthogonality relations follow from (4):

$$\{U^\alpha, U^\beta\} = 0, \quad \alpha + \beta \neq 0. \tag{12}$$

This relationship is also preserved in the case when ε and μ are symmetrical complex tensors. In an absorptionless medium (ε and μ are Hermitian tensors), expression (12) is replaced by the following one:

$$\{U^\alpha, (U^\beta)^*\} = 0, \quad \alpha + \beta^* \neq 0. \tag{13}$$

In the case of constant values of ε and μ, expression (12) is simplified, as is well known, and has the form [12]:

$$\iint_D [E^\alpha, H^\beta]\,dx_1\,dx_2 = 0, \quad \alpha \neq \beta.$$

Let the frequency ω be such that there are exactly N propagating modes in W.

The field generated by the source J^+ has the following form when $x_3 > l_1$ (all subsequent formulas are written with a precision of down to the inhomogeneous modes):

$$U^+(x)=\sum_{\alpha=1}^{N} V_\alpha{}^+ U^\alpha(x).$$

We shall normalize the eigenfunctions with the condition $\{U^\alpha, U^{-\alpha}\} = 1$. We shall locate electrical and magnetic dipole radiators at the point $x^i \in S$, $1 \leq i \leq 2N$, where the axes of the radiators fall in the plane (x_1, x_2). We pose the following problem: Select the amplitudes and axes of the radiators such that the field produced by them is equal to $-U^+(x)\theta(x_3 - l_2)$. This problem is substantially nonunique because of the arbitrary nature of the orientation of the radiators; we shall orient them in the same way, in the g direction. Here, g is a 6-vector, for which even one of the first three and even one of the last three components can be different from zero. We write the compensating field in the form:

$$U^*(x)=\sum_{i=1}^{2N} y_i g_i(x),$$

where $g_i(x)$ is the field of a radiator located at the point x^i, i.e.:

$$g_i(x)=\sum_{\alpha=1}^{N} C_{i\alpha}{}^{\pm} U^{\pm\alpha}(x),\ C_{i\alpha}{}^{\pm}=(U^{\mp\alpha}(x^i), g).$$

From the conditions for the field U*, we find the following from Cramer's rule:

$$y_i=\frac{\Delta_i}{\Delta},\quad \Delta=\det\|C_{i\alpha}{}^{\pm}\|.$$

The problem posed is solvable if $\Delta \neq 0$. This condition is of the nature of a prohibition on the positioning of the points x^i.

By way of example, we shall consider a very simple problem: a waveguide with a rectangular cross-section, $0 \leq x_1 \leq a$, $0 \leq x_2 \leq b$, $a > b$ and ε and μ are constants. Let $\pi/a < k\sqrt{\varepsilon\mu} < \pi b$. Then only the H_{10} mode can propagate in the waveguide. Its nonzero components have the form (after division by $\exp(\mp i\gamma x_3)$):

$$E_2{}^{\pm}=-k\mu \sin\frac{\pi}{a}x_1,$$

$$H_1{}^{\pm}=\pm\gamma \sin\frac{\pi}{a}x_1, H_3{}^{\pm}=i\frac{\pi}{a}\cos\frac{\pi}{a}x_1.$$

The plus or minus signs are chosen for waves traveling to the right (or to the left), $\gamma=\sqrt{k^2\varepsilon\mu-(\pi/a)^2}$. . The external fields have the form $U^{\pm}(x) = (4\pi/c)A^{\pm}H_{10}^{\pm}$ when $x_3 > l_1$ and $x_3 < l_2$ respectively ($l_1 < l_2$). The problem consists in cancelling the field $U^+(x)$ in the region $x_3 > l_2$, without radiating anything in this case into the region $x_3 < l_2$. Let $l_1 = 0$. We place electrical and magnetic dipole receivers at the point $P^0 = (x_1^0, x_2^0, 0)$ of the section $x_3 = 0$, orienting them along the Ox_2 and Ox_1 axes respectively. Then, based on measurements of the total field U at this point, one can find the amplitude A^+ of the field U^+:

$$A^+=[k\mu H_1(P^0)-\gamma E_2(P^0)]\frac{c\gamma k\mu}{8\pi\sin(x_1^0\pi/a)}.$$

We shall place electrical and magnetic dipole radiators having the same orientation as above at the point $P^1 = (x_1^1, x_2^1, l_2)$. These radiators generate the fields:

$$U_p=\frac{4\pi}{c\gamma ab}\sin\left(\frac{\pi}{a}x_1^1\right)H_{10}^{\pm}(x);$$

$$U_m=\frac{4\pi}{ck\mu ab}\sin\left(\frac{\pi}{a}x_1^1\right)H_{10}^{\pm}(x)\operatorname{sgn}(x_3-l_2).$$

Knowing A^+ we determine the amplitudes p and m of the radiators:

$$p=-\frac{\gamma abA^+}{2\sin(x_1^1\pi/a)};\quad m=-\frac{k\mu abA^+}{2\sin(x_1^1\pi/a)}.$$

Then the compensating field $U^*(x)$ has the form:

$$U^*(x)=pU_p(x)+mU_m(x)=-\frac{4\pi}{c}A^+H_{10}^+(x)\Theta(x_3-l_2),$$

i.e., such a pair of radiators cancels the field U^+ when $x_3 > l_2$, and does not radiate into the region $x_3 < l_2$.

BIBLIOGRAPHY

1. G.D. Malyuzhinets, "Ob odnoy teoreme dlya analiticheskikh funktsiy i yeye obobshcheniye dlya volnovykh potentsialov" ["On One Theorem for Analytic Functions and Its Generalization for Wave Potentials"], in the collection, "III Vsesoyuznyy simpozium po difraktsii voln, Referaty dokladov" ["The Third All-Union Symposium on Wave Diffraction. Abstracts of Reports"], Nauka Publishers, 1964.

2. G.D. Malyuzhinets, "Nestatsionarnyye zadachi difraktsii dlya volnovogo uravneniya s finitnoy pravoy chast'yu" ["Nonsteady-state Diffraction Problems for the Wave Equation with a Finite Right Side"], TRUDY AKUST. IN-TA [ACOUSTICAL INSTITUTE PROCEEDINGS], 1971, No 15, p 124.

3. M.V. Fedoryuk, "O rabotakh G.D. Malyuzhintsa po teorii volnovykh potentsialov" ["On the Papers of G.D. Malyuzhinets on Wave Potential Theory"], TRUDY AKUST. IN-TA, 1971, No 15, p 169.

4. M. Jessel, "Acoustique Theorique", Paris, 1973.

5. A.A. Mazanikov, V.V. Tyutekin, AKUST. ZH. [JOURNAL OF ACOUSTICS], 1974, 20, No 5, p 807.

6. A.A. Mazanikov, V.V. Tyutekin, AKUST. ZH., 1976, No 22, p 5.

7. J.H.B. Poole, H.G. Leventhal, J. OF SOUND AND VIBRATION, 1976, 49, No 2, p 257.

8. A.A. Mazanikov, V.V. Tyutekin, A.T. Ukolov, AKUST. ZH., 1977, 23, No 3, p 485.

9. G. Mangiante, "Les absourbeurs acoustiques actifs" ["Active Acoustic Absorbers"], Third Conference on Noise Abatement, Warsaw, 1973.

10. M.V. Fedoryuk, ZH. VYCHISL. MATEM. I MATEM. FIZIKI [JOURNAL OF COMPUTATIONAL MATHEMATICS AND MATHEMATICAL PHYSICS], 1976, No 4, p 1065.

11. V.Yu. Prikhod'ko, AKUST. ZH., 1976, 22, No 3, p 462.

12. L.D. Landau, Ye.M. Lifshits, "Elektrodinamika sploshnykh sred" ["The Electrodynamics of Continuous Media"], GTTI Publishers, 1957.
[40-8225]

8225
CSO: 1860

UDC 551.501.8

DETERMINATION OF THE MOISTURE CONTENT OF A CLOUDLESS ATMOSPHERE FROM MEASUREMENTS OF OUTGOING MICROWAVE RADIATION FROM ON BOARD AN AIRCRAFT

Gor'kiy IZVESTIYA VYSSHIKH UCHEBNYKH ZAVEDENIY, RADIOFIZIKA in Russian Vol 22 No 9, 1979 pp 1077-1084 manuscript received 12 Jul 78

[Article by V.A. Rassadovskiy, Scientific Research Radio Physics Institute]

[Text] Regression equations are obtained for determining the moisture content of both all the strata of the atmosphere and in the layer below flight altitude from measurements of outgoing radio-frequency radiation in the vicinity of water vapor absorption line $\lambda = 1.35$ cm from an altitude of $H = 3$ km above the water surface. Estimates are made of the sensitivity of the method in measurements of outgoing radio-frequency radiation over different surfaces. The procedure and results are given of an experimental determination of the total moisture content of the atmosphere above a water surface. Several possibilities are discussed for determining moisture content characteristics from two-channel difference measurements.

At the present time the determination of the total moisture content of a cloudless atmosphere from measurements of outgoing radio-frequency radiation in the water vapor absorption line centered at $\lambda = 1.35$ cm has been worked out the most completely both on the theoretical and experimental planes in [1-5]. A generalization of the results obtained is contained in monograph [12]. The triviality of optical thicknesses, τ, of the atmosphere in this line for a wide range of values of the total mass of water vapor, Q, in a column of the atmosphere is the physical basis for the procedure, based on linear regression equations relating the brightness temperature of the outgoing radio-frequency radiation measured at altitude H to the unknown values of Q. In this study are investigated the possibilities of further developing this procedure. In particular, a comparison is made (in terms of accuracy of determination of the unknown parameter) of measurements at different wavelengths, and the results are given of a determination of the total mass of water vapor from vertical absorption of the atmosphere (the proper method has certain advantages for the case of a cloudy atmosphere).

1. In the required linear regression equations

$$T_{\text{я}\lambda} = a_\lambda + b_\lambda Q'; \tag{1}$$

$$\tau_{0\lambda} = c_\lambda + d_\lambda Q' \tag{2}$$

an estimate of unknown coefficients can be made by different methods. The authors of [2] made such an estimate from a family of $T_{\text{уа}\,\lambda}(Q)$ curves, obtained on the basis of model calculations for different states both of the underlying water surface and of meteorological parameters of the atmosphere. In estimating the coefficients of equations (1) and (2) we used the following procedure. From summer data from aerological sounding for a number of years in the central section of the European sector of the USSR were calculated values of $T^1_{\text{уа}\,\lambda}$ and $\tau^1_{0\lambda}$ for the case of observing the nadir from a flight altitude of $H_1 = 3$ km, for each i-th sonde from the equation

$$T_{\text{я}\lambda} = (1 - R_\lambda) T_0 \exp(-\tau_\lambda) + \int_0^{H_1} T(h)\,\gamma(h) \exp\left[-\int_h^{H_1} \gamma(h')\,dh'\right] dh + \\ + R_\lambda \exp(-\tau_\lambda) \int_0^{H} T(h)\,\gamma(h) \exp\left[-\int_0^{h} \gamma(h')dh'\right] dh. \tag{3}$$

(3)

In (3) H_i is the aircraft's flight altitude, $\tau_\lambda = \int_0^{H_1} \gamma(h)dh$, H is the altitude of the upper limit of the atmosphere, R_λ is the mirror reflection coefficient for the surface in terms of power, T_0 is the kinetic temperature of the underlying surface, T(h) is the atmosphere's temperature profile, and $\gamma(h) = \gamma_{O_2}(h) + \gamma_{H_2O}(h)$ is the absorption coefficient of a cloudless atmosphere, determined by the contributions of water vapor and molecular oxygen. The expression for $\gamma(h)$ was taken from [6], where it is presented while taking into account corrections for experimental values of $\gamma_{O_2}(h)$ and for nonlinear absorption in terms of ρ (absolute humidity). The values of R_λ for observation above a smooth water surface were calculated from the equations in [7]. We have disregarded the contribution of cosmic radio-frequency radiation re-echoed from the surface on account of its triviality and the possibility of taking it into account in processing measurement results.

For purposes of comparing the feasibility of sounding at different wavelengths, calculations were made at two frequencies: $\nu_1 = 20.83$ GHz and $\nu_2 = 22.22$ GHz.

Then the coefficients of regression equations and confidence intervals for coefficients were calculated by the method of least squares. The equations obtained relate the brightness temperatures of the outgoing radio-frequency

radiation and absorption in the $0\text{-}H_1$ (km) layer to the mass of the water vapor, Q' (g/cm^2), in atmosphere column $0\text{-}H_1$ (km). For frequency ν_2, for purposes of comparing feasibility and processing experimental data, was obtained the regression equation

$$T_{\text{я}\lambda} = n_\lambda + m_\lambda Q, \tag{4}$$

where Q is the total mass of water vapor in all layers of the atmosphere.* Results of calculations are given in table 1.

Table 1.

1) Частота, ГГц	20,83	22,22
a	124,0	127,3
Δa	2,68	3,49
b	17,2	22,3
Δb	1,32	1,72
c	0,0067	0,0074
Δc	0,0074	0,0104
d	0,0483	0,0679
Δd	0,0036	0,0051
n		122,3
Δn		3,28
m		18,9
Δm		1,22

Key:
1. GHz

In regression equations for radio brightness temperatures (1) and (4), coefficient n_λ contains the brightness temperature of the underlying surface and the radiation of molecular oxygen (both direct and re-echoed). In coefficient a_λ, in addition to the components indicated, is contained also the radiation, re-echoed from the surface, of the water vapor of strata of the atmosphere above the flight altitude (averaged for the ensemble of sondes employed). Coefficients b_λ and m_λ, characterizing the sensitivity of the brightness temperature to changes in mass of the water vapor, depend heavily on the type and state of the underlying surface.

In fig 1 is given the dependence of the mean sensitivity of the radio brightness temperature to changes in the total mass of water vapor, $\overline{m}_\lambda$, on the surface's

*According to our estimates, the correlation factor between the brightness temperature measured from an altitude of H_1 = 3 km and the total mass of water vapor, Q (g/cm^2), can reach 0.989, which confirms the possibility of obtaining information on Q over a water surface with microwave measurements from relatively not too great altitudes.

R_λ , computed for sonde realizations of Q in the range of 1 to 3 g/cm^2, and with an altitude distribution corresponding to an exponential model with a characteristic altitude of 2.2 km. It is obvious from this figure that for values of R_λ corresponding to a smooth water surface $\bar{m}_\lambda \simeq 16°K/g \cdot cm^{-2}$, which is considerably lower than the values obtained by us. This discrepancy represents a reflection of the fact that the dependence shown in fig 1 was obtained for conditions of independence of the state of the atmosphere (in this case of its moisture content) on the state of the underlying surface. Under real conditions the water vapor in the atmosphere by its nature is related to the state of the underlying surface, and there can be observed both a shortage of moisture [13] (arid areas), and an excess of it (e.g., as the result of cyclone activity). Over vast water surfaces water vapor on average is of a convective nature. In this case the amount of water vapor in the atmosphere is on average greater for states of the surface corresponding to higher temperatures. The brightness temperature of outgoing radiation of the atmosphere per se can be represented in the form

$$T_я = T_{ср}(1 - e^{-\tau}), \tag{5}$$

and the mean temperature of the atmosphere in the form

$$T_{ср} = T(0) - \Delta T, \tag{6}$$

where T(0) is the temperature of the air at the surface, which correlates well with T_0 in the case of a water surface, and ΔT is the correction for the nonisothermicity of the atmosphere [8]. From (5) and (6) follows a greater (than that caused only by an increase in Q) growth in T_{ya} for "hotter" surfaces. This fact also results in an increase in $\bar{m}_\lambda$ with regard to the data in fig 1. Thus, the coefficients of regression equations for $T_{ya\lambda}$ depend in a complex manner also on the nature, unknown beforehand, of interaction between the atmosphere and the underlying surface. Hence it follows that substantial refinement of coefficients for a specific realization (in particular, by refining the temperature of the surface as compared with the mean seasonal by means of an additional receiver in the centimeter band) meets with considerable difficulties. It is interesting to note that the accuracy of a determination of Q in terms of $T_{ya\lambda}$, which can be obtained from confidence intervals for coefficients of the regression equations given in table 1, is in good agreement with the data of [2,4], in spite of the difference in the coefficients themselves caused by the selection of statistical data on the atmosphere and underlying surface. In our opinion, this agreement is the consequence of the factors mentioned above. When observing over sections of dry land having lower values of R_λ as compared with the water surface, the relative contribution of the reasons discussed for the variability of the sensitivity of the brightness temperature to changes in the total mass of water vapor increases, which together with real errors in measurement of brightness temperatures severely worsens the method's capabilities even when observing over homogeneous sections of dry land.

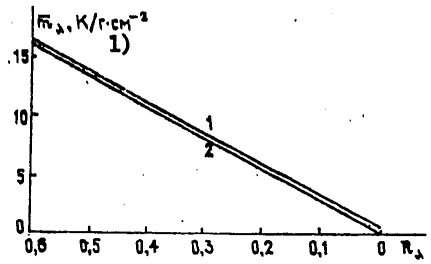

Figure 1. Dependence of the Sensitivity, $\bar{m}_\lambda$, of the Radio Brightness Temperature at $\lambda = 1.35$ cm to Changes in the Total Mass of Water Vapor, on the Mirror Reflection Coefficient, R_λ, of the Surface (Observation Toward the Nadir from an Altitude of $H_1 = 3$ km): 1--Surface Temperature of 278°K; 2--Surface Temperature of 293°K

Key:
1. °K/g·cm^{-2}

In [9] are given model calculations of variations in brightness temperature caused by variations in the altitude distribution of water vapor with an unchanged moisture content when observing from an altitude of $H_1 = 3$ km . The variations in brightness temperatures for frequencies of 20.83 GHz and 22.22 GHz equaled approximately 3°K with fixed T_0 . In the real statistics of sondes, the contribution of these variations is completely "washed away" by the factors mentioned above. A comparison of the equations obtained for different frequencies from the viewpoint of "zero errors" in the method does not make it possible to give preference to any of them. However, if the errors in measuring $T_{ya\,\lambda}$ are taken into account, then a determination of the integral moisture content is made better at a frequency of 22.23 GHz, since here with equal errors in $T_{ya\,\lambda}$ are obtained lower errors in Q .

A substantial improvement can be reached in the accuracy of determining Q by using equations not for brightness temperatures but for absorption. Interest in this changeover has grown considerably in the case of a cloudy atmosphere by reason of the additivity of absorption, but at the present time a practical procedure has not been worked out for determining the total vertical absorption from on board an aircraft.

2. Experimental measurements of outgoing radio-frequency radiation on line $\lambda = 1.35$ cm were made in May-June 1976 from on board an IL-14 aircraft in the area of the Rybinskoye Reservoir in keeping with a joint scientific

program with the USSR Academy of Sciences IFA [Institute of Physics of the Atmosphere]. The reception of radio-frequency radiation was accomplished with a horn antenna with a directivity diagram width in relation to the half-power level of 10°, installed in the nadir direction, by means of a modulation-type radiometer with a fluctuation threshold of sensitivity of 0.4°K. The design of the radiometer and its characteristics are given in [10]. Calibration of the receiver in relation to the antenna temperature was accomplished with reference to an internal reference noise signal source. For the purpose of calibrating the radiometer's scale in terms of radio brightness temperature, a series of flights was made under conditions of stable weather conditions, after which the factors for the conversion from antenna temperatures measured in this series to computed radio brightness temperatures were found by the method of least squares. As the reference level for the brightness temperature during the days of the following measurement cycle was used the radio-frequency radiation of a surface covered by a forest, in view of its independence, noted above, on the state of the atmosphere. Since aerological sounding was not carried out immediately in the flight area (the nearest sounding station was located at a distance of 50 km on average from the meaurement area), we made a measurement of vertical absorption, $\tau_{0\lambda}$, of the atmosphere in the 0.1 to 3 km layer, not requiring calibration of the radiometer. Actually, using equation (3) and the equation for the relationship between the brightness and antenna temperatures, it is possible to demonstrate that

$$\frac{T_{A2}^{л} - T_{A2}^{в}}{T_{A1}^{л} - T_{A1}^{в}} = \exp(-\tau_0),$$

where superscripts л and в indicate antenna temperatures measured above a forest and above water, respectively, and subscripts 1 and 2, antenna temperatures measured above surfaces at altitudes of 0.1 and 3 km, respectively. By virtue of the triviality of absorption, the differences of antenna temperatures at different altitudes are approximately equal and the accuracy of determining the relationship is determined by the stability of the equipment and the accuracy of making readings (the influence of the receiver's internal noise is not important, since forest-water contrasts are sufficiently high). Therefore measurements of $\tau_{0\lambda}$ according to the procedure described served for us as a criterion for eliminating gross errors in measurements of the brightness temperature of outgoing radio-frequency radiation.

The results of measurements of brightness temperatures and absorption are shown in table 2. In fig 2 is shown the variation in the integral moisture content during the observation period, computed from the data of aerological sounding. Given there also are values of Q computed from measured values of brightness temperatures and absorption. The agreement of the values of Q computed in relation to $T_{va\lambda}$ and $\tau_{0\lambda}$, even without taking into account the error in measurement of the radio brightness temperature, which equaled approximately 5°K when calibrating by the procedure described, makes it possible to conclude that there is considerable variability in the integral moisture content of the atmosphere on relatively not too great spatial scales.

Table 2.

1) Дата	2) $T_{н}^{выч}$, К	3) $T_{н}^{изм}$, К	4) $\tau^{выч}$, Непер	5) $\tau^{изм}$, Непер
24.05.76	152,8	133	0,084	0,029
25.05.76	149,9	134	0,073	0,039
26.05.76	156,5	158	0,092	0,080
28.05.76	142,6	144	0,054	0,046
30.05.76	151,3	—	0,075	0,079
4.06.76	153,9	156	0,098	0,112
5.06.76	146,6	164	0,073	0,157
6.06.76	148,4	156	0,071	0,086
7.06.76	156,5	153	0,101	0,049

Key:
1. Date
2. T_{ya}^{vych} [calculated], °K
3. T_{ya}^{izm} [measured], °K
4. τ^{vych}, nepers
5. τ^{izm}, nepers

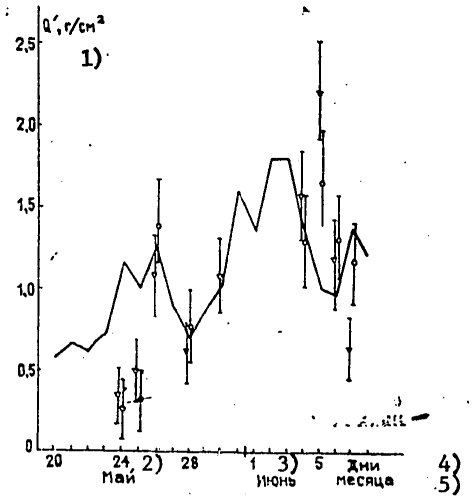

Figure 2. Variation in Mass of Water Vapor, Q' (g/cm^2), in a 0-3 km Atmosphere Column During the Observation Period:
[Caption continuation and key on following page]

solid line--data from aerological sounding; circles--values of Q' computed from measurements of T_{ya}; triangles--values of Q' computed from measurements of τ_0

Key:
1. g/cm^2
2. May
3. June
4. Days
5. Months

3. Let us now dwell briefly on the feasibility of further refining moisture content characteristics in connection with making multi-frequency measurements of outgoing radio-frequency radiation. Let us turn, in particular, to two-channel measurements, in favor of which can be presented the following arguments. First, the kernels of integral equations for outgoing radio-frequency radiation at different frequencies in the vicinity of $\lambda = 1.35$ cm can in a first approximation be approximated by linear functions of altitude, at least up to an altitude of 6 km [11]. By virtue of this fact, measurements at just two frequencies will be independent, which in turn speaks in favor of the ability to obtain information from such measurements of two parameters of the moisture content of the atmosphere.

Secondly, the variations in brightness temperatures for variations in the altitude distribution of water vapor are not too great [9], and with the modern sensitivity of equipment it is possible to rely on measurement of just maximum contrast (in terms of the line's slope).

Thirdly, since the difference in frequencies for measurement of these contrasts is not too high (approximately 1.5 GHz), it is possible to make a radiometer which would measure directly the difference in brightness temperatures. Furthermore it is possible to improve measurement accuracy by increasing the accuracy of calibration of the receiver and reducing the influence of the state of the underlying surface.

In fig 3 is given the ensemble of ΔT_{ya} calculated for frequencies of 20.83 GHz and 22.22 GHz for the ensemble of sondes employed in sec 1, when observing over a water surface. Plotted there also is the line of least squares. As was expected, the difference in brightness temperatures proved to be sufficiently sensitive to variations in characteristic altitude H_ρ in order for it to be able to be recorded reliably. The brightness temperatures for days with a different altitude distribution of water vapor can differ by 5 to 6°K with an identical integral moisture content. At the same time the set of points corresponding to identical H_ρ is approximated with high accuracy by a straight line regardless of the temperature of the underlying water surface. The line of least squares corresponds to $H_\rho = 2.2$ km (white dots). As is obvious from this figure, the maximum differences from a straight line are not greater than approximately 0.5°K for sondes with the H_ρ in question, although the surface temperature for them fluctuated over a wide range ($\pm$ 10°K).

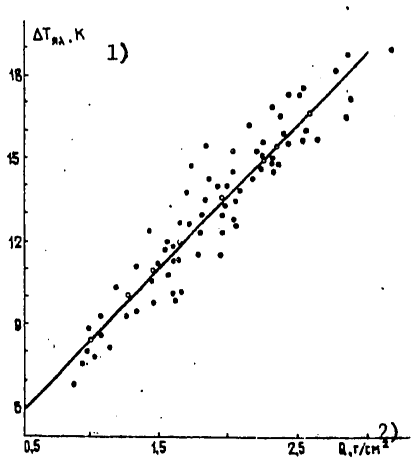

Figure 3. Ensemble $\Delta T_{ya} = T_{ya\ \nu_2} - T_{ya\ \nu_1}$, Calculated from Aerological Sounding Data for the Summer Months of a Number of Years in the Central Section of the European Sector of the USSR

Key:
1. $\Delta T_{ya\ \lambda}$, °K
2. Q, g/cm^2

Thus, it can be concluded already from a brief analysis that in observations at least over a water surface it is possible to refine information on moisture content characteristics, although, of course, the procedure for obtaining this information must be different from the regression equation procedure. The development of such a procedure, it can be hoped, will make it possible to achieve a substantial improvement in the accuracy of determining moisture content characteristics from measurements of outgoing radio-frequency radiation, as compared with the regression equation procedure, whose possibilities have by this time been apparently exhausted to a considerable extent.

The author wishes to express deep gratitude to A.P. Naumov for assistance in formulation of the problem and discussion of results, to M.S. Malkevich and A.P. Orlov for active assistance in performing the experiment and to M.B. Zinicheva for making calculations.

Bibliography

1. Gorchakova, I.A., Demin, V.V. and Yershov, A.T. IZV. AN SSSR, FIZIKA ATMOSFERY I OKEANA, 7, No 8, 841 (1971).

2. Rabinovich, Yu.I. and Shchukin, G.G. TRUDY GLAVNOY GEOFIZICHESKOY OBSERVATORII, No 222, 62 (1968).

3. Rabinovich, Yu.I. and Shchukin, G.G. TRUDY GLAVNOY GEOFIZICHESKOY OBSERVATORII, No 309, 3 (1974).

4. Uilkheyt, T.T., Fauler, M.G., Stembakh, G. and Gloersen, R. In "Sovetsko-amerikanskiy eksperiment 'Bering'" [The Soviet-American "Bering" Experiment], Gidrometeoizdat, Leningrad, 1975, p 15.

5. Gurvich, A.S. and Demin, V.V. IZV. AN SSSR, FIZIKA ATMOSFERY I OKEANA, 6, No 8, 771 (1970).

6. Rabinovich, Yu.I. and Melent'yev, V.V. TRUDY GLAVNOY GEOFIZICHESKOY OBSERVATORII, No 235, 78 (1970).

7. Zhevakin, S.A. and Naumov, A.P. IZV. VUZOV, RADIOFIZIKA, 10, Nos 9-10, 1213 (1967).

8. Kislyakov, A.G. IZV. VUZOV, RADIOFIZIKA, 9, No 3, 451 (1966).

9. Naumov, A.P. and Rassadovskiy, V.A. IZV. AN SSSR, FIZIKA ATMOSFERY I OKEANA, 14, No 7, 716 (1978).

10. Khrulev, V.V., Samoylov, R.A., Fedyantsev, B.K., Zborovskiy, V.S. and Larionova, L.F. IZV. VUZOV, RADIOFIZIKA, 21, No 2, 295 (1978).

11. Staelin, D.H. J. GEOPHYS. RES., 71, No 12, 2875 (1966).

12. Basharinov, A.Ye., Gurvich, A.S. and Yegorov, S.T. "Radioizlucheniye Zemli kak planety" [Radio-Frequency Radiation of Earth as a Planet], Izdatel'stvo Nauka, Moscow, 1974.

13. Boldyrev, V.G., Koprova, L.I. and Malkevich, M.S. IZV. AN SSSR, FIZIKA ATMOSFERY I OKEANA, 1, No 7, 703 (1965).

CSO: 1860
8831

UDC 621.371.242.7

SOME FEATURES OF THE RAY TRAJECTORY IN THE PROPAGATION OF RADIO WAVES IN AN IRREGULAR IONOSPHERIC WAVEGUIDE

Gor'kiy IZVESTIYA VYSSHIKH UCHEBNYKH ZAVEDENIY, RADIOFIZIKA in Russian Vol 22 No 9, 1979 pp 1061-1069 manuscript received 9 Oct 78

[Article by M.V. Tinin, Irkutsk State University]

[Text] By the averaging method an investigation is made of the behavior of a ray in a three-dimensionally inhomogeneous ionospheric waveguide. For ray variations are obtained expressions which are suitable both at great and at short distances.

1. Introduction

In recent times a number of studies have appeared, devoted to the waveguide propagation of signals in an inhomogeneous medium, important, in particular, in the long-range ionospheric propagation of short radio waves [1-4]. Waveguide propagation has been studied quite well for layered media [5]. Of great interest is the investigation of irregular waveguides whose properties vary along the route. In a geometrical optics approximation such an analysis involves asymptotic integration of the ray trajectory [6]. When the properties of a waveguide vary fairly slowly along the route, for a number of estimates is used the condition of constancy of the adiabatic invariant [3,4].

For the purpose of determining variations in the ray trajectory in the horizontal plane in a three-dimensionally inhomogeneous medium, in [3,7] is used an adiabatic approximation. However this approach is valid only with a great distance between correspondents and does not agree with certain results [8-11] of the usual perturbation method, which is applicable at least with short distances. In this study, for the purpose of analyzing ray variations in a three-dimensionally inhomogeneous medium is used the averaging method [12-14], which has made it possible to obtain expressions valid both at short and at long distances.

2. Application of the Averaging Method to the Ray Equation

Let us consider the behavior of a ray in a waveguide formed in an inhomogeneous medium whose dielectric constant equals

$$\varepsilon = \varepsilon(\nu x,\ \nu y,\ z). \tag{1}$$

Here by adding minor parameter $\nu << 1$ we explicitly take into account the slow variation in the medium in the horizontal plane. The behavior of the ray is described by the following system:

$$\frac{dz}{dx} = \operatorname{ctg}\psi; \tag{2}$$

$$\frac{dy}{dx} = \operatorname{tg}\varphi; \tag{3}$$

$$\frac{d\psi}{dx} = \frac{1}{2\varepsilon}(1 + \sin^2\psi\operatorname{tg}^2\varphi)\left(\frac{\partial\varepsilon}{\partial x}\operatorname{ctg}\psi - \frac{\partial\varepsilon}{\partial z}\right); \tag{4}$$

$$\frac{d\varphi}{dx} = \frac{1}{2\varepsilon}(1 + \cos^2\varphi\operatorname{ctg}^2\psi)\left(\frac{\partial\varepsilon}{\partial y} - \frac{\partial\varepsilon}{\partial x}\operatorname{tg}\varphi\right). \tag{5}$$

In (1) to (5) z, x and y are the Cartesian coordinates of the ray, ψ is the angle between the z axis and the projection onto plane xz of the tangent to the ray and ϕ is the azimuthal angle.

In order to employ the averaging method [12-14], it is necessary first to transform system (2) to (5). For this purpose we introduce new "slow" (α, τ, σ) and "fast" (K) variables:

$$\tau = \nu x; \tag{6}$$

$$\sigma = \nu y; \tag{7}$$

$$\alpha = \frac{\varepsilon(\tau,\ \sigma,\ z)\sin^2\psi}{1 + \sin^2\psi\operatorname{tg}^2\varphi}; \tag{8}$$

$$K = \frac{1}{T}\int^{z}\frac{\sqrt{\alpha}\cos\varphi\,dz}{\sqrt{\varepsilon\cos^2\varphi - \alpha}} + K_0, \tag{9}$$

where

$$T = 2\int_{z_1}^{z_2} \frac{\sqrt{\alpha}\cos\varphi}{\sqrt{\varepsilon\cos^2\varphi - \alpha}} \tag{10}$$

is the period of oscillation of the ray trajectory. The integrals in the right halves of (9) and (10) are taken with fixed values of parameters α, ϕ, τ and σ, and the turning points, $z_{1,2}(\tau,\sigma)$, are determined from the condition

$$\varepsilon(\tau, \sigma, z_{1,2})\cos^2\varphi - \alpha = 0. \tag{11}$$

The meaning of the symbols in (8) and (9) is sufficiently clear for a horizontally homogeneous medium. In this case ϕ = const and α takes on the value of a constant in the Snell's law,

$$\alpha = \varepsilon(z)\sin^2\beta = \text{const}, \tag{12}$$

where the angle of incidence, β, is determined from the equation

$$\sin^2\beta = \frac{\sin^2\psi}{1 + \sin^2\psi\,\mathrm{tg}^2\varphi}. \tag{13}$$

For a horizontally homogeneous medium, K, as is obvious from definition (9), represents the horizontal range of the oscillating ray normalized for period T. Therefore in a layered medium the waveguide trajectory is a periodic (with a period equal to 1) function of K.

In the symbols of (6) to (10) ray trajectory equations assume the following form:

$$\frac{dK}{dx} = \frac{1}{T(\alpha, \tau, \sigma, \varphi)} + \nu S(\alpha, \tau, \sigma, \varphi, K); \tag{14}$$

$$\frac{d\alpha}{dx} = \nu\frac{\partial\varepsilon}{\partial\tau}(\tau, \sigma, K); \tag{15}$$

$$\frac{d\sigma}{dx} = \nu \operatorname{tg}\varphi; \tag{16}$$

$$\frac{d\varphi}{dx} = \nu \frac{\cos^2\varphi}{2\alpha}\left[\frac{\partial \varepsilon}{\partial \sigma}(\tau, \sigma, K) - \operatorname{tg}\varphi \frac{\partial \varepsilon}{\partial \tau}(\tau, \sigma, K)\right]; \tag{17}$$

$$\frac{d\tau}{dx} = \nu, \tag{18}$$

where S is the result of differentiating in terms of τ the right half of equation (9) with fixed z :

$$S = \frac{dK}{d\tau}\Big|_z = \frac{\partial K}{\partial \tau} + \operatorname{tg}\varphi \frac{\partial K}{\partial \sigma} + \frac{\partial \varepsilon}{\partial \tau}\frac{\partial K}{\partial \alpha} + \\ + \frac{\cos^2\varphi}{2\alpha}\left[\frac{\partial \varepsilon}{\partial \sigma} - \operatorname{tg}\varphi \frac{\partial \varepsilon}{\partial \tau}\right]\frac{\partial K}{\partial \varphi}. \tag{19}$$

System (14) to (18) is a system with a rapidly rotating phase [12,13]. The right halves of equations (14) to (18) are periodic functions of fast variable K and, consequently, permit averaging. Therefore it is possible to apply to this system the usual arrangement of the averaging method [12,14], similarly to how this was done for a two-dimensionally inhomogeneous medium in [15].* As a result we get

$$K = \eta + \nu v_1 + \nu^2 v_2 + \dots; \tag{20}$$

$$\alpha = \bar{\alpha} + \nu u_1^{(1)} + \nu^2 u_2^{(1)} + \dots; \tag{21}$$

$$\sigma = \bar{\sigma} + \nu u_1^{(2)} + \nu^2 u_2^{(2)} + \dots; \tag{22}$$

$$\varphi = \bar{\varphi} + \nu u_1^{(3)} + \nu^2 u_2^{(3)} + \dots, \tag{23}$$

*Cf. also [16].

Where

$$u_1 = T\int_0^{\eta} [b - F_1]\Big|_{K=\eta} d\eta + u_{10}; \tag{24}$$

$$v_1 = T\int_0^{\eta} \left[S + u_1\frac{\partial}{\partial\xi}\frac{1}{T} - \Phi_1\right]\Big|_{K=\eta} d\eta + v_{10}; \tag{25}$$

$$u_2 = T\int_0^{\eta} \left[u_1\frac{\partial b}{\partial\xi} + v_1\frac{\partial b}{\partial\eta} - \Phi_1\frac{\partial u_1}{\partial\eta} - F_1\frac{\partial u_1}{\partial\xi} - F_2\right]\Big|_{K=\eta} d\eta + u_{20}; \tag{26}$$

$$F_1 = \overline{b}; \tag{27}$$

$$F_2 = \overline{\left[u_1\frac{\partial b}{\partial\xi} + v_1\frac{\partial b}{\partial\eta} - F_1\frac{\partial u_1}{\partial\xi}\right]}; \tag{28}$$

$$\Phi_1 = \overline{\left[S + u_1\frac{\partial}{\partial\xi}\frac{1}{T}\right]}. \tag{29}$$

Equations (24) to (29) are written in vector form by means of the following vectors introduced:

$$u_1 = \{u_1^{(1)}, u_1^{(2)}, u_1^{(3)}\}; \tag{30}$$

$$u_2 = \{u_2^{(1)}, u_2^{(2)}, u_2^{(3)}\}; \tag{31}$$

$$\xi = \{\overline{\alpha}, \overline{\sigma}, \overline{\varphi}\}. \tag{32}$$

The components of vector b are the right halves of equations (15) to (17). In equations (27) to (29) the line above indicates averaging in terms of fast variable η. Variables $\overline{\alpha}$, $\overline{\sigma}$ and $\overline{\phi}$ are determined from the averaged equations

$$\frac{d\xi}{dx} = \nu F_1 + \nu^2 F_2 + \ldots \tag{33}$$

3. Adiabatic Approximation

Let us plot the ray trajectory with an accuracy of up to terms of the first order of triviality:

$$K = \eta + O(\nu); \tag{34}$$

$$\alpha = \bar{\alpha} + O(\nu); \tag{35}$$

$$\sigma = \bar{\sigma} + O(\nu); \tag{36}$$

$$\varphi = \bar{\varphi} + O(\nu). \tag{37}$$

As is obvious from (34) to (37), in this approximation for the purpose of determining the ray trajectory it is sufficient to solve the averaged equations:

$$\frac{d\eta}{dx} = \frac{1}{T(\xi_2)} + \nu\Phi_1(\xi_1) + O(\nu^2); \tag{38}$$

$$\frac{d\xi_1}{dx} = \nu F_1(\xi_1). \tag{39}$$

In view of the fact that we are constructing an asymptotic solution to the ray equation with a long range of $x = O(1/\nu)$, in the right halves of (38) and (39) should be retained terms on the order of ν. For the same reason in the first term of the right half of (38) it is necessary to substitute slow variables determined from an equation of the following order of accuracy:

$$\frac{d\xi_2}{dx} = \nu F_1(\xi_2) + \nu^2 F_2(\xi_2). \tag{40}$$

Let us note that with a known solution to equation (39) the solution to equation (40) is easily determined by means of the usual perturbation method. Let us transcribe system (39) as follows:

$$\frac{d\bar{\alpha}}{dx} = \nu\frac{\overline{\partial\varepsilon}}{\partial\tau} = 2\nu\frac{\sqrt{\bar{\alpha}}\cos\bar{\varphi}}{T}\int_{z_1}^{z_2}\frac{\frac{\partial\varepsilon}{\partial\tau}dz}{\sqrt{\varepsilon\cos^2\bar{\varphi}-\bar{\alpha}}}; \tag{41}$$

$$\frac{d\bar{\sigma}}{dx} = \nu \operatorname{tg} \bar{\varphi}; \tag{42}$$

$$\frac{d\bar{\varphi}}{dx} = \nu \frac{\cos^2 \bar{\varphi}}{2\bar{\alpha}} \left(\frac{\overline{\partial \varepsilon}}{\partial \sigma} - \operatorname{tg} \bar{\varphi} \frac{\overline{\partial \varepsilon}}{\partial \tau} \right) = \nu \frac{\cos^2 \bar{\varphi}}{2\bar{\alpha}} \left(\frac{\overline{\partial \varepsilon}}{\partial \sigma} - \operatorname{tg} \bar{\varphi} \frac{d\bar{\alpha}}{d\tau} \right) = \tag{43}$$

$$= \frac{\nu \cos^2 \bar{\varphi}}{2\bar{\alpha}} \left(\frac{2\sqrt{\bar{\alpha}} \cos \bar{\varphi}}{T} \int_{z_1}^{z_2} \frac{\frac{\partial \varepsilon}{\partial \sigma} dz}{\sqrt{\varepsilon \cos^2 \bar{\varphi} - \bar{\alpha}}} - \operatorname{tg} \bar{\varphi} \frac{d\bar{\alpha}}{d\tau} \right).$$

In the last equations, (41) and (43), it is taken into account that in a first approximation averaging in terms of variable η can be substituted by integration in terms of z by virtue of the equation

$$d\eta = dK + O(\nu) = \frac{\sqrt{\bar{\alpha}} \cos \bar{\varphi} \, dz}{T \sqrt{\varepsilon \cos^2 \bar{\varphi} - \bar{\alpha}}} + O(\nu). \tag{44}$$

It is not difficult to verify that by virtue of (41) to (43) on the ray trajectory is fulfilled the condition of constancy of the adiabatic invariant*

$$I = \int_{z_1}^{z_2} \sqrt{\varepsilon - \frac{\bar{\alpha}}{\cos^2 \bar{\varphi}}} \, dz = \int_{z_1}^{z_2} \sqrt{\varepsilon - \varepsilon(z_{1,2})} \, dz = \text{const}. \tag{45}$$

Condition (45), as we know [3,4] is very useful for making a direct analysis of conditions for further propagation. Unlike the two-dimensional case, where satisfaction of condition (45) is equivalent to solving an averaged system, in the three-dimensional case the solution of functional equation (45) does not eliminate the need to integrate system (41) to (43), but only lowers its order of magnitude.

*Let us note that the adiabatic invariant remains constant only along the ray trajectory. Therefore the derivation of equations for the "projection of a ray" onto Earth in [7], which does not take this into account, is not completely correct.

Thus, plotting the trajectory in a first approximation has been reduced to solving system (41) to (43) in the range of $O(1/\nu)$.

Unlike original system (2) to (5), system (41) to (43) does not contain rapidly fluctuating factors; therefore, it can be solved numerically with considerably less expenditure of machine time. Moreover, in some cases system (41) to (43) permits the use of analytical approximation methods.

4. Variations of Arrival Angles on Routes of Different Lengths

Let us assume, in addition to a large characteristic amount of horizontal inhomogeneity, a not too great amount of change in parameters of the ionosphere along the propagation route.

Let

$$\varepsilon = \varepsilon_0(z) + \lambda\varepsilon_1(\tau, \sigma, z) \quad (\lambda \ll 1). \tag{46}$$

Then system (41) to (43) can be written as

$$\frac{d\bar{\alpha}}{d\tau} = \lambda \frac{\overline{\partial \varepsilon_1}}{\partial \tau}; \tag{47}$$

$$\frac{d\bar{\sigma}}{d\tau} = \operatorname{tg}\bar{\varphi}; \tag{48}$$

$$\frac{d\bar{\varphi}}{d\tau} = \lambda \frac{\cos^2\bar{\varphi}}{2\bar{\alpha}} \left[\frac{\overline{\partial \varepsilon_1}}{\partial \sigma} - \operatorname{tg}\bar{\varphi} \frac{\overline{\partial \varepsilon_1}}{\partial \tau} \right]. \tag{49}$$

System (47) to (49) in the range of $\tau = \nu x \sim 1$ can be solved by the perturbation method. The first approximation with initial conditions of

$$\bar{\alpha}(0) = \alpha_0, \quad \bar{\sigma}(0) = \sigma_0 \ll 1, \quad \bar{\varphi}(0) = \varphi_0 \ll 1 \tag{50}$$

has the form

$$\bar{\alpha} = \alpha_0 + \lambda \int_0^{\tau} \frac{\overline{\partial \varepsilon_1}}{\partial \tau}\Big|_{\substack{z=\varphi=0 \\ \alpha=\alpha_0}} d\tau; \tag{51}$$

$$\bar{\varphi} = \varphi_0 + \frac{\lambda}{2\alpha_0}\int_0^{\tau} \left.\frac{\overline{\partial \varepsilon_1}}{\partial \sigma}\right|_{\substack{\alpha=\alpha_0\\ \sigma=\varphi=0}} d\tau; \tag{52}$$

$$\bar{\sigma} = \sigma_0 + \varphi_0 \tau + \frac{\lambda}{2\alpha_0}\int_0^{\tau} (\tau - s) \left.\frac{\overline{\partial \varepsilon_1}}{\partial \sigma}\right|_{\substack{\alpha=\alpha_0\\ \sigma=\varphi=0}} ds. \tag{53}$$

By means of equations (52) and (53) it is possible also to solve the problem of the variation in arrival angles with a fixed position of the source and observer, i.e., to solve the two-point trajectory problem:

$$\sigma(x_t) = \sigma(0) = \sigma_0. \tag{54}$$

For this purpose it is necessary by means of (53) and (54) to exclude from (52) angle ϕ_0 :

$$\bar{\varphi}_t \equiv \bar{\varphi}(x_t) = \frac{\lambda}{2\alpha_0 \tau}\int_0^{\tau} s \frac{\overline{\partial \varepsilon_1}}{\partial \sigma} ds. \tag{55}$$

Expressions (51) to (55) are outwardly similar to the corresponding equations obtained by the usual perturbation method [8-11]. The difference is that included in the integrands in (51) to (55) are not the derivatives themselves of ε , but their average in terms of the period of oscillations of the unperturbed trajectory.

Equations (51) to (55) are valid at great--on the order of $1/\nu$--distances, where the equations of the ordinary perturbation method are no longer valid. On the other hand, equations (51) to (55) cease to be valid at short--on the order of 1--distances, since then $\tau \sim \nu$ and the retained averaged terms in (51) to (55) prove to be commensurate with the discarded periodic corrections determined by equations (24) to (26). If of the latter the highest in value are retained, then it is possible to obtain an equation which smoothly converts into the ordinary equations at short distances. In particular, for two-point problem (54) we have

$$\varphi_t = \frac{\lambda}{2\alpha_0 x_t}\int_0^{x_t} s \frac{\partial \varepsilon_1}{\partial y}[z_0(s),\ \nu x_t,\ 0]\, ds - \frac{\lambda}{2\alpha_0 x_t}\int_0^{x_t} \frac{s^2}{2}\frac{\partial}{\partial s}\frac{\overline{\partial \varepsilon_1}}{\partial y} ds, \tag{56}$$

where $z_0(x)$ is the ray trajectory in a regular waveguide ($\nu = 0$). It is not difficult to verify that at a long distance, where $x = O(1/\nu)$, in (56) an important contribution is made by the second term, from which it is possible to derive (55) by integration by parts. At short distances of $x \lesssim O(1)$ dominant in (56) is the first term, which (taking into account that $\nu \ll 1$) converts into the equation for the variation in azimuth obtained in [11] by the usual perturbation method (by a straight Poincaré expansion).

From equation (56) and similar equations which can be obtained by means of the averaging method for other parameters of the trajectory, can be concluded this pattern for the change in properties of waveguide trajectories with distance.* At short distances the shape of $\phi_t(x_t)$ has rapid changes (on the order of the trajectory's period). With distance is evidenced a slow component (the second term in (56)) of variations in arrival angles, which becomes dominant at a great distance.

5. Example. Irregular Waveguide with a Parabolic Profile for the Dielectric Constant

As an example of application of the averaging method, let us consider the behavior of the trajectory of a ray with long-range propagation in a waveguide formed in a medium whose dielectric constant varies with height parabolically, and whose parameters are slow functions of the horizontal coordinates:

$$\varepsilon = \varepsilon_m - \left(\frac{z - z_m}{d}\right)^2$$
$$(\varepsilon_m = \varepsilon_m(\tau, \sigma), \quad z_m = z_m(\tau, \sigma), \quad d = d(\tau, \sigma)). \tag{57}$$

In this case the application of the averaging method for the trajectory gives

$$z = z_m + \sqrt{cd}\sin 2\pi\eta + \nu\left\{\frac{\sqrt{d\bar{\alpha}c}}{4}\cos(2\pi\eta)\left[\frac{dd}{d\tau} - \frac{1}{4\bar{\alpha}}\frac{c}{d}\frac{\partial d}{\partial\tau}\right] + \right.$$
$$\left. + \frac{c}{2\sqrt{\bar{\alpha}}}\frac{\partial z_m}{\partial\tau}\sin(4\pi\eta) - \frac{c}{16}\sqrt{\frac{c}{d\bar{\alpha}}}\frac{\partial d}{\partial\tau}\cos(6\pi\eta)\right\} + O(\nu^2); \tag{58}$$

*Let us note that equation (56) is valid both at short and long distances, but with different absolute accuracy. The relative accuracy, nevertheless, remains the same--$O(\lambda) + O(\nu)$.

$$y = \bar{y} - \nu \frac{\sqrt{cd}}{2}\left[2\frac{dz_m}{dn}\sin(2\pi\eta) - \frac{1}{4}\frac{dd}{dn}\sqrt{\frac{c}{d}}\cos(4\pi\eta)\right] + O(\nu^2), \tag{59}$$

where

$$\frac{d}{d\tau} \equiv \frac{\partial}{\partial\tau} + \operatorname{tg}\bar{\varphi}\frac{\partial}{\partial\sigma}, \qquad \frac{d}{dn} \equiv \frac{\partial}{\partial\sigma} - \operatorname{tg}\bar{\varphi}\frac{\partial}{\partial\tau}.$$

Function $\bar{\alpha}(\tau)$ and $\bar{y}(\tau) = \bar{\sigma}/\nu$ are found from the following system of averaged first-approximation equations:

$$\frac{d\bar{\alpha}}{dx} = \nu\left\{\frac{\partial\varepsilon_m}{\partial\tau} + \frac{1}{d}\left[\varepsilon_m - \frac{\bar{\alpha}}{\cos^2\bar{\varphi}}\right]\frac{\partial d}{\partial\tau}\right\} + O(\nu^3); \tag{60}$$

$$\frac{d\bar{\sigma}}{dx} = \nu\operatorname{tg}\bar{\varphi} + O(\nu^3); \tag{61}$$

$$\frac{d\bar{\varphi}}{dx} = \nu\frac{\cos^2\bar{\varphi}}{2\bar{\alpha}}\left\{\frac{\partial\varepsilon_m}{\partial\sigma} - \operatorname{tg}\bar{\varphi}\frac{\partial\varepsilon_m}{\partial\tau} + \right.$$
$$\left. + \frac{1}{d}\left(\frac{\partial d}{\partial\sigma} - \operatorname{tg}\bar{\varphi}\frac{\partial d}{\partial\tau}\right)\left(\varepsilon_m - \frac{\bar{\alpha}}{\cos^2\bar{\varphi}}\right)\right\} + O(\nu^2). \tag{62}$$

Equation (60) can be substituted by a functional equation following from the condition of constancy of the adiabatic invariant (45),

$$d\left[\varepsilon_m - \frac{\bar{\alpha}}{\cos^2\bar{\varphi}}\right] = \text{const} = c. \tag{63}$$

Equations (60) to (63) can be solved either by means of the perturbation method (cf. above) or strictly, when variables are separated. Here it is necessary to note that averaged equations can permit the separation of

variables, whereas in the initial ray equations (2) to (5) it is impossible to separate variables. In particular, in the case of the model of the medium discussed, (57), averaged equations (60) to (63) do not contain $z_m(\tau,\sigma)$, and, consequently, are solved easily when the variable in model (57) is only the height of axis z_m.

By definition (cf. (38) where $\Phi_1 = 0$) the value of η in equations (58) and (59) equals

$$\eta = \int_0^x \frac{dx}{2\pi d(\nu x, \bar{\sigma})\sqrt{\bar{\alpha}}} + \eta_0. \tag{64}$$

As we know from [12], at a long distance of $x \sim 1/\nu$ by virtue of integration operation (64) the "phase," η, is determined with less accuracy than the "slow" variables α, σ and ϕ. Thus, in this case the error in variables α, σ and ϕ determined from equations (60) to (62) will be on the order of ν^2, and the error in η determined by equation (64) equals $O(\eta)$. At short distances of $x \leq O(1)$ the accuracy of all the values determined becomes the same, and as a result it is possible to obtain the equations of the usual perturbation method.

As is obvious from (58) to (62), the irregularity of a parabolic waveguide results at a long distance in the fact that in addition to variations in the ray of a rapid nature and low amplitude (on the order of ν) slow variations are evidenced, the characteristic scale of variation of which is on the order of the dimensions of inhomogeneities. The amplitude of the latter variations at a long distance exceeds the amplitude of "fast" variations. Taking into account the motion of inhomogeneities in the ionosphere, from the three-dimensional pattern obtained can be concluded a similar pattern for the variation over time in the parameters of a radio wave in an ionospheric waveguide. Thus, in the observation of arrival angles, polarization, etc., must be observed relatively fast fluctuations with a period on the order of the ratio of the trajectory's period of oscillation to the velocity of the inhomogeneity, the parameters of which (amplitude and frequency) vary slowly, but over a considerably wide range, in time.

Bibliography

1. Kazantsev, A.N. and Lukin, D.S. KOSMICHESKIYE ISSLEDOVANIYA, Vol 4, No 2, 221 (1966).

2. Wong, M.S. RADIO SCI., 1, No 10, 1214 (1966).

3. Gurevich, A.V. and Tsedilina, Ye.Ye. GEOMAGNETIZM I AERONOMIYA, 13, 283 (1973).

4. Tsedilina, Ye.Ye. GEOMAGNETIZM I AERONOMIYA, 14, 1008 (1974).

5. Brekhovskikh, L.M. "Volny v sloistykh sredakh" [Waves in Layered Media], Izdatel'stvo Nauka, Moscow, 1975.

6. Kinber, B.Ye. and Kravtsov, Yu.A. RADIOTEKHNIKA I ELEKTRONIKA, 22, No 12, 2470 (1977).

7. Baranov, V.A., Yegorov, I.B. and Popov, A.V. In "Difraktsionnyye effekty dekametrovykh radiovoln v ionosfere" [Diffraction Effects of High-Frequency Radio Waves in the Ionosphere], Moscow, Izdatel'stvo Nauka, 1977, p 31.

8. Baranov, V.A. and Kravtsov, Yu.A. IZV. VUZOV, RADIOFIZIKA, 18, No 1, 52 (1975).

9. Gusev, V.D., Makhmutov, N.A. and Khuri, A. RADIOTEKHNIKA I ELEKTRONIKA, 19, No 9, 1809 (1974).

10. Lewis, R.P.W. PROC. PHYS. SOC., B66, No 4, 308 (1953).

11. Tinin, M.V. In "Issledovaniya po geomagnetizmu, aeronomii i fizike Solntsa" [Studies in Geomagnetism, Aeronomy and Solar Physics], No 41, Moscow, Izdatel'stvo Nauka, 1977, p 40.

12. Volosov, V.M. and Morgunov, B.I. "Metod osredneniya v teorii nelineynykh kolebatel'nykh sistem" [Averaging Method in the Theory of Nonlinear Oscillatory Systems], Moscow, MGU, 1971.

13. Moiseyev, N.N. "Asimptoticheskiye metody nelineynoy mekhaniki" [Asymptotic Methods of Nonlinear Mechanics], Moscow, Izdatel'stvo Nauka, 1969.

14. Bogolyubov, N.N. and Mitropol'skiy, Yu.A. "Asimptoticheskiye metody v teorii nelineynykh kolebaniy" [Asymptotic Methods in the Theory of Nonlinear Oscillations], Moscow, Izdatel'stvo Nauka, 1974.

15. Tinin, M.V. In "Issledovaniya po geomagnetizmu, aeronomii i fizike Solntsa," No 39, Moscow, Nauka, 1976, p 166.

16. Tinin, M.V. IVZ. VUZOV, RADIOFIZIKA, 20, No 12, 1906 (1977).

CSO: 1860
8831

UDC 621.391.2

THE MEASUREMENT OF THE COORDINATES OF A POINT OBJECT OBSERVED THROUGH A TURBULENT ATMOSPHERE

Moscow RADIOTEKHNIKA I ELEKTRONIKA in Russian Vol 24 No 10, 1979 pp 2027-2034 manuscript received 12 Jul 78

[Article by A.B. Aleksandrov and V.A. Loginov]

[Text] Algorithms are synthesized for the measurement of the range and angular coordinates of a point object, taking into account fluctuations in the level and phase which arise during the propagation of the radiation in a turbulent medium. A comparative analysis is made of the quality of the synthesized and nonoptimal algorithms, and the influence of level and phase fluctuations in the received field on the measurement errors is ascertained.

Introduction

One of the major obstacles which makes it difficult to use the high potential capabilities of information systems is the disruption of the coherency of laser radiation when it propagates in the atmosphere. Distortions which have the nature of multiplicative interference, $exp[\psi(r, t) + is(r, t)]$, appear in an electromagnetic wave which passes through a layer of a randomly inhomogeneous medium. The function $s(r, t)$ describes the random phase changes due to the passage of the wave through the inhomogeneity of a medium; fluctuations in the level of the wave (amplitude fluctuations), which arise with the interference of secondary waves scattered at these inhomogeneities, are designated in terms of $\chi(r, t)$.

Up till now, questions of synthesizing and analyzing algorithms for processing the data contained in a laser signal were treated without taking the amplitude fluctuations into account. This is related to the intuitive notion that the major factor limiting the information capacity of a signal when it propagates in a turbulent medium is the disruption of its phase structure. The model of a signal distorted solely by phase fluctuations is used, for example, in papers [1, 2]. Moreover, the question of the influence of amplitude fluctuations on the quality of the discrimination

of information has remained unclear up to the present. This problem is studied in this paper as applied to the problem of measuring the coordinates of a point object observed through a turbulent atmosphere.

1. The Formulation of the Problem

We shall assume that the duration of the probe signal is short as compared to the characteristic time for the change in the complex phase $\psi(r, t) = \chi(r, t) + is(r, t)$ (for the atmosphere, this time is on the order of 10^{-3} seconds) and we shall neglect the dependence of $\chi(r, t)$ and $s(r, t)$ on time. The field reflected from the object and observed in the time interval $0 \leq t \leq T$ at the point R of the receiving aperture is represented in the form:

$$y(\mathbf{r}, t)=\sqrt{2E}\,\mathrm{Re}\left\{u(t-\tau)\exp\left[i\omega_0\left(t-\frac{R+|\mathbf{R}-\mathbf{r}|}{c}\right)+\right.\right. \tag{1}$$
$$\left.\left.+\chi(\mathbf{r})+is(\mathbf{r})\right]\right\}+n(\mathbf{r}, t).$$

Here, E is the surface energy density of the signal; u(t) is the complex law governing its modulation $\left(\int_0^T |u(t)|^2\,dt=1\right)$; ; ω_0 and c are the carrier frequency and the speed of light; R is a radius vector directed from the center of the aperture to the object; $R = |\mathbf{R}|$ is the range to the object; $\tau = 2R/c$ is the time delay of the signal; n(r, t) is the background interference, which in the following we shall consider to be normal white noise with a zero mean value and a correlation function of:

$$\langle n(\mathbf{r}_1, t_1)n(\mathbf{r}_2, t_2)\rangle=N_0\delta(\mathbf{r}_1-\mathbf{r}_2)\delta(t_1-t_2).$$

The parameters being measured are the range R (the time delay τ) and the angular coordinates of the object, determined by the projections n_x and n_y of the vector $\mathbf{n} = \mathbf{R}/R$ on to the coordinate axes, related to the receive aperture.

2. The Synthesis of the Algorithms. The Interpretation of Optimal Processing

The logarithm of the probability ratio of the signal and noise mixture (1) has the form [3]:

$$z[y(\mathbf{r}, t)]=\frac{\Delta}{N_0}\sum_{j=1}^{N}a_j^2- \tag{2}$$
$$-\frac{1}{2}\sum_{j,k=1}^{N}[B_{jk}A_jA_k+2B_{j,k+N}A_j\theta_k+B_{j+N,k+N}\theta_j\theta_k].$$

This expression was derived given the following assumptions:

1. The receiving aperture is broken down into discrete cells, Δ_j (j = 1, ..., N) with an area $\Delta = S_A/N$ (S_A is the aperture area) in such a manner that the continuous functions $\chi(r)$ and $s(r)$ are described quite well by the set of their own values χ_j and s_j in these cells, while the difference in the phase changes in the adjacent cells is much less than 2π. The a priori law governing the distribution of the quantities $\chi_1, \ldots, \chi_N, s_1, \ldots, s_N$ is assumed to be normal:

$$P_{zN}(\gamma) = (2\pi)^{-N} \det{}^{-1/2} \mathbf{K} \exp\left\{-\frac{1}{2}(\gamma-\gamma_0)^T \mathbf{K}^{-1}(\gamma-\gamma_0)\right\},$$

where $\gamma^T = (\chi_1, \ldots, \chi_N, s_1, \ldots, s_N)$, $\gamma_0^T = (\langle\chi\rangle, \ldots, \langle\chi\rangle, 0, \ldots, 0)$; $\mathbf{K} = \|K_{jk}\|$ is the correlation matrix of the levels and phases, $K_{jk} = \langle(\gamma_j - \gamma_{0j})(\gamma_k - \gamma_{0k})\rangle$, j, k = 1, ... , 2N. This hypothesis is justified in the range of small amplitude fluctuations, where the wave propagation in an inhomogeneous is described quite well in the approximation of the method of continuous perturbations (MPV), and in the range of saturation of the intensity fluctuations. The methods of wave propagation theory for a randomly inhomogeneous medium allow for the calculation of the correlation functions of the level $K_{\chi\chi}(\rho)$, the phase $K_{ss}(\rho)$ and the cross-correlation function $K_{\chi s}(\rho)$, so that we shall consider the matrices K and K^{-1} to be specified.

2. The signal-to-noise ratio is considered to be rather high, so that the a posteriori measurement precision for the values χ_j and s_j in each cell is enormously better than the a priori scatter in the indicated quantities. This assumption permits the use of the asymptotic Laplace method when averaging the likelihood ratio with respect to the random levels of χ_j and phases of s_j.

The following symbols are introduced in (2):

$$y_j = \frac{1}{\Delta}\int_{\Delta_j}\int_0^T y(\mathbf{r}, t)\, u(t-\tau) \exp\left[i\omega_0\left(t - \frac{R+|\mathbf{R}-\mathbf{r}|}{c}\right)\right] dt\, d\mathbf{r}, \tag{3}$$

$$a_j = |y_j|, \quad \theta_j = -\arg y_j, \quad A_j = \ln\frac{2a_j}{\sqrt{2E}} - \langle\chi\rangle,$$

where $\langle\chi\rangle$ is the mean value of the wave level. The elements of the matrix B_{jk} (j, k = 1, ... , 2N) are specified by the expressions:

$$B_{jk} = K_{jk}^{-1} - \frac{1}{D}\sum_{m=1}^{N} K_{j,m+N}^{-1} \sum_{n=1}^{N} K_{k,n+N}^{-1}, \tag{4}$$

$$D = \sum_{m,n=1}^{N} K_{m+N,n+N}^{-1}.$$

Maximizing expression (2) makes it possible to ascertain the optimal operations when estimating the time delay τ and the direction n to the object. In this case, the fact that the first term in (2),

$$z_1=(\Delta/N_0)\sum_{j=1}^{N}a_j^2,$$

which is proportional to the signal/noise ratio, significantly exceeds the second term and is practically independent of the angular coordinates, must be taken into account. For this reason, it is to be used when finding the estimate of the delay $\hat{\tau}$. On the other hand, the information on the angular coordinates is basically contained in the second term of (2), and by maximizing it with respect to the unknown values of n_x and n_y, one can find the maximum likelihood estimates of $\hat{n}_x$ and $\hat{n}_y$.

In order to interpret the nature of optimal processing when measuring the delay, we shall choose the origin for the time readout so that $u(t) \equiv 0$, $t \geq 0$, and set $|R-r| \approx R(1-nr/R+r^2/2R^2)$. Then a_j^2 can be written in the form:

$$a_j^2=a_j^2(\tau)=\frac{1}{\Delta^2}\left|\int_{\Delta_j}Y(\mathbf{r},\tau)\exp\left[\frac{i\omega_0}{c}(nr-r^2/2R)\right]dr\right|^2, \tag{5}$$

where

$$Y(\mathbf{r},\tau)=\int_0^{\tau}y(\mathbf{r},t)\,u(t-\tau)\exp[i\omega_0(t-\tau)]\,dt. \tag{6}$$

Now, the generation of $z_1 \sim \sum_{j=1}^{N} a_j^2$ can be treated thusly: the received field $y(r, t)$ is passed through a filter with a pulse response of $h(t) = \mathrm{Re}[u(-t)\cdot\exp(-i\omega_0 t)]$, and is then fed to a system of lenses, the apertures of which coincide with the regions Δ_j; if photodetectors are installed in the focal plane on the axes of the lenses, where the photodetectors generate the squares of the absolute values of the field incident on them, and sum their outputs, then the result proves to be proportional to the quantity z_1. In this case, the output of the circuit at the current point in time τ corresponds to the tuning for the range $R = c\tau/2$, i.e., timewise scanning of the output signal with respect to the delay is realized in it. When observing in a time interval T, determined by the a priori coverage of the range being measured, the position of the maximum of the output signal $\hat{\tau}$ is the estimate of the delay, while the quantity $\hat{R} = c\hat{\tau}/2$ is the estimate of the range to the object.

We will note that an important feature of the processing being discussed here is the partitioning of the receiving aperture into cells, the dimensions of which do not exceed the effective size of the field coherency region; this assures coherent storage of the energy from the entire aperture. The engineering realization of such processing does not present any fundamental difficulties.

When finding the estimates $\hat{n}_x$ and $\hat{n}_y$, which maximize the second term in (2), the fact that the information on the angular coordinates is contained only in the phases θ_j of the field being observed is to be taken into account, as well as the dependence of θ_j on the parameters n_x and n_y being measured, where this is described by the expression:

$$\theta_j \simeq -\frac{\omega_0}{c}(n_x x_j + n_y y_j),$$

where x_j and y_j are the coordinates of the vector r_j. If the aperture is symmetrical with respect to the x and y axes, while the object is located close to the normal to the aperture, running through the origin of the coordinates, then the explicit expressions for $\hat{n}_x$ and $\hat{n}_y$ are as follows:

$$\hat{n}_x = \frac{c}{\omega_0}\cdot\frac{\sum_{j,k=1}^{N} x_k(B_{j,k+N}A_j + B_{j+N,k+N}\theta_j)}{\sum_{j,k=1}^{N} x_j x_k B_{j+N,k+N}}, \tag{7}$$

$$\hat{n}_y = \frac{c}{\omega_0}\cdot\frac{\sum_{j,k=1}^{N} y_k(B_{j,k+N}A_j + B_{j+N,k+N}\theta_j)}{\sum_{j,k=1}^{N} y_j y_k B_{j+N,k+N}},$$

where A_j, θ_j and a_j are defined by expressions (3), in which the following is to be substituted:

$$y_j = \frac{1}{\Delta}\int_{\Delta_j}\int_{0}^{T} y(\mathbf{r}, t)\,u(t-\hat{\tau})\exp(i\omega_0 t)\,dt\,d\mathbf{r}. \tag{8}$$

As was noted in papers [2, 4], the estimation of the angular coordinates of the radiation source reduces to the calculation of the smoothed average slope of the phase front of the received field with respect to the coordinate axes, chosen at the aperture. The processing of (7) is treated in precisely the same way. The difference consists in the fact that during the smoothing, not only the direct correlation relationships between the values of the phases θ_j in the different cells of the aperture are taken into account, but also their relationships in terms of the field levels A_j. In engineering terms, processing of the form of (7) is considerably more difficult to realize than operations of range estimation. In any case, the issue is one of the necessity of registering the levels and the phases of the received field in the cells Δ_j, with subsequent digital processing.

3. The Precision in the Measurement of the Time Delay in Optimal Processing. A Comparison with Nonoptimal Algorithms.

We shall analyze the errors in the measurement of the time delay τ with the assumption that the object being observed is located close to the normal to the aperture passing through its center.

The estimate $\hat{\tau}$ which maximizes the function

$$z(\tau)=\sum_{j=1}^{N}\left|\int\limits_{\Delta_j}\int\limits_{0}^{T} y(\mathbf{r},t)\,u(t-\tau)\exp(i\omega_0 t)\,dt\,d\mathbf{r}\right|^2,$$

satisfies the likelihood equation:

$$\left.\frac{\partial z(\tau)}{\partial \tau}\right|_{\tau=\tau}=0.$$

The left side of this equation can be expanded in a series at the point $\hat{\tau} = \tau$ (τ is the true value of the delay), and by linearizing the difference $\hat{\tau} - \tau$ with respect to the noise component, one can obtain the following expression for the dispersion of the estimate:

(9) $$\sigma_\tau^2=\left\langle\frac{\left[\frac{\partial z_{ш}(\tau)}{\partial\tau}\right]^2}{\left[\frac{\partial^2 z_c(\tau)}{\partial\tau^2}\right]^2}\right\rangle,$$

where $z_C(\tau)$ and $z_Ш(\tau)$ are the signal and noise components of $z(\tau)$. The angular brackets in (9) indicate averaging with respect to the noise and the fluctuations of the level and phase of the signal. Omitting a number of mathematical derivations, we shall given the final expression for σ_τ^2:

(10) $$\sigma_\tau^2=\frac{1}{q\Delta\omega^2}\left\langle\left(\frac{1}{N}\sum_{j=1}^{N}e^{2z_j}\right)^{-1}\right\rangle.$$

Here, $q = ES_A/N_0$ is the signal-to-noise ratio in the aperture, while $\Delta\omega^2$ is the square of the root mean square spectral width of the signal modulation:

(11) $$\Delta\overline{\omega^2}=\frac{1}{2\pi}\int_{-\infty}^{\infty}\omega^2|u(i\omega)|^2\,d\omega-\left(\frac{1}{2\pi}\int_{-\infty}^{\infty}\omega|u(i\omega)|^2\,d\omega\right)^2.$$

The low frequency modulation spectrum of the probe signal is designated as $u(i\omega)$ in (11). The fact that σ_τ^2 is proportional to the quantity $1/q\Delta\omega^2$ does not require any special commentary: with an increase in the signal to noise ratio and the spectral width of the modulation, the precision in the measurement of the delay deteriorates. The factor $\gamma =$

$$\gamma=\left\langle\left((1/N)\times\sum_{j=1}^{N}e^{2z_j}\right)^{-1}\right\rangle$$

reflects the influence of the amplitude fluctuations of the field on this error for the case of optimal processing. We shall estimate this quantity

in the limiting cases of small and large apertures (as compared to the coherency region of the received field). In the first case, we shall assume that for all j, $\chi_j = \chi$, i.e.:

$$\gamma = \left\langle \left(\frac{1}{N} \sum_{j=1}^{N} e^{2\chi_j} \right)^{-1} \right\rangle = \langle e^{-2\chi} \rangle = \exp(4\sigma_\chi^2). \tag{12}$$

For a large aperture, the quantity $(1/N) \sum_{j=1}^{N} e^{2\chi_j}$ differs little from its mean value, $(1/N) \sum_{j=1}^{N} \langle e^{2\chi_j} \rangle = 1$, so that in this case $\gamma = 1$. The reduction in the factor γ with an increase in the dimensions of the aperture is related to its averaging effect. The limits for the variation in γ are determined by the quantity $\exp(4\sigma_\chi^2)$ and can be quite considerable (in the saturation region of the intensity fluctuations, $\sigma_\chi^2 \approx 0.7$, so that $\exp(4\sigma_\chi^2) \approx 16$.

It is interesting to calculate that potential gain in the delay measurement accuracy which optimum processing yields as compared to algorithms in which the processing of the amplitude fluctuations is absent. One of these algorithms, which is used in practice, effects the storage from the entire aperture Ω; this processing is optimal if the signal is regular, while its initial phase is randomly and uniformly distributed in the range of $(-\pi, \pi)$. With this method, the estimate $\hat{\tau}$ maximizes the quantity:

$$L_1(\tau) = \left| \int_{\Omega} \int_{0}^{T} y(\mathbf{r}, t)\, u(t-\tau) \exp(i\omega_0 t)\, dt\, d\mathbf{r} \right|^2.$$

As yet another method, we shall consider an algorithm which maximizes the following expression with respect to τ:

$$L_2(\tau) = \sum_{j=1}^{N} \left| \frac{1}{\Delta} \int_{\Delta_j} \int_{0}^{T} y(\mathbf{r}, t)\, u(t-\tau) \exp(i\omega_0 t)\, dt\, d\mathbf{r} \right|.$$

As follows from [2], this algorithm is optimal when only the phase fluctuations of the signal are taken into account.

By considering the signal-to-noise ratio to be high, and linearizing $L_1(\tau)$ and $L_2(\tau)$ with respect to the noise components, one can derive the following formulas for the errors of the algorithms considered here:

$$\sigma_{\tau 1}^2 = \gamma_1 / q\Delta\omega^2 = \frac{1}{q\Delta\omega^2} \left\langle \left| \frac{\int_{\Omega} \exp[\chi(\mathbf{r}) + is(\mathbf{r})]\, d\mathbf{r}}{S_A} \right|^{-2} \right\rangle \tag{13}$$

$$\sigma_{\tau 2}^2 = \gamma_2 / q\Delta\omega^2 = \frac{1}{q\Delta\omega^2} \left\langle \left(\frac{1}{N} \sum_{j=1}^{N} e^{\chi_j} \right)^{-2} \right\rangle. \tag{14}$$

The dependence of $\sigma_{\tau 1}^2$ and $\sigma_{\tau 2}^2$ on the signal to-noise ratio q and the spectral width of the modulation is precisely the same as in (10). The influence of the amplitude fluctuations on the error is described by the coefficients γ_1 and γ_2. It is not difficult to see that in the case of a small aperture, the quantities γ, γ_1 and γ_2 agree. This is not surprising, since each of the three algorithms considered in this case accomplish coherent spatial processing of the field. More interesting is the relationship of the quantities γ, γ_1 and γ_2 with large aperture dimensions, since specifically in this region does the optimality or nonoptimality of the processing have an effect. In this case, $\gamma = 1$, while the quantities γ_1 and γ_2, which characterize the corresponding gain in precision, are represented in the form:

$$\gamma_1 = \left(\frac{1}{S_A^2}\int\int_{\Omega\Omega} \Gamma_2(\mathbf{r}_1-\mathbf{r}_2)\,d\mathbf{r}_1\,d\mathbf{r}_2\right)^{-1}, \quad \gamma_2 = \exp(\sigma_\chi^2), \tag{15}$$

where $\Gamma_2(r_1 - r_2)$ is a second order coherency function of a spherical wave distorted in a turbulent atmosphere. It can be seen from (15) that the quantity γ_1 is of the order S_A/S_k, where S_k is the size of the field coherency region, while the maximum value of γ_2 is approximately 2 (when $\sigma_\chi^2 = 0.7$).

The estimates cited here provide a qualitative notion of the precision characteristics of the each of the algorithms considered.

4. The Precision in the Measurement of Angular Coordinates for the Case of Optimal Processing. A Comparison with a Nonoptimal Algorithm.

The dispersion of the error in the measurement of angular coordinates can be calculated using expression (7) for the estimates. By linearizing the right sides of (7) with respect to the random component, it is easy to show that the error consists of two components: a noise and a fluctuation component. The first is determined by the presence of additive noise in the field being processed; its dispersion is inversely proportional to the signal-to-noise ratio q. When $q \gg 1$, the second component is more important, which is due to the spatial fluctuations of the level and phase of the signal. Limiting ourselves to the treatment of only this component, the following expression can be derived for its dispersion:

$$\sigma_{\phi n}^2 = \frac{c^2}{\omega_c^2 D_0}, \tag{16}$$

where

$$D_0 = \sum_{j,k=1}^{N} x_j x_k B_{j+N,k+N}, \tag{17}$$

while the elements of the B matrix are determined by formulas (4). It follows from (17) that the value of $\sigma_{\phi n}^2$ [$\sigma_{f1.}^2$] depends substantially on the

ratio of the dimensions of the aperture and the characteristic scales which describe the spatial fluctuations of the phase and level. This function can be clearly illustrated in the limiting cases of small and large apertures.

In the first case, it is sufficient for the estimate to limit ourselves to the quadratic of the correlation functions $K_{\chi\chi}(\rho)$, $K_{ss}(\rho)$ and $K_{\chi s}(\rho)$ and to derive the following expression:

$$\sigma^2_{\phi n} = \frac{c^2}{\omega_0^2}\left(\beta_{ss} - \frac{\beta^2_{\chi s}}{\beta_{\chi\chi}}\right), \tag{18}$$

where

$$\beta_{\chi\chi} = -\frac{\partial^2 K_{\chi\chi}}{\partial\rho^2}\Big|_{\rho=0};$$

$$\beta_{\chi s} = -\frac{\partial^2 K_{\chi s}}{\partial\rho^2}\Big|_{\rho=0}; \tag{19}$$

$$\beta_{ss} = -\frac{\partial^2 K_{ss}}{\partial\rho^2}\Big|_{\rho=0}.$$

The quantity which determines the relative contribution of the amplitude fluctuations to the dispersion $\sigma^2_{fl.}$ is $\gamma = \beta_{\chi s}/\sqrt{\beta_{\chi\chi}\beta_{ss}}$. This parameter coincides with the cross correlation factor for the level and phase of a plane wave, determined in [5]. It follows from the estimates given in this paper that the quantity γ^2 does not exceed a few percent, so that in (18), one can assume $\sigma^2_{fl.} = (c^2/\omega_0^2)\beta_{ss}$. The result obtained is extremely characteristic: with a decrease in the aperture, the fluctuation error ceases to depend on its size, and is determined by the parameter β_{ss}. The physical explanation of this fact is obvious: with small apertures, the portion of the wave phase front being processed can be considered planar, and for this reason, the precision in the angular position of the source is determined only by the fluctuations in the angle of incidence of the wave, the dispersion of which is proportional to β_{ss}.

The other limiting case occurs if the area of the aperture significantly exceeds the dimensions of the coherency regions of the fluctuations of the level and phase. In this case, a changeover must be made from discrete quantities to continuous ones in expressions (4) and (17), and when solving the resulting integral equations, one must make use of the Fourier transform of the correlation functions $K_{\chi\chi}$, $K_{\chi s}$ and K_{ss}. The final expression for $\sigma^2_{fl.}$ has the form:

$$\sigma^2_{\phi n} = \frac{3c^2}{4\omega_0^2 h^2}\left(F_{ss} - \frac{F^2_{\chi s}}{F_{\chi\chi}}\right), \tag{20}$$

where:

$$F_{xx}=\Phi_{xx}(\varkappa_1, \varkappa_2)\,|_{\varkappa_1=\varkappa_2=0};$$
$$F_{xs}=\Phi_{xs}(\varkappa_1, \varkappa_2)\,|_{\varkappa_1=\varkappa_2=0}; \quad (21)$$
$$F_{ss}=\Phi_{ss}(\varkappa_1, \varkappa_2)\,|_{\varkappa_1=\varkappa_2=0}.$$

Φ_{XX}, Φ_{XS} and Φ_{SS} take the form of two-dimensional spatial spectra of the corresponding correlation functions; 2h is the linear dimension of the aperture.

It follows from formulas (18) and (21) that the presence of amplitude fluctuations and their correct processing leads to a reduction in the fluctuation component of the measurement error for the angular coordinates (we will note that the first terms in (18) and (21) correspond to the error in the measurement of the angular coordinates using only phase processing. The explanation of this unexpected results is that in a turbulent atmosphere, the amplitude and phase fluctuations prove to be markedly correlated, and for this reason, the processing of the signal levels allows for the extraction of additional information on the angular coordinates. As has already been noted, for the case of a small aperture, this reduction is also small (a few percent), and in the case of a large aperture, the resulting in the error is determined by the quantity $\mu = 1 - F_{XS}^2(F_{XX}F_{SS})^{-1}$. The expressions for the spectra Φ_{XX}, Φ_{XS} and Φ_{SS}, computed in [5] for the case of a plane wave propagating in a turbulent atmosphere, yield a value of $\mu = 0.25$. This figure eloquently speaks of the necessity of taking into account the amplitude fluctuations when synthesizing algorithms for the measurement of the angular coordinates.

In conclusion, the authors would like to express their deep gratitude to P.A. Bakut for his useful discussions and attention to the work.

BIBLIOGRAPHY

1. A.A. Kuriksha, RADIOTEKHNIKA I ELEKTRONIKA, 1968, 13, 5, p 771.

2. P.A. Bakut, K.N. Sviridov, I.N. Troitskiy, N.D. Ustinov, RADIOTEKHNIKA I ELEKTRONIKA, 1977, 22, No 5, p 935.

3. A.B. Aleksandrov, P.A. Bakut, V.A. Loginov, "Obrabotka opticheskogo signala, rasprostranyayushchegosya v sluchayno-neodnorodnoy srede" ["The Processing of an Optical Signal Propagating in a Randomly Inhomogeneous Medium"], "Doklady VII Vsesoyuznoy konferentsii po teorii kodirovaniya i peredachi informatsii" ["Reports of the Seventh All-Union Conference on Coding and Information Transmission Theory"], Part VI, p 6, 1978.

4. P.A. Bakut, V.A. Loginov, I.N. Troitskiy, RADIOTEKHNIKA I ELEKTRONIKA, 1977, 22, No 2, p 286.

5. V.I. Tatarskiy, "Rasprostraneniye voln v turbulentnoy atmosfere" ["Wave Propagation in a Turbulent Atmosphere"], Nauka Publishers, 1967.
[40-8225]

8225
CSO: 1860

Electron Tubes; Electrovacuum Technology

UDC 621.385.6

MICROWAVE AMPLIFIERS WITH CROSSED FIELDS

Moscow SVERKHVYSOKOCHASTOTNYYE USILITELI SO SKRESHCHENNYMI POLYAMI in Russian 1978, signed to press 27 Dec 77 p 2, 278-280

[Annotation and table of contents from book by Mikhail Borisovich Tseytlin, Mikhail Aleksandrovich Fursayev and Oleg Vladimirovich Betskin, Sovetskoye radio, 550 copies, 280 pages]

[Text] This book describes methods for calculating and analyzing microwave amplifiers with crossed fields (type M). Beam amplifiers are considered (with an electron-optical system removed from the interaction space). Besides a general theory of interaction between the electron flow and the retarded electromagnetic wave in the large signal mode, considerable attention is given to investigating new arrangements and various operating modes of beam devices. In the section dedicated to the amplitron, an analysis is given of basic electrical characteristics, as well as a calculation of the output parameters of the amplifier.

The book is intended for engineers and scientific staff workers in the area of microwave electronics and radiophysics, as well as for instructors and students in higher educational schools. It may also be used as a textbook for course and diploma theses.

Pictures 157; tables 8; bibliography 175 titles.

Contents

[266-2291]

2291
CSO: 1860

BOOK ON EXPERIMENTAL RADIOOPTICS

Moscow EKSPERIMENTAL'NAYA RADIOOPTIKA in Russian 1979 pp 1, 254-256

[Annotation and table of contents from book by N. M. Borovitskaya, et al, Nauka, total copies unknown, 256 pages]

[Text] Methods of coherent and incoherent optics, radiovision and acoustics are discussed within the framework of a single radiooptical approach, and corresponding installations and devices are described. The part on coherent optics includes: investigation of the laser radiation spectrum, holography, picture multiplexing, optical methods for processing data, the study of statistical characteristics (noises) of data carriers, as well as the investigation of the intensity blips of laser radiation propagating in the atmosphere. Incoherent and partially coherent light are used to solve problems of spatial filtration and the correlation analysis of pictures, and for making integral Fourier and Fresnel transformations. Descriptions of most installations are provided with circuits, practical recommendations etc. which are sufficient for use in laboratory courses.

Table 1; illustrations 117; bibliography 95 titles.

Contents

Table of Contents

Table of Contents

Table of Contents

2291
CSO: 1860

General Circuit Theory and Information

PHASE-LOCKED LOOPS WITH SAMPLING COMPONENTS

Moscow SISTEMY FAZOVOY AVTOPODSTROYKI CHASTOTY S ELEMENTAMI DISKRETIZATSII (Phase-Locked Loops with Sampling Components) in Russian 1979 signed to press 15 Jan 79 pp 2, 224

[Annotation and table of contents from book by Vagen Vaganovich Shakhgil'-dyan, Aleksandr Alekseyevich Lyakhovkin, Vladimir Leonidovich Karyakin, Vladimir Anatol'yovich Petrov and Valentina Nikolayevna Fedoseyeva, edited by V. V. Shakhgil'dyan, Svyaz', 4300 copies, 224 pages]

[Text] This book studies phase-locked loops (FAPCh) containing components for sampling its coordinates of state (with respect to time, level).

The authors introduced a classification of systems containing sampling components. They discussed methods of the analysis and computation of radio-pulse, pulsed, digital, and continuous sampling FAPCh systems. They analyzed the stability, dynamics, and noise immunity of these systems and gave recommendations on designing and calculation of such systems.

The book is intended for scientists engaged in the development and use of synchronization devices.

Contents

[31-10,233]

10,233

CSO: 1860

UDC 389.14:006.354.065

METROLOGICAL CONTROL SYSTEM FOR PRODUCTION

Moscow IZMERITEL'NAYA TEKHNIKA in Russian, No 10, 1979 pp 7-8

[Article by L. A. Pronin]

[Text] Raising the quality of products manufactured by the tool plants of the Minstankoprom [Ministry of Machine Tool and Tool Building Industry] is a complex and responsible problem impossible to solve without metrological control (MO) of production.

To the "Kalibr" Plant that produces a broad range of measuring devices (SI) for linear dimensions and angles, with a great variety of controlled parameters, metrological control problems are especially important. MO provides for the following:

analyzes the condition of measurements at the enterprise and, on the basis of the analysis of the data, develop measures for improving the MO;

develops and introduces modern measuring methods; establishes efficient nomenclature for the SI used;

introduces government and industrial standards, develops enterprise standards that regulate precision norms, introduces methods for making the measurements, checks and tests;

obtains expert metrological opinion on the technical-norm, design and technological documentation;

checks and obtains metrological certification of the SI used at the plant.

Moreover, the plant deals with MO problems related to coordinating government standards for the SI series produced by the plant which complicates high precision measurements; participating in metrological tests of special design devices and automatic monitoring facilities, assimilated in accordance with the plans for new equipment; the study of the operating properties of the SI, produced by domestic industry; develop local checking arrangements that establish the order of transferring the dimensions of units of

length and angles from Gosstandart standards and master SI to working SI used at the plant, as well as for the entire list of SI products made by the plant.

The Central Metrological Service (Department of Chief Metrologist) at the plant was organized according to the "Regulation on Metrological Service of the Minstankoprom" and typical regulations of the Gosstandart on departmental metrological services. The creation of a centralized metrological service made it possible to implement a single policy in the area of metrology, create and introduce a metrological production control system and conditions where the head of the metrological service is responsible for all kinds of measurements, the right SI selection, metrological supervision over the measuring equipment and the introduction of new SI.

At the "Kalibr" Plant, as in many other enterprises of the Minstankoprom, the Department of the Chief Metrologist (OGM) was organized on the basis of a central measurements laboratory and the KIP[Monitoring measuring devices] service.

The specialization of the OGM subdivisions (see arrangement) by individual sections of the MO of production provided a single approach to the problems of the metrological preparation for production,and the fullest and most efficient utilization of metrologists-specialists.

The OGM puts special importance on the expert metrological analysis of design and technological documentation which permits solving beforehand the problems related to the MO development and product manufacturing, i.e., to determine the possibility of the accuracy of the monitoring norms called for in the documentation, evaluate the authenticity of the established methods, determine the necessity for developing facilities and methods for measurements, as well as providing the necessary conditions for production and testing.

One of the most important aspects of MO for production is developing and introducing nonstandardized SI and monitoring-measuring fixtures. In our opinion, the greatest effect in solving these problmes may be achieved when OGM designers become involved in developing the indicated SI. In this case, proper planning and the timely design of the SI; the measurement arrangements of units and parts of monitoring-measuring fixtures should be standardized.

The large product list of parts and units with similar measured parameters should be taken into account.

The efficiency of this approach is confirmed by the experience of several other Minstankoprom enterprises, especially the Kaunass Plant imeni Dzerzhinskiy [1]

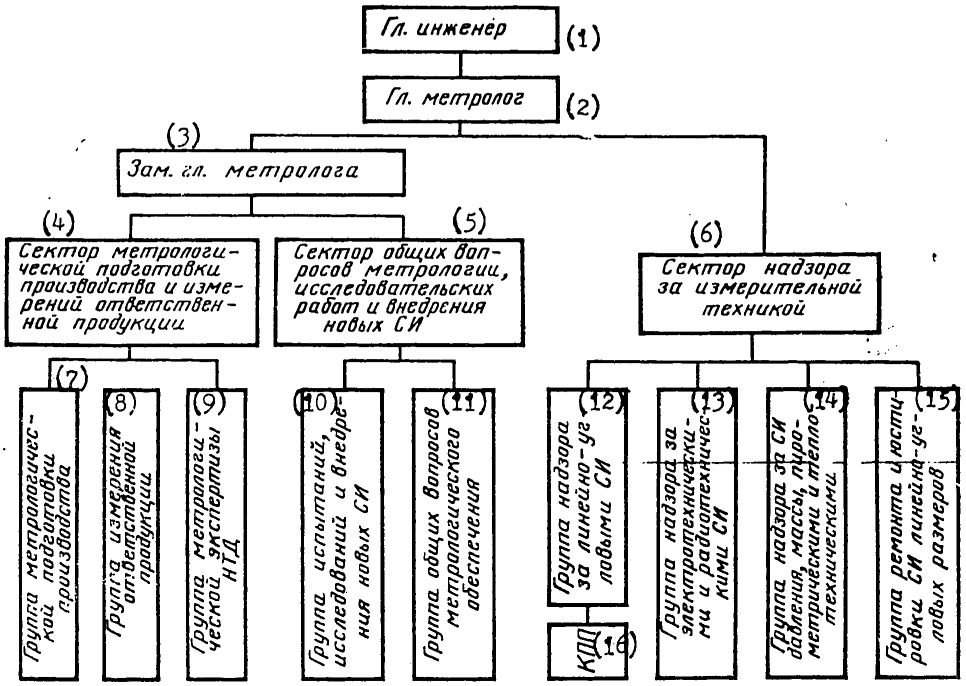

1. Chief engineer
2. Chief metrologist
3. Deputy chief metrologist
4. Sector for metrological preparation for production and measurements of critical products
5. Sector for general metrological problems, research and introduction of new SI
6. Sector for supervision of measuring techniques
7. Group for metrological preparation for production
8. Group for measuring critical products
9. Group for metrological expert analysis NTD [Norm-technical documentation]
10. Group for testing, investigating and introducing new SI
11. Group for general questions on metrology
12. Group for supervising linear and angular SI
13. Group for supervising electric and radio SI equipment
14. Group for supervising pressure, weight, pyrometric and heat SI
15. Group for repair and adjustment of SI for linear and angular measurements
16. KPP [Control and check point]

At present a design bureau was organized at the OGM of the plant. In addition to developing nonstandard SI and monitoring-measuring fixtures, it is involved in problems of introducing in production active and automatic monitoring, and developing technical tasks on designing special complex SI.

Since 1977, certification was introduced in the Minstankoprom system to improve the MO [2]. The certificate, which is the basic document that characterizes the state of the MO at the enterprise on 1 January of each year, includes information on the structural subdivisions of the metrological service and data on cadres, rooms, master and working SI etc.

The introduction of MO certificates, besides obtaining authentic and operational information on the state of the MO in the industry, permits the metrological service of the enterprise to evaluate the development of the MO and the results of the work of the metrological service and to detect shortcomings.

The MO system is a component part of the KS UKP [expansion unknown] introduced at the plant. At present, a number of STP [expansion unknown] operate at the plant. They regulate the order of the MO of production, in particular, the metrological supervision of the SI; plant monitoring tests; expert metrological analysis of design and technological documentation; development and manufacturing monitoring-measuring fixtures; methods and facilities for checking the SI produced by the plant etc.

Solving MO problems of production of precision measuring equipment is impossible without highly skilled metrologists. The enterprise has a continuous system for preparing metrologists-specialists and raising their skills. All OGM inspectors and metrology technicians are trained in courses to increase their qualifications according to two programs. The first includes a general course on the principles of the interchangeability theory, metrology and the technique of linear measurements; the second -- a course on the organization and methods of checking certain kinds of the SI.

Study in these courses is stimulated by an order established at the plant, according to which the class of inspector is raised depending upon the results of the training. Engineers-metrologists raise their skills by studying at the institutes of the Minstankoprom or Gosstandart for raising these skills.

The metrological service of the "Kalibr"Plant is developing scientific-technological cooperation with leading metrological organizations in the country.

At present, metrological and technical services and the entire "Kalibr" Plant collective are faced with critical problems related to raising the technical standards and quality of output. These problems can be solved by metrological control in developing new products, expert metrological analysis

of design and technological documentation at all stages of production, the assimilation of the latest measurement techniques and measurement methods and the improvement of metrological supervision of the SI etc.

1. IZMERITEL'NAYA TEKHNIKA, No 5, 1977 pp 7-21.

2. Markov, N. N.; Zinin, B. S., IZMERITEL'NAYA TEKHNIKA, No 8, 1977.

[56-2291]

2291
CSO:1860

Instruments, Measuring Devices and Testors;
Methods of Measuring

UDC 535.214.4

PLANE RADIOMETERS MADE WITH SEMICONDUCTOR DEVICES

Moscow RADIOTEKHNIKA in Russian No 9 1979, signed to press 23 Jan 79
pp 42-45

[Article by A. G. Semin, Yu. B. Khapin, A. N. Sharapov]

[Text] In radiometric investigations from planes of the atmosphere and underlying surfaces, multifrequency measuring methods are the most preferable. They make it possible to increase the measurement accuracy of geophysical parameters and approach the measurement of atmosphere and surface parameters as a single problem of remote sounding.

In creating radiometric complexes that span a broad range of frequencies, including the shortwave part of the millimeter range, difficulties arise that are related to the implementation of simple and reliable systems with high sensitivity and stability. One promising way to overcome these difficulties is the use of semiconductors. At present, semiconductor radiometers can be made for the entire millimeter range of wavelengths.

The IKI [Institute of Space Research] of the USSR AN developed a complex of semiconductor radiometric receivers of the superheterodyne type with mixers at the input for experimental investigations of the atmosphere and underlying surfaces. The radiometers operate at frequencies of 89 gigaHz (λ = 0.34 cm), 37 gigaHz (λ = 0.8 cm) and 20 gigaHz (λ = 1.5 cm). The radiometers showed high operational characteristics during the operation of the complex under various seasonal and climatic conditions. A brief description of the radiometers and their individual units is given below.

Radio meter for an 0.34 cm wavelength. The special features of a radiometer: transfer output modulation to an intermediate frequency (PCh) and use a mixer operating on the second harmonic of the heterohynes* [3]. The noted features made it possible to reduce losses considerably in the input channel due to the breakdown of the SVCh [Microwave frequency] modulator

* In literature, they are sometimes called mixers with subharmonic pumping.

and the decoupling devices, as well as to use a semiconductor heterodyne with an avalanche-transit diode, operating at 40 gigaHz. The block diagram of the radiometer is shown in Fig. 1, where the following designations are used: S -- mixer; M -- modulator; G -- heterodyne; A -- Attenuator: ST -- system for stabilizing the mixer current; GSh -- noise oscillator; PU and UTD -- parametric and tunnel amplifiers; D -- detector and preliminary UNCh [Ultralow frequency]; F -- Faraday switch of polarization plane; NF -- directional filter; V -- rectifier; K -- signal switches; R -- recorder; BP -- power supply units.

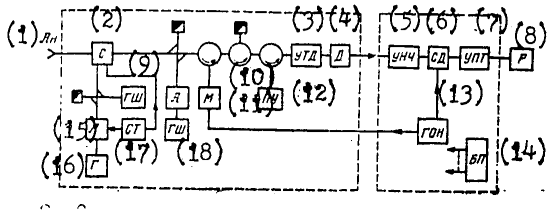

Fig. 1

1. Ln [line]
2. S
3. UTD
4. D
5. UNCh
6. SD
7. UPT
8. F
9. GSh
10. L
11. M
12. PU
13. GON
14. BP
15. A
16. G

The basic sources of the instability of the radiometer with PCh modulation are: the mixer, the transmission coefficient and the external noise temperature which depends on the heterodyne input power. The problem of obtaining a highly stable receiver with PCh modulation may be solved by two methods: by designing a mixer insensitive to changes in heterodyne power or by the rigid stabilization of the heterodyne power. In [3], a calculation is given of the allowable instability of the heterodyne power, which should not exceed 0.025% at a sensitivity of the PCh channel of 0.05K at the modulator input. In the experimental modulator, described there, a heterodyne power stabilization system that would maintain the mixer input power with the required accuracy was used.

A more efficient method for eliminating the effect of the instability of the heterodyne power on the mixer operation is the use of a system to stabilize the operating currents of the mixer. The system operates in the following manner. The initial shift of the operating point of the mixer diode is provided by the stable voltage source. A reference resistor is placed in the DC circuit of the diode; voltage changes across the resistor, related to the heterodyne power changes, control an amplifier in whose input circuit is placed an attenuator for regulating the transmission coefficient of the heterodyne channel. The instability of the mixer operating currents in this device was $< 0.01\%$ for a heterodyne voltage changes of $\pm$ 25%.

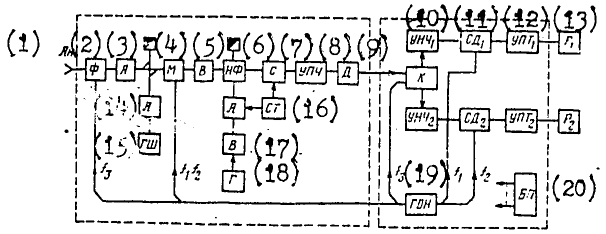

Fig. 2

1. Ln (line)
2. F
3. A
4. M
5. V
6. NF
7. S
8. UPCh
9. D
10. $UNCh_1$
11. CD_1
12. UPT_1
13. R_1
14. A
15. GSh
16. ST
17. V
18. G
19. GON
20. BP

A signal is sent to the diode in the mixer over a 2.4 x 1.2mm^2 waveguide which is reduced to a third in the connection plane of the diode. The heterodyne voltage is brought to the mixer over a 5.2 x 2.6mm^2 waveguide. Transformed PCh signal passes through a low frequency filter (FNCh) into a 23 x 2mm^2 waveguide and then to an intermediate frequency channel. A Schottky barrier diode (DBSh) with parameters: series resistance

R_s = 10 ohms and barrier capacitance C_o = 0.022 picofarads, were used in the mixer. The mixer operates in a single-band mode.

The first UPCh stage is a degenerated parametric amplifier in the 3-cm range with a noise temperature of 150K and a 13db amplification coefficient. The following three UPCh stages are tunnel diode amplifiers. The total UPCh amplification coefficient is equal to 52db with a non-uniformity of about 15db in the amplitude-frequency characteristic (AChKh).

Radiometer for 0.8cm wavelength. This radiometer receives radiation from one of two orthogonal polarities as well as simultaneously from both polarities. As may be seen from the block diagram (Fig. 2, where the designations are the same as in Fig. 1), the receiver has only one receiving antenna that receives radiation in two orthogonal planes and one SVCh channel. The switching of the antenna for receiving one of the polarities is done by a switch operating on the Faraday effect basis.

When the polarities are received simultaneously in two planes, a three-frequency signal selection method of different polarities is used. A frequency of $f_1 = f_o$ voltage is sent to the synchronism detector of the first channel from a reference voltage oscillator, and frequency $f_2 = f_o/2$ voltage is sent to the second synchronism detector. The Faraday switch switches the antenna from one polarity to the other with a frequency of $f_3 = f_o/32$. A frequency f_1 modulating voltage is applied to the modulator during the first half period $T_3 = 1/f_3$ and an f_2 frequency voltage is applied during the second half period T_3. The signal selection of various polarities is done by synchronism detectors and signal switches that switch corresponding inputs of the low frequency channels at a frequency of f_3. Frequencies f_1, f_2, f_3 are rigidly synchronized. Decoupling between various polarity channels is about 25db and is determined basically by the decoupling properties of the Faraday switch. The use of signal switches is not compulsory. Switching period T_3 of the antenna is selected so that during time $T_3/2$ the spot of the radiation pattern is shifted by not more than 2% when the plane is at a height of about 300m.

The transformation of the signal frequency into the intermediate frequency is done by a single diode mixer with an encased diode (DBSh). The waveguide height (cross section 7.2 x 3.4mm) was reduced to 1/6-th in order to match the impedances at the mixer input. The signal and the intermediate frequencies are separated by a band FNCh. To stabilize the operating mode of the mixer, a stabilizing system of mixer operating currents is used which is similar to the 0.3-centimeter channel.

A Hanna diode oscillator is used as a heterodyne. Noise suppression of the heterodyne is done by single-resonance directed filter with the following parameters: central frequency of the filter -- 37.1 gigaHz; passband at 3db -- 100 megaHz; transit attenuation -- about 2.6db; directivity -- about 7eb; losses in the direct channel outside the band $<$ 0.1db.

The use of a high Q-factor directional filter made it possible to utilize a comparatively low frequency transistor amplifier for the intermediate frequency with the following characteristics: operating range -- 300 to 1000 megaHz; amplification coefficient about 55db; nonuniformity of the amplitude-frequency characteristic -- 1.5db; integral noise coefficient -- about 3.9db.

It should be noted that with simultaneous reception on the two polarities, the radiometer sensitivity is halved.

Radiometer for 1.5cm wavelength. The radiometer is made with a circuit similar to Fig. 2. It was designed for receiving the radiation of only one polarity. It has no Faraday switch and no second low frequency channel.

The radiometer uses a two-diode mixer with opposite connection of the diodes, similar to the one described in [4]. The special feature of this mixer is the separation of odd ($n\omega_r \pm \omega_0$; $n = 1, 3, 5, \ldots$) and even ($n = 0, 2, 4, \ldots$) combination frequencies into orthogonal modes, with the odd having a waveguide type of oscillations and the even -- coaxial. Thus, decoupling is provided between the signal and the intermediate frequencies. Encased barrier Schottky diodes are used in the mixer. A Hanna oscillator is used as a heterodyne, frequency stabilized by a high Q-quality resonator. Heterodyne noise suppression is done by means of a directional filter with the following parameters: central frequency of the filter -- 20.1 gigaHz; passband at 3db level -- 50 megaHz; transit attenuation -- about 2.4db; directivity -- about 7db.

The intermediate frequency amplifier has the following characteristics: operating frequency range -- 250 to 260 megaHz; amplification coefficient -- about 55db; AChKh nonuniformity -- 1.5db; integral noise coeffient -- about 3.6db. In all other respects, the radiometer is similar to the 0.8cm receiver.

Attenuators made with p-i-n diodes are used as attenuators and modulators in the radiometers. Semiconductor noise oscillators using avalanche diodes are used for introducing noise when operating in the quasi-zero mode and calibrating the amplification coefficient. Power sources for important units of the radiometers have instability coefficients not worse than 10^{-4}.

Structurally, the radiometers are placed in thermally controlled housings on a rotary platform in a plane hatch. The platform makes it possible to measure rising radiation at angles of 0 to 45 degrees from the nadir. The radiometers have horn antennas with the width of the radiation pattern of 6° for a 3db level.

The basic characteristics of the radiometers and their units are shown in the Table where the designations are: losses in the antenna-feeder channel -- $L_{a.f}$; mixer transformation losses -- L_{cm} (for single-band reception for λ = 0.34cm and for two-band reception for λ = 0.8 and 1.5cm); noise coefficient -- F_{sh} and UPCh bandpass Δf; noise temperature T_{sh}. Radiometer sensitivities ΔT_m are measured aboard the plane by the difference of measured radio brightness temperatures at a time constant of one second of the integrating circuit and are reduced to the antenna input. The instability of the amplification coefficient δ K/K was measured for 5 hours of operation after an hour of heating.

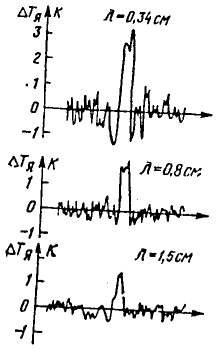

Fig. 3

Table

λ, см	(1) $L_{а.ф.}$, дБ	(2) $L_{см}$, дБ	(3) $F_{ш}$, дБ	(4) Δf, МГц	(5) $T_{ш}$, К	ΔT_m, К	$\delta K/K$, %
0,34	0,5	7	4	700	5900	0,3	5
0,8	1,5	2,7	3,9	700	2700	0,15	2
1,5	1,0	2,5	3,6	400	2100	0,15	2

1. $L_{a.f}$
2. db
3. F_{sh}
4. megaHz
5. T_{sh}

Fig. 3 shows an example of synchronous recording of a petroleum film on the Caspian Sea at the three wavelengths made on 24 May 1978.

In conclusion, the authors express their deep gratitude to V. S. Etkin for his constant interest and help.

BIBLIOGRAPHY

1. Basharinov, A. Ye.; Gurevich, A. A.; Yegorov, S. T. "Radio Radiation from Earth as a Planet," Moscow, Nauka, 1974.

2. Norman C. Grody. Trans. IEEE, 1974, v. AP-24, No 2.

3. Bordonskiy G. S.,et. al. Preprint IKI AN SSSR, Pr-321, Moscow, 1977, No 2565-77 Dep.

4. Baulin, V. A.; Strukov, I. A. "Second All-Union School-Seminar on Microwave Radio-Receiving Devices," Yerevan, 1974.

[35-2291]

2291
CSO: 1860

HIGH-FREQUENCY METHOD FOR MEASURING NONELECTRICAL QUANTITIES

Moscow VYSOKOCHASTOTNYY METOD IZMERENIYA NEELEKTRICHESKIKH VELICHIN (High-Frequency Method for Measuring Nonelectrical Quantities) in Russian 1978 signed to press 20 Sep 78 pp 2, 277-280

[Annotation and table of contents from book by Vladimir Andreyevich Viktorov, Boris Vasil'yevich Lunkin and Aleksandr Sergeyevich Sovlukov, Nauka, 2600 copies, 280 pages]

[Text] This monograph generalizes the results of studies and development of measuring devices for nonelectric quantities (level, amount, position of interfaces, continuity, small distances, flow rate, etc) using the properties of electromagnetic systems of distributed parameters (long lines, waveguides, resonators, etc). The authors discuss the fundamentals of the theory and the principles of the construction and use of measuring devices for general industrial and individual purposes.

Contents

[30-10,233]

10,233
CSO: 1860

Microelectronics [including microcircuits; integrated circuits]

UDC 62-503

ASSURANCE OF LINEARITY OF CONVERSION IN DEVELOPING LARGE-SCALE HYBRID INTEGRATED CIRCUITS OF A PRECISION ANALOG-DIGITAL CONVERTER

Moscow RADIOTEKHNIKA in Russian No 9, 1979 signed to press 2 Feb 79
pp 18-22

[Article by G. Ya. Gensirovskaya, A. A. Kotkin, A. V. Krivosheykin, V. I. Moskvitin, M. A. Stolypin]

[Text] The possibility of obtaining high indicators when making digital analog converters (TsAP) by microelectronic technology methods predetermines greatly the attention given them by microelectronics.

Depending upon the required TsAP characteristics, two technological directions became apparent for their realization: semiconductor -- for making relatively inexpensive compact TsAP; and hybrid-film -- for making multibit, high precision [1-5] TsAP. The TsAP theory is highly developed with respect to principles of operation and design [6]. However, there are a number of problems related to the organization of their production. Therefore, speaking about the special features of development, we will keep in mind the solving of the problem of BGIS*TsAP production. To obtain the basic TsAP parameters most fully (accuracy, linearity, fast action) [i] a BGIS TsAP (see Fig. 1) [7] based on the current summation principle is used.

We will consider the possibilities of the given implementation according to the basic characteristics when building with hybrid-film components, taking into account the existing technological standards.

The problem consists of the following:

identify TsAP parameters monitored in the process of production;

determine sources of errors of these parameters for a given TsAP and their quantitative evaluation;

*[Large-scale hybrid integrated circuits.]

consider methods for compensating for errors or technical methods for their elimination;

substantiate the expediency of using this or another method for error compensation.

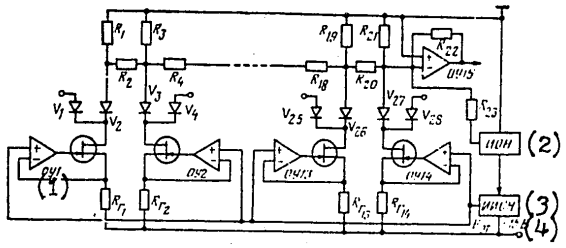

Fig.

1. OUI
2. ION
3. IION
4. Volts

For basic TsAP parameters, such as accuracy, linearity and fast action, the norms for the allowable errors are set for any code combination at the TsAP input. Thus, to monitor these parameters, it is necessary to consider all code combinations which, for an n-bit TsAP, is equal to 2^n. It is obvious that to measure the characteristic of each TsAP would require a long time and is unacceptable in series production. Therefore, an accuracy measurement is made at a limited number of points, permitted by GOST 14015-68, which, however, does not guarantee that requirements will be met at all points. The situation is complicated considerably for precision TsAP. Actually, the absolute accuracy of the TsAP output for any number of bits should not exceed ½ of the voltage, corresponding to the least significant digit (MZR) [6]. Even for 12 bits, the relative accuracy should be no worse than 0.012%. Apparatus should be used for measurement that has an accuracy corresponding to that of domestic devices for making metrological checks, which is impossible to achieve in production. The solution is considerably worse when the number of bits increases. Therefore, accuracy cannot be the parameter monitored in the process of production. A quantizing step can be used as such a parameter.

Let a sequence of binary digits (code combinations) be sent to the digital input of the TsAP, with each one of them numbered in increasing order $m=\overline{1, 2^n}$; n -- number of bits.

A stepped signal is formed at the TsAP output. Voltage differences $U^{(m)}$, $U^{(m-1)}$, corresponding to adjacent numbers in sequence m, m-1, are called quantizing steps Δ_m .

Linearity requirements designate the accuracy requirements of a quantizing step for any $m \in (1,2^n)$. Thus, by monitoring the parameter quality of a quantizing step, we will monitor the linearity.

We will prove that the number of monitoring points in a sequence of binary digits may be equal to n. We will write the expression for a quantizing step with number m:

$$\Delta_m = U^{(m)} - U^{(m-1)} = \sum_{j=1}^{n} b_j^{(m)} U_j - \sum_{j=1}^{n} b_j^{(m-1)} U_j, \quad m \in [1, 2^n]. \qquad (1)$$

where U_j -- voltage at the TsAP output, corresponding to a binary digit with one unit in the j-th bit; coefficients $b_j^{(m)}$, $b_j^{(m-1)}$ assume values 0 or 1 depending on the value of the corresponding bit in binary digits with numbers m and (m-1), while for $m = 1$ $b_j^{(m-1)} = 0, j = \overline{1, n}$. Since these number differ by unity, there is always such a number of bit k, for the considered binary digits, that:

1) the code combinations will coincide up to the (k-1)-th high order bit;

2) for the m-th code combination, the value of the k-th bit is 1, while the value of lower bits is equal to 0, i.e.,
$$b_k^{(m)} = 1, \; b_j^{(m)} = 0, \; j = \overline{k+1, n};$$

3) for the (m-1) code combination, the following relationships hold:

$$b_k^{(m-1)} = 0, \quad b_j^{(m-1)} = 1, \; j = \overline{k+1, n}.$$

Taking these properties into account (1) can be written in form

$$\Delta_m = \sum_{j=k}^{n} b_j^{(m)} U_j \sum_{j=k}^{n} b_j^{(m-1)} U_j = U_k - \sum_{j=k+1}^{n} U_j, \quad m \in [1, 2^n]. \qquad (2)$$

Since voltages U_k, $k = \overline{1, n}$ are independent, then in correspondence with (2) there are such n linearly independent quantation steps Δ_{mk}, $k = \overline{1, n}$, that any quantizing step Δ_m, $m = \overline{1, 2^n}$. coincides with one of them. The truth of the reverse assertion also follows from (2).

Therefore, it may be asserted that the linearity error of any quantizing step Δ_m, $m \in [1, 2^n]$, does not exceed a given value only when the error in n quantizing steps Δ_{mk} does not exceed the same value. Therefore, the necessary and sufficient number of monitoring points is equal to n, which was to be proven. Monitoring steps Δ_{mk} are formed by voltage differences at the TsAP output when only the k-th bit and simultaneously all preceding lower order bits are included.

Before proceeding to the study of the basic sources of errors, we will consider the circuit shown in the Figure in greater detail. Current oscillators, controlled by voltage $E_{эт}$ produce equal currents in each bit determined by formula

$$I_{rk} = E_{эт} S_k, \quad k = \overline{1, n}, \tag{3}$$

where $S_k = 1/R_{rk}$ -- transconductance of current oscillators; R_{rk} -- corresponding master current resistor of resistive matrix R_r; source of reference voltage (ION) and the inverting ION (IION) are intended respectively for obtaining a sign-changing voltage at the TsAP output and the voltage for reference source $E_{эт}$. Resistive matrix R-2R divides these currents at the TsAP output, and switches V_1, V_2, ..., 00 switch the oscillator currents in the bits.

The basic error sources in the TsAP parameters are:

1) errors in manufacturing components of resistor matrices R-2R and R_r;

2) input currents $I_{вх}$ and bias voltages $E_{см}$ of operational amplifiers (OU), used in current oscillators;

3) inverse currents $I_{обр}$ of the switching switches.

KP-308 field transistors in the diode connection are used as switches in such a way that the inverse current of the switches is equal to the shut-off current and does not exceed one nanoampere. This makes it possible to neglect the third source of errors. Sources of errors due to parameters OU-$E_{см}$, $I_{вх}$, in accordance with (3) may be reduced to equivalent deviations from nominal values of the master current resistors of current regenerators according to formula

$$\delta R^E_{rk} = -E_{см}/E_{эт}, \quad \delta R^I_{rk} = I_{вх}/I_{rk}, \quad k = \overline{1, n}, \tag{4}$$

where δR^E_{rk}, δR^I_{rk} -- equivalent relative deviations of resistors R_{rk}. Thus, in calculating the TsAP parameter errors, it is possible to consider only the effect of resistor matrices R-2R, R_r taking into account the equivalent errors in their components. This applies also to the determination of the temperature relationships.

Here the following values were assumed: $E_{эт}$ = 10 v, I_{rk} = 1ma; R_{rk} = 10 kohms (S_{rk} = 10^{-4} ohms), k = $\overline{1.14}$; resistances of the matrix resistors R-2R are equal to one to two kohms.

Substituting these values into (4), as well as typical values [8] for OU- $|E_{CM}| \leq$ 8 mv, $I_{BX} \leq$ 50 nanoamperes, we will obtain for the current resistor evaluations:

$$|\delta R^{E}_{rk}| \leqslant 0{,}08\%,\ |\delta R^{I}_{rk}| \leqslant 0{,}005\%.$$

The random deviation of the value of each component is the sum of two independent random values [9]. The first of them is common to all components and may assume large values. The second is individual and determines the error in the ratios of component values. Since the errors in the TsAP characteristics are determined basically by the errors in the ratios, we will keep in mind the second error component. At the existing technological level, with the individual adjustment of resistors, it is possible to obtain an accuracy of 0.01% which corresponds to an error value in manufacturing resistor matrices of

$$|\delta R| \leqslant 0{,}005\%.$$

We will consider the possibilities for reducing parameter errors of the TsAP due to errors in its components. Obviously, up to a certain level, the accuracy of the TsAP parameters may be insured only by the precision of manufacture. In the following, the effect of uncontrolled OU errors in the production of the TsAP becomes essential. At this stage, an additional technological operation -- functional (selective) assembly [10, 11], may be introduced to meet parameter requirements. It consists of finding those that have small errors among the UO and installing them in current oscillators of several of the higher order bits. The remaining ones are installed in oscillators of the lower order bits. A further reduction in TsAP parameter errors is possible only by using functional tuning as a compulsory stage in the technological production process [3,5]. In this case, the necessity for making accurate resistor matrices is eliminated; however, the functional assembly must be maintained because it solves the problem of temperature stability of the TsAP parameters [12].

Therefore, the error value in the TsAP parameters, at which it is sound practice to introduce the functional assembly and then functional tuning is of great importance. A method described in [13] solves the problem of synthesizing tolerances in the TsAP components for accuracy requirements at each quantizing step equal to 1/3 MZP. The Table shows the calculated values for the tolerances in percentages for the TsAP components for various numbers of bits.

(1)

Число разрядов	(2) Элементы										
	R_1-R_9	R_{10}	R_{11}	R_{12}	R_{13}	R_{14}	R_{15}	R_{16}	R_{17}	R_{18}	R_{19}
8	1	0,90	1	0,50	0,75	0,40	0,19				
9	1	0,72	1	0,38	1	0,22	0,33	0,16	0,083		
10	1	0,65	1	0,33	1	0,18	0,63	0,10	0,150	0,077	0,038
11	1	0,59	1	0,29	1	0,15	1	0,08	0,280	0,017	0,071
12	1	0,55	1	0,27	1	0,14	1	0,072	0,550	0,038	0,13
13	1	0,50	1	0,26	1	0,13	1	0,065	1	0,033	0,25
14	1	0,49	1	0,25	1	0,12	1	0,06	1	0,031	0,50

Число разрядов	Элементы									
	R_{20}	R_{21}	R_{22}	R_{23}	R_{24}	R_{25}	R_{26}	R_{27}	$R_{r1}-R_{r3}$	R_{r4}
8									1	1
9									1	1
10									1	1
11	0,035	0,018							1	1
12	0,022	0,033	0,017	0,008					1	1
13	0,018	0,063	0,01	0,016	0,008	0,004			1	1
14	0,016	0,12	0,009	0,03	0,005	0,007	0,004	0,002	1	0,96

Число разрядов	Элементы									
	R_{r5}	R_{r6}	R_{r7}	R_{r8}	R_{r9}	R_{r10}	R_{r11}	R_{r12}	R_{r13}	R_{r14}
8	0,74	0,37	0,18	0,09						
9	0,66	0,33	0,16	0,08	0,041					
10	0,60	0,30	0,15	0,077	0,038	0,019				
11	0,56	0,28	0,14	0,07	0,035	0,017	0,008			
12	0,54	0,27	0,13	0,067	0,033	0,016	0,008	0,001		
13	0,50	0,25	0,12	0,06	0,03	0,015	0,008	0,001	0,002	
14	0,48	0,24	0,12	0,06	0,03	0,015	0,008	0,004	0,002	0,001

1. Number of bits 2. Components

By comparing these results and the error values cited above, the following conclusions can be made:

1. Required TsAP parameters with a number of bits not greater than eight may be provided by accurate manufacturing of resistor matrices.

2. Functional assembly must be introduced for a number of bits greater than nine.

3. Functional tuning must be introduced for a number of bits 12 and greater, with tolerances of 1% allowed for components of the resistor matrices R-2R and R_r.

We will now evaluate the possibility of introducing a functional assembly for the 11-bit TsAP.

For simplicity, we will neglect errors in manufacturing resistors of matrix R_r.

From the data in the Table, it follows that in higher order bits, it is necessary to install OU with equivalent deviations of resistors

$$|\delta R^E_{r1}| \leq 0{,}008\%, \quad |\delta R^E_{r2}| \leq 0{,}017\%, \quad |\delta R^E_{r3}| \leq 0{,}035\%, \quad |\delta R^E_{r4}| \leq 0{,}07\%,$$

which correspond to the following requirements to bias voltages

$$|E_{см1}| \leq 0{,}64 \text{ мВ}, \quad |E_{см2}| \leq 1{,}36 \text{ мВ}, \quad |E_{см3}| \leq 2{,}8 \text{ мВ}, \quad |E_{см4}| \leq 5{,}6 \quad \text{mB = m volts.}$$

We will assume a normal distribution law for bias voltages and a value of 3 σ for the boundary value $|E_{см}| = 8$ m volts. Then, to an accuracy of 0.99, it may be stated [14] that for 100 units from 1100 units of TsAP, not less than 179 OU will meet the requirements of the first higher order bit; not less than 391 -- of the second; not less than 741 -- of the third and not less than 1045 -- of the fourth higher order bit. Since the required number of OU is 100 for each bit, cited evaluations attest to the actual possibility of introducing the functional assembly with a considerable surplus of OU available in a lot above the required number.

It should be noted that monitoring the quantizing steps, i.e., the conversion linearity, in the process of production does not guarantee meeting requirements of other parameters, for example, the value of the transconductance of the conversion characteristic. When this parameter is important, tuning of the transconductance should be introduced along with other adopted measures for insuring linearity, by using resistor R_{22} of the input OU (see Figure) for this purpose.

The investigation made it possible to develop a microcircuit for the TsAP, which is a hybrid integrated circuit of the third degree of integration and has over 800 components. All components are connected to the switching board and housing crosspieces by wires. A ceramic 30 x 48mm substrate is used to made a two-layer thick-film switching plate. Electron beam piercing of holes in the ceramic substrates with the following metallization of the holes by stenciling them is used as a basis for the technology of forming interlayer switching of components. The BGIS TsAP is made in a metal-glass housing with 40 pin terminals with an average distance of 2.5mm between them.

The measured parameters of the manufactured samples of BGIS TsAP using functional assembly meet linearity requirements of 12 bits in a temperature range of -60 to +80°C, which is very close to the evaluations cited above. The power used does not exceed 0.8 watts and the setting time does not exceed eight microseconds.

Thus, the results obtained in this paper make it possible to solve problems related to manufacturing TsAP. In spite of the concreteness of the examples, a number of conclusions are general enough and, in that sense, serve as an addition to the information known in theory.

In conclusion, the authors express their gratitude to R. I. Grushvitskiy, S. M. Pavlov, O. N. Selyutin, S. M. Tolpygo and G. P. Shlykov for the useful contacts with them that facilitated the clarification of the essence of the considered problems.

BIBLIOGRAPHY

1. Malinin, V. V. "Electron Equipment Reviews," series 3. MIKROELEKTRONIKA. Issue 3 (467), Moscow, TsNII, ELEKTRONIKA , 1977.

2. Koyl. -- ELEKTRONIKA, 1977, v. 50, No 15.

3. "Fourteen-Bit TsAP for Operation in the Oto 70°C Range." ELEKTRONIKA, 1977 v. 50, No 15.

4. Mattera. ELEKTRONIKA, 1977, v. 50, No 18.

5. "Analog-Digital Converter with Setting Time of 200 Nanoseconds," ELEKTRONIKA, 1977, v. 50, No 21.

6. "Microelectronic with Digital-Analog and Analog-Digital Data Converters," Edited by V. B. Smolov, Energiya, 1976.

7. Mel'nichenko, A. T.; Lundin, V. A. Rakhmanin, N. M.; Kotov, B. A. "Information Sheet," No 602-76. Leningrad, LMTTsNTIiP, 1976.

8. Balakay, V. G.; I. P. Lukyanov, L. M. "Integrated ATsP and TsAP Circuits," Energiya, 1978.

9. "Integrated Circuits" translated from the English. Edited by K. I. Martyushov, Moscow. SOVETSKOYE RADIO, 1970.

10. Ponkratov, L. V. et al. "Communications Facilities Equipment," series Radio Measuring Equipment, 1977, issue 2.

11. Lopukhin, V. A. in book "Design-Technological problems in Micro-miniaturization of Radio Electronic Apparatus." Leningrad, LETI, 1977, issue 114.

12. Galimova, R. G. "Radio Electronics Abroad." 1976, No 5.

13. Krivosheykm, A. V. IZVESTIYA VUZOV SSSR, series Radioelektronika, 1977, v. 20, No 12.

14. Van-der Varden, B. L. "Mathematical Statistics." Moscow, IIL, 1960.

[35-2291]

2291
CSO: 1860

Radars, Radio Navigation Aides, Direction Finding

UDC 621.396.96

SUPERREGENERATIVE DETECTOR

Moscow RADIOTEKHNIKA in Russian No 9, 1979 signed to press after completion 10 Apr 79 pp 50-53

[Article by G. I. Kravchenko, V. L. Gurevich, L. P. Mochalina]

[Text] Problems are considered in [1] of the interference stability of a superregenerative pulse signal receiver. An analysis is given below of a superregenerator acoustic locator, the block diagram of which is shown in Fig. 1, intended for detecting objects in a given zone (in a given distance element). The designations in the Figure are: 1 -- supergenerator (GS), 2 -- superregenerator (Sr); 3 -- threshold device (PU), 4 -- receiving-transmitting acoustic converter (Pr), 5 -- object.

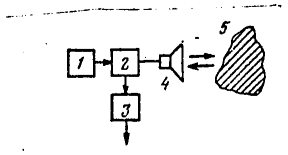

Fig. 1

Principle of locator operation. If there is no object in the detection zone, Sp operates in a linear mode by its internal or external noises and its output pulses (flashes) have a low altitude, fluctuating around an average value A_a. The appearance of an object (target) in the zone leads to an origination of a positive feedback (reflected pulses enter the Sr at the moment of generation of successive flashes) which produces an incremental pulse process in the system, that ends at some level A_p when the mechanism for limiting the amplitude becomes active in the Sr.

When the object leaves the detection zone, a change occurs during one period of supergeneration of large (amplitude A_p) to small (amplitude A_n) oscillations. PU compares the flash amplitude with a given level and produces an answer on the presence of a target.

As follows from the principle of operation, the locator has an adaptivity with respect to the radiated power: in the absence of a target it radiates comparatively low power which increases only when the object appears. Ratio $D = A_p/A_a$ is the measure of adaptivity.

We will determine the characteristics of the detection device, using equation (1) with designations given in [1], assuming that R(t) takes into account the negative resistance changing with time and, moreover, internal losses and losses introduced by the acoustic converter; $\mathcal{E}(t)$ is the emf of the acoustic converter translated to the Sr circuit. We will find the output voltage u(t) (voltage across capacitance Sr) in the form.

$$u(t) = q(t)/C = a(t)\sin\omega_0 t - b(t)\cos\omega_0 t, \qquad (1)$$

where $\omega_0 = 1/\sqrt{LC}$ -- internal frequency of Sr. We consider that the continuous law of supergeneration $\delta(t) = R(t)/2L$ provides for a single start of Sr and satisfies requirement $\delta(t) < 0$ for $t_2 < t < t_4$, $\delta(t) > 0$ for $t_4 < t < t_2$, while $2\delta(t)/\omega_0 \ll 1$.

By analogy with [1], by the method of slowly changing amplitudes [2] and using the procedure of partial contraction [3] we find

$$\begin{pmatrix} a(t) \\ b(t) \end{pmatrix} = K_c h_2(t)\,\omega_0 \int_{-\infty}^{t} h_1(t)\,\varepsilon(t) \begin{pmatrix} \cos\omega_0 t \\ \sin\omega_0 t \end{pmatrix} dt, \qquad (2)$$

where

$$K_c = \exp\int_{t_4}^{t} \delta(t)\,dt$$

-- amplification coefficient due to superregeneration;

$$h_1(t) = \exp\int_{t_1}^{t} \delta(t)\,dt;\quad h_2(t) = \exp\int_{t}^{t_4} \delta(t)\,dt.$$

To obtain high interference stability, we will require that voltage u(t) coincides with the optimal input signal of Sr, found in [1] for the case of receiving signals with a background of white noise, to a precision up to a constant shift. We will call an Sr, meeting this requirement, self-matched. As follows from [4], the properties of a self-matched Sr coincides with the properties of a linear undistorting active quadripole without demodulation.

We will determine the supergeneration law that provides for self-matching. For this purpose, we will select on the time axis, points t_1, t_s and t_5 so that the following equation is fulfilled

$$\int_{t_1}^{t_2} \delta(t)dt - \int_{t_2}^{t_3} \delta(t)dt - \int_{t_4}^{t_5} \delta(t)dt - \int_{t_4}^{t_5} \delta(t)\,dt = \ln \sqrt{K_c}.$$

We will also assume that $\sqrt{K_c} \gg 1$. This provides a basis, assuming error $\mu = 1/\sqrt{K_c}$ in the determination of

$$\begin{pmatrix} a(t) \\ b(t) \end{pmatrix}$$

and neglecting the values of

$$\begin{pmatrix} a(t) \\ b(t) \end{pmatrix},$$

smaller than

$$\mu \begin{pmatrix} a(t_4) \\ b(t_4) \end{pmatrix},$$

to replace functions $h_{1,2}(t)$ in (2) by simpler (contracted) relationships $H_{1,2}(t)$ that correspond to

$$H_1(t) = h_1(t),\ t_1 \leqslant t \leqslant t_2,\ H_1(t) = 0,\ t_2 < t < t_1,$$
$$H_2(t) = h_2(t),\ t_3 \leqslant t \leqslant t_5,\ H_2(t) = 0,\ t_5 < t < t_3.$$

If the supergeneration law δ (t) is selected so that the following relationship is fulfilled

$$H_1(t) = H_2(t - \tau_c) = H_0(t), \qquad (3)$$

where $\tau_c = t_4 - \tau_2$. Sr converts, to a precision up to a constant shift in phase to fill the flash, into an undistorting linear active quadripole without demodulation, i.e., it becomes self-matched.

Actually, assuming that instead of (1) at the Sr output, the following process takes place

$$u(t) = a(t)\cos(\omega_0 t + \varphi) + b(t)\sin(\omega_0 t + \varphi),$$

where $\varphi = -\omega_0\tau_c$, the formula that ties u(t) and $\varepsilon(t)$ can be written thus:

$$u(t) = \omega_0 K_c \left[H_0(t-\tau_c)\cos\omega_0(t-\tau_c)\int_{-\infty}^{t} H_0(t)\,\varepsilon(t)\cos\omega_0 t\,dt + H_0(t-\tau_c)\sin\omega_0(t-\tau_c)\times\right.$$
$$\left.\times\int_{-\infty}^{t} H_0(t)\,\varepsilon(t)\sin\omega_0 t\,dt\right].$$

This is the algorithm of the sought for quadripole, supplemented by an amplifier with amplification coefficient K_0. For multiple incoherent (independent) starts with period T_c we have

$$u(t) = \omega_0 K_c\left[H_0(t-nT_c-\tau_c)\cos\omega_0(t-\tau_c)\int_{t-\tau_c}^{t} H_0(t-nT_c)\,\varepsilon(t)\cos\omega_0 t\,dt + \right.$$
$$\left. + H_0(t-nT_c-\tau_c)\sin\omega_0(t-\tau_c)\int_{t-\tau_c}^{t} H_0(t-nT_c)\,\varepsilon(t)\sin\omega_0 t\,dt\right], \qquad (4)$$

where n = o, 1, 2, ... -- number of starts.

The functional circuit, implementing algorithm (4), is shown in Fig. 2 (within the broken line). We will call this circuit a mathematical model of a self-matched Sr.

We obtain the model of the detector as a whole (the linear version) by supplementing the Sr with delay line τ_{u_1} and attenuator β (Fig. 2). Delay line τ_{u_1} is equal to the delay of the reflected signals, while the value of β corresponds to the ratio of the amplitudes of the probing and reflected pulses at the Pr terminals. Thus, the detector represents a closed pulse system whose two links take into account the characteristics of the object.

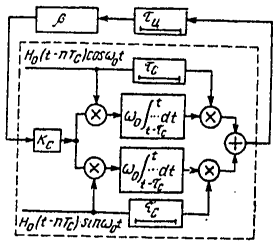

Fig. 2

We will open the circuit in Fig. 2 between attenuator β and amplifier K_c and will make the following experiment mentally. We will send to the amplifier input a sequence of pulses $B_1 H_0(t-nT_c-\tau_u-\tau_c)\cos(\omega_0 t+\psi)$, B_1, $\psi=\text{const}$, measure amplitude B_2 of pulses at the attenuator output. We will designate ratio B_2/B_1 by S. Then, we will change τ_{u_1} and β simultaneously to reproduce a discrete radial movement of the target after which we repeat the measurement of S. After a number of similar tests, we will obtain relationship $S(\tau_{u_1})$, which in correspondence to (4) should have the form

$$S(\tau_u) = \text{const}\,\beta(\tau_u)\,S_0(\tau_u - mT_c - \tau_c),\quad S_0(\tau_u) = \int_{-\infty}^{\infty} H_0(y-\tau_u)\,H_0(y)\,dy,$$

where m = 1, 2, 3, ... -- numbers of the detection zone; $\beta(\tau_{u_1})$ -- function of attenuation of β with the delay time.

Returning to the closed circuit, we conclude that it will lose stability in intervals $\Delta\tau_{u_1}$, where (y)

In a real locator, there exists some mechanism for limiting the amplitude at level A_p. In this case, stability regions (τ_{u_1} outside of intervals $\Delta\tau_{u_1}$) will coincide in the linear and nonlinear cases. As far as values of τ_{u_1} within intervals of $\Delta\tau_{u_1}$ are concerned, a stable state with amplitude A_p corresponds to the instability of the linear circuit, in a nonlinear device here. Thus, we may consider a superregenerative locator a device whose stable state with respect to the amplitude of the radiated pulses has two levels -- 0 and A_p, with the "switching" of the system from state "0" to state "A_p" (and conversely) being done by movement of the target.

We will determine the detection characteristics. For this, we will assume that the Sr input receives, besides reflected signals e(t), also normal delta-correlated noise η (t) with a two-sided spectral density N_0. We will consider the simplest situation where the target appears at the center of any detection zone.

Since a self-matched Sr implements a quadratic-correlation processing of mixture e(t) + η (t), detection characteristics of the considered locator coincide with the similar characteristics of a monopulse locator which is equipped with a quadratic-correlation receiver and radiates a pulse coinciding with flash Sr in the mode of large oscillations. The system differs from the indicated locator by the detection time and the presence of a threshold for the reflection area of the targets.

Detection time $T_{o\delta_H}$ is practically equal to the duration of the circuit transition from the zero state to the state with amplitude A_p. We will use recurrent formula $A_i = S(\tau_u)A_{i-1}$, where A_i and A_{i-1} are amplitudes of the i-th and (i-1) flashes during the transition process for calculating $T_{o\delta_H}$. It follows from the formula that

$$T_{обн} = T_c \frac{\ln D}{\ln S(\tau_u)}. \qquad (5)$$

The expression found not only evaluates $T_{обн}$, but also shows that the system has a threshold for the target reflection area. The threshold condition is inequality $S(\tau_u) > 1$: targets that have an insufficient reflection area and do not meet the requirements of this inequality are not detected.

Thus, compared to the traditional locator which is equipped with a quadratic-correlation receiver and radiates one pulse which coincides with flash Sr in the large oscillations mode, the considered device has a greater detection time [see (5)] and, moreover, is characterized by a threshold effect in accordance with the reflection area of the targets. These properties are a "price" for the adaptivity.

For objects in the center of any detection zone, condition $S(\tau_u) = 1$ will be fulfilled, if $E_c = 2N_0$ where E_c is the energy of the reflected signal at the Sr input. An experimental check of this condition is a convenient method for determining the interference stability of the system (closeness to the quadratic-correlation device).

A capacitive acoustic head with a 10^o radiation pattern was used in the laboratory model of the detector. Along with units shown in Fig. 1, the model included a voltage converter that provided a constant bias of 100 volts to the head. The PU role was fulfilled by an amplitude detector, a DC amplifier and a photodiode indicator. The device was fed by a 4.5 volt battery and consumed two milliamperes. The GS (multivibrator) had T_c regulation limits from 6 to 100 milliseconds; the Sr (natural frequency 25k Hz) was designed in accordance with the circuit shown in [5]. The self-matching mode was obtained by measuring $H_{1,2}(t)$ characteristics and selecting components of the device to meet condition (3). The following experimental data was obtained: maximum detection range of an object with a reflection area -- 20m (D = 6db), minimum range -- 1.5m (D = 46db), adaptivity D = 40db at a distance of 4m.

To evaluate the interference stability of the system, the object was located in the center of the first detection zone; then the amplification of Sr was reduced to a level at which the circuit "switched over" to the small oscillation mode. The period of T_c was changed and voltage from head Pr was fed to a measuring amplifier with a passband equal to the noise band of Sr. The signal/noise ratio was evaluated at the amplifier output and threshold condition $E_c = 2N_0$ was checked by calculation. The calculated value $E_c = 2.2N_0$ coincided well with the theoretical value.

BIBLIOGRAPHY

1. Kravchenko, G. I.; Markov, V. F.; Mochalina, L. P. RADIOTEKHNIKA, 1976, v. 31, No 5.

2. Andronov, A. A.; Vitt, A. A.; Khaykin, S. E.; "Theory of Oscillations," Moscow, Fizmatgiz, 1968.

3. Karasik, G. Ya.; Kravchenko, G. I.; Markov, V. F. RADIOTEKHNIKA I ELEKTRONIKA, 1974, v. 19, No 8.

4. Svistov, V. M. "Radar Signals and Their Processing," Moscow, SOVETSKOYE RADIO, 1977.

5. Kravchenko, G. I.; Markov, V. F.; Gurevich, V. L.; Koryakin, N. M. RADIOTEKHNIKA, 1978, v. 33, No 6.

[35-2291]

2291
CSO: 1860

UDC 621.396.96+51.007

COMPUTER SIMULATION IN RADAR

Moscow MODELIROVANIYE V. RADIOLOKATSII (Computer Simulation in Radar) in Russian 1979 signed to press 6 Mar 79, p 2, 263-264

[Annotation and table of contents from book by Aleksandr Ivanovich Leonov, Vladimir Nikolayevich Vasenev, Yuriy Ivanovich Gaydukov, et al, edited by Aleksandr Ivanovich Leonov, Sovetskoye radio, 7000 copies, 264 pages]

[Text] This book is on the subject of the use of computer simulation for the evaluation of technical solutions, efficiency, and main characteristics of radar stations during the stages of their development and testing. General principles and methods of radar simulation are examined.

The book is intended for specialists engaged in the development and testing of radar stations, as well as for those engaged in the problems of the use of digital computers for simulation.

Contents

[46-10,233]
10,233
CSO: 1860

UDC 621.396.96:621.391.82

OPTIMIZING DIGITAL COHERENT WEIGHTED PROCESSING OF RADAR SIGNALS

Kiev IZV. VUZ: RADIOELEKTRONIKA in Russian Vol 22 No 8, 1979 pp 90-93
manuscript received 26 May 78, after revision 3 Jan 79

[Article by D.I. Popov and V.I. Koshelev]

[Text] The structure of an optimal signal discrimination system for the two extreme cases of strongly correlated and uncorrelated white noise interference is distinguished by the presence or absence respectively of a rejection filter at the input to the coherent store, where the filter takes the form of a repeated interperiod compensation device (ChPK) [1]. In the intermediate case, as well as for a combination of correlated interference and white noise, the optimal system is not realized using traditional rejection filters and storage devices. However, when selecting the order of the rejection filter and the weighting factors of the store in accordance with the interference parameters and the signal to noise ratio, one can design a quasi-optimal system (KS) [QS], which approaches the efficiency of the optimal system.

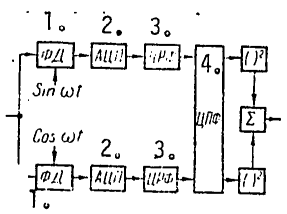

Figure 1.

The optimization of the coherent weighting factors for a storage device is treated below, and various QS's are compared.

Let sample values of an additive mixture of the signal, interference and noise, characterized by the n-dimensional gaussian column vector $S = ||s_k \exp i\ (\phi_0 + \phi_{дк})||$ be fed to the input of the digital QS depicted in Figure 1, where s_k and ϕ_0 are the absolute value and initial phase respectively of the k-th sample, while $\phi_{дк}$ [ϕ_{dk}] is the doppler phase shift over k periods. The quadrature components of the input samples formed at the output of the phase detectors (FD) [1.] are converted to digital codes in the analog-to-digital converters (ATsP) [2.], and the codes are fed to the digital rejection filters (TsRF) [3.], which suppress the interference and can be characterized by the pulse characteristic coefficients, g_k, where k = 0, m-1. The rejection residues are fed to the digital bandpass filter (TsPF) [4.], which can be

characterized by a (n - m)-dimensional complex column vector of coefficients of the pulse characteristic $W = \|\dot{w}_k\|$.

It is convenient to characterize the passage of the input vector through the digital rejection filters by an n-dimensional square rejection matrix G, the elements of which are $G_{jh} = g_{j-k}$ when $k \leq j \leq \min(n, m+k)$, and $G_{jk} = 0$ when $1 \leq j < k$ and $m + k + 1 \leq j \leq n$. To take into account the curtailment of the sample being processed due to the transient response in the digital rejection filters, we shall introduce the n-dimensional column vector $H = \|\dot{h}_k\|$, where $\dot{h}_k = 0$ when $1 \leq k \leq m$, $\dot{h}_k = \dot{w}_{k-m-1}$, when $m < k \leq n$. Then the output quantity of the digital bandpass filter is V = SGH, the dispersion of which with a zero mathematical expectation of the input data is $\sigma_V^2 = \overline{V^*V}/2 = H^{T*}G^T\overline{S^{T*}S}GH/2$. By definition, $\overline{S^{T*}S}/2 = \sigma^2 R$, where σ^2 and R are the dispersion and the normalized correlation matrix of the input vector respectively. Then the passage of the process through the system is described by the quantity $\sigma_V^2/\sigma^2 = H^{T*}G^TRGH$.

We shall characterize the efficiency of the QS by the coefficient of improvement in the signal/(interference plus noise) ratio, the size of which, without taking into account level quantization errors, is

$$\mu_0 = \frac{(\sigma_V^2/\sigma^2)_c}{(\sigma_V^2/\sigma^2)_{n+\text{ш}}} = \frac{H^{T*}G^TR_cGH}{H^{T*}G^T(R_n + \lambda I)GH}(1 + \lambda), \qquad (1)$$

where λ is the noise/interference ratio with respect to power; I is a unit matrix.

The quantity μ_0 is related to the threshold signal q by the false alarm F and detection D probabilities by the formula $D = F^{1/1+\mu_0 q}$ [1]. The quantity μ_0 depends to a significant extent on the a priori unknown parameters ϕ_{dk} and the spectral width of the interference fluctuations, p_π, which determines the elements of the matrix R_π.

In this regard, it is expedient to optimize the digital bandpass filter coefficients based on the criterion of an improvement in the coefficient averaged over these parameters and having the form:

$$\mu_{cp} = \frac{1}{k_\pi \Delta p_\pi} \int_0^{k_\pi} \int_{p_{\pi H}}^{p_{\pi H}+\Delta p_\pi} \mu_0(p_\pi, \varphi_{дk})\, dp_\pi d\varphi_{дk}, \qquad (2)$$

where $p_{\pi H}$ and Δp_π are the lower boundary and the possible range of change respectively in the spectral width of the interference fluctuations. For first and second order rejection filters, which are usually employed in QS's, binomial coefficients are close to optimal [2]. We shall make use of the well known weighting functions of Dolf-Chebyshev and Kaiser, which are distinguished by properties of optimality in the frequency range, to approximate the coefficients of the digital bandpass filter. As calculations have shown, the Dolf-Chebyshev function has proved to be more efficient for the problem under consideration here, where this function has the following form for even n:

$$|\dot{w}_k| = \frac{2}{n}\left[\alpha + 2\sum_{j=1}^{n/2-1} T_{n-1}\left(z_0 \cos\frac{\pi j}{n}\right)\cos\frac{2\pi j}{n}\left(k - \frac{n+1}{2}\right)\right],$$

where α is a parameter which determines the width of the main lobe and its amplitude with respect to the first sidelobe; T_{m-1} is a Chebyshev polynomial; $z_0 = \mathrm{ch}\left(\frac{1}{n-1}\operatorname{arch}\alpha\right)$.

In carrying out the search based on the parameter α, one can achieve a compromise between the width of the main lobe and the level of the sidelobes, where the efficieny of the QS estimated by formula (1) or (2) will be maximal. We shall write the target function of the optimization problem in the form $\mu_{av} \rightarrow \max_{\alpha}$. The problem posed here can be solved by one dimensional search methods which allow for the determination of a series of local extrema, and by sorting through these, the global extremum is found. The critierion for the completion of the optimization procedure is the condition $|\mu_{av\ j} - \mu_{av\ (j+1)}|/\mu_{av\ j} \leq \varepsilon$, where $\mu_{av\ j}$ and $\mu_{av\ (j+1)}$ are the values of the target function in the j-th and (j+1)-th optimization step; ε is a specified error in the determination of the optimum. With this criterion, the "method of the golden mean" is the most suitable approach [3].

In the numerical calculations, the resonance and gaussian curves which characterize the normalized spectral width of the fluctuations at a level of 0.5 of the maximum are used as the approximations for the energy spectrum of the signal and interference respectively. The doppler velocity of the interference is considered to be compensated, while it is constant for the signal ($\phi_{dk} = k\phi_d$), where n = 10 and $p_c = 0.015$.

The curves for the threshold signal as a function of the noise/interference ratio at the input are shown in Figure 2a where $F = 10^{-3}$, D = 0.5, p_π = o.1, $\phi_d = \pm(2k - 1)\pi$, k = 0, 1, 2, ..., for the optimal system (curve 1, computed in accordance with [4]), the ChPK-2 QS - weighted storage device (VN) (curve 2), the ChPK-1 QS - VN (curve 3), the QS without the rejection filter in the case of weighted storage (curve 4), the ChPK-2 QS - equilibrium store (RN) (curve 5) and the ChPK-1 QS - RN (curve 6). It can be seen from Figure 2a that the ChPK-2-VN QS and the ChPK-1-VN QS approach the optimum system in terms of efficiency, being no more than 2-3 dB inferior to it. With a simplification of the QS structure, its inferiority to the optimal system increases, attaining 15 dB when λ = -80 dB for the coherently weighted storage system. Weighted processing permits a substantial improvement in QS efficiency, in which case, the improvement is greater for the system with ChPK-1 than for the system with ChPK-2. The curves of Figure 2a correspond to fixed values of the doppler shift of the signal with respect to the interference and the widths of its fluctuation spectrum, but despite this limitation, they allow for a clear evaluation of the extent to which the efficiency of the various QS's approach the potential results.

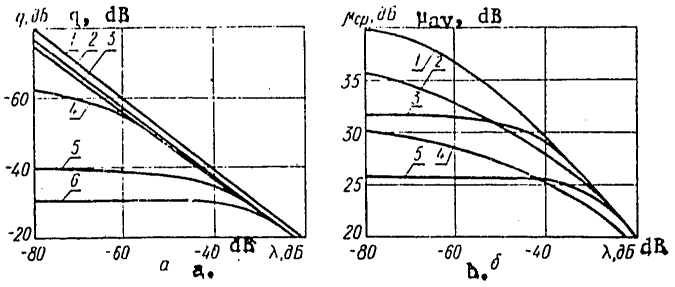

Figure 2.

The curves of $\mu_{av}(\lambda)$ for various QS's for the case of optimization of the digital bandpass filter coefficients are shown in Figure 2b where $p_{ПН} = 0.05$ and $\Delta p_{п} = 0.15$. Curve 1 corresponds to the ChPK-2-VN system; 2 corresponds to ChPK-1-VN; 3 corresponds to the ChPK-2-RN; 4 corresponds to the weighted storage system and 5 corresponds to the ChPK-1-RN. It follows from Figure 2b that the optimization of the weighting factors increases QS efficiency not only in the case of fixed and known parameters of the interference (Figure 2a), but also under conditions of their apriori ambiguity. Thus, when λ = -60 -- -80 dB, the gain in the quantity μ_{av} because of the transition from equilibrium to weighted storage in the ChPK-2-VN system amounts to 5-80 dB, and 8-10 dB in the ChPK-1-VN system. With an increase in the white noise level, the gain due to the weighted processing falls off, while the weighted store degenerates into an equilibrium store. The weighted storage system when λ = -60 -- -80 dB has an advantage over the ChPK-1-RN QS (by 3.5 to 5 dB) and is inferior to it by a slight amount when λ > -40 dB. We will note that with other weighting functions, both of these systems prove to be comparable in terms of effectiveness [5]. The functions cited here make it possible to select a system on the basis of data on the level of internal noise which delivers the requisite efficiency with minimal complexity.

TABLE 1

QS / КС	λ, дБ / dB	-80	-60	-40	-20
1. ЧПК-2-ВН		182	76	30	30
2. ЧПК-1-ВН		1917	288	51	30
3. ВН		3000	3000	350	30

Key: 1. ChPK-2-VN [interperiod compensation - 2 - weighted store];
2. ChPK-1-VN;
3. VN.

The optimal values of the parameter α_{opt} for various QS's and values of λ given in Table 1, from which it can be seen that with an increase in the overall interference spectrum at the input to the digital bandpass filter

of the uncorrelated component (both as a result of increasing λ and as a result of the decorrelation of the interference in the digital rejection filter), there is a decrease in the quantity α_{opt}, something which is due to the necessity of narrowing the width of the main lobe in this case.

Thus, when optimizing the weighting factors of the digital bandpass filter, QS efficiency under certain conditions approaches the efficiency of the optimal system. In this case, the expediency of increasing the complexity of the rejection factor, as well as introducing weighted processing into the digital bandpass filter, depends on the noise/interference ratio and falls off with an increase in this ratio.

BIBLIOGRAPHY

1. "Voprosy statisticheskoy teorii radiolokatsii" ["Questions in Statistical Radar Theory"], Edited by G.P. Tartakovskiy, Moscow, Sovetskoye Radio Publishers, 1963, 1.

2. Murakami, T., Johnson, R.S., "Clutter Suppression by Use of Weighted Pulse Trains", RCA REV., 1971, Sept., 32.

3. Wild, D.J., "Metody poiska ekstremum" ["Extremum Search Methods"], Moscow, Nauka Publishers, 1967.

4. Popov, D.I., "Kharakteristiki obnaruzheniya pri optimal'noy obrabotke signalov na fone korrelirovannykh pomekh" ["Detection Characteristics for the Case of Optimal Signal Processing Against a Background of Correlated Interference"], IZV. VUZOV - RADIOELEKTRONIKA [PROCEEDINGS OF THE HIGHER EDUCATIONAL INSTITUTES - RADIOELECTRONICS], 1971, 14, No 10, p 1198.

5. Babanov, A.A., Baranov, P.Ye., Galyus, A.V., Khudin, V.I., "Issledovaniye effektivnosti sistemy kogerentno-vesovoy obrabotki" ["A Study of Coherent Weighted System Processing Efficiency"], IZV. VUZOV - RADIOELEKTRONIKA, 1976, 19, No 4, p 33.]
[16-8225]

8225
CSO: 1860

UDC 621.396.962.8

RADAR WITH ADAPTIVE TUNING

Kiev IZV. VUZ: RADIOELEKTRONIKA in Russian Vol 22 No 8, 1979 pp 15-22
manuscript received 14 Apr 78, after revision 26 Sep 78

[Article by L.S. Mettus]

[Text] An analysis is made of the operation of adaptive radar detection with carrier frequency control, which employs a finite automat as the adaptive device. A procedure for calculating the detection characteristics is treated and an example is adduced.

It is well known that the effective scattering area (EPR) of a target as a function of the angular coordinates depends substantially on the transmit frequency. Minima of the EPR can be observed in the case of mutual motions of the target and the radar, something which leads to the attenuation of the radar return and possible loss of target. To avoid such situations, radars were proposed having a random (equiprobable in a specified range of frequencies) pulse by pulse tuning of the frequency. It was shown in [1, 2] that there is a gain both in the detection characteristics (for acquisition radars) and the tracking precision (for tracking radars). A further development of this idea is the effort to control the random frequency retuning for the purpose of increasing the operation time at that frequency where the EPR of the target is maximal [3], i.e., the use of adaptation is proposed by means of retuning the carrier frequency. In this case, as was to be anticipated, we will obtain yet an additional gain in the detection characteristics.

Moreover, the specific goal oriented control of the carrier frequency can prove to be useful when a radar operates under conditions of nonuniform spectral density of the interference, when there is the possibility of selecting that working frequency where the interference intensity is minimal.

Given below is an analysis of the operation of an adaptive acquisition radar with control of the carrier frequency, which uses a finite automat as the adaptive device.

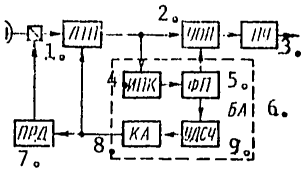

Figure 1.

A block diagram of an adaptive radar is shown in Figure 1, where LTP [1] is the linear receiver channel, which processes the one-time signal; PRD [7] is the transmitter with the controlled carrier frequency; UOP [2] is the packet [pulse train] processor; PU [3] is the threshold gate; BA [6] is the adaptation unit; IPK [4] is the quality indicator meter; FP [5] is the functional converter; UDSCh [9] is the controllable random number generator; and KA [8] is the finite automat.

The radar considered here differs from a conventional one in the presence of the adaptation unit. The adaptation unit is intended for improving the quality indicators of the radar in the process of packet processing, and specifically, for assuring the predominant operation of the radar at the "favorable" carrier frequency. For this, an entire packet of volume N is broken down into n subpackets, each of which contains m signals (N = nm). The quality indicator is measured within the limits of a subpacket, and in this case, the carrier frequency remains constant. A change in frequency can occur only from one subpacket to another.

The given radar, just as any adaptive system, pursues a specific goal: the maximization of the correct detection probability (given a constant false alarm probability) by means of changing the carrier frequency. Any quantity which is monotonically related to the correct detection probability, for example, the signal-to-noise ratio or the difference between the signal and interference power, can play the part of the quality indicator.

We shall limit the discussion to finite automats [4] with a binary input alphabet, i.e., consisting of two elements (reactions of the media): "win" (+1) and "lose" (-1). The input signal ("win" or "lose") is a discrete random quantity specified by the "win" probability. In order for the entire system to have a goal oriented behavior, it is necessary that the "win" probability, obtained by the automat for the performed action (the transmission at a specific carrier frequency) be monotonically related to the quality indicator.

The functional converter maps the set of permissible values of the quality indicator in the range [0, 1]. The controlled random number generator generates "wins" with probabilities equal to the values of the output signal of the functional converter and "losses" with the complementary probability. The operational principle of the automat consists in the fact that in realizing random wandering through the set of actions (the values of the carrier frequencies), it makes an effort to predominantly perform that action, for which the "win" probability is the highest.

Thus, with the appropriate selection of the quality indicator, the functional converter and the automat, a radar which is equipped with an adaptation unit

will operate predominantly at that carrier frequency for which the correct detection probability is maximal. We will note that not only an acquisition radar, but also a tracking radar, can be equipped with such an adaptation unit.

In calculating the detection characteristics, we shall assume that at the output of the linear receiver channel, a random sequence is observed, the elements of which are independent random quantities. This sequence is generated either by a mixture of signal and interference (the H_1 hypothesis), or only by interference (the H_0 hypothesis). In this case, it is more convenient to adopt double indexing of the elements of a sequence (a packet), and specifically: the first subscript ($i = \overline{1, n}$) will designate the number of a subpacket, while the second ($j = \overline{1, m}$) designates the ordinal number of an element in a subpacket, $x_{11}, \ldots, x_{1m}; \ldots; x_{i1}, \ldots, x_{ij}, \ldots, x_{im}; \ldots; x_{n1}, \ldots, x_{nm}$, $x \quad (-\infty, \infty)$.

The carrier frequency is constant within the limits of a subpacket, but is a discrete random quantity which takes on values from a finite set $\{f^{(k)}; k = \overline{1, l}\}$. Then, within the limits of a packet, the carrier frequency forms a discrete random process. Thus, there are two dependent random processes in the general case. One is generated by the random nature of the interference and the radar return, while the other is produced by the random variation in the carrier frequency from one subpacket to another. Their dependence is due to the fact that it is desirable by means of the second process to realize goal directed control of the first based on the observations of the latter. It follows from this that the composite multidimensional probability density of the observation vector and the carrier frequency vector is:

$$w(x_{11}, \ldots, x_{nm}; f_1, \ldots, f_n) = w(f_1, \ldots, f_n) \prod_{i=1}^{n} \prod_{j=1}^{m} w(x_{ij} | f_1, \ldots, f_n)$$

The probability density of the random quantity x_{ij} depends on the value of the carrier frequency of the transmitted signal in the i-th subpacket, i.e. on f_i, but in no case (if the interference does not depend on the signal) does it depend on the values of the carrier frequencies in the other subpackets. For this reason:

$$w(x_{11}, \ldots, x_{nm}; f_1, \ldots, f_n) = w(f_1, \ldots f_n) \prod_{i=1}^{n} \prod_{j=1}^{m} w(x_{ij} | f_i). \qquad (1)$$

We shall assume that the parametric family of distribution functions $w(x_{ij} | f_i)$ is unknown, which is determined by the models adopted for the signal and interference. There then remains the determination of $w(f_1, \ldots, f_n)$, which describes the functioning of the adaptation unit.

Taking into account the discrete nature of the random quantity f_i, we represent $w(f_1, \ldots, f_n)$ in the following form:

$$w(f_1, \ldots, f_n) = \sum_{k_1=1}^{l} \sum_{k_n=1}^{l} R(f_1^{(k_1)}, \ldots, f_n^{(k_n)}) \delta(f_1 - f_1^{(k_1)}; \ldots; f_n - f_n^{(k_n)}), \qquad (2)$$

where $k_i = \overline{1, l}$ for all $i = \overline{1, n}$; $R(f_1^{(k_1)}, \ldots, f_n^{(k_n)})$ is the probability of the event that in the first subpacket, the value of the frequency is $f^{(k_1)}$, in the second it is $f^{(k_2)}$, etc.,(the probability of the realization of the carrier frequencies); $\delta(\ldots)$ is a multidimensional delta function. We will note that the realizations of the carrier frequencies form a complete group of events, i.e.:

$$\sum_{k_1=1}^{l} \sum_{k_n=1}^{l} R(f_1^{(k_1)}, \ldots, f_n^{(k_n)}) = 1. \tag{3}$$

We shall now move on to a discussion of the packet processor. Let the packet processor realize the functional transformation $z = \phi(x_{11}, \ldots, x_{nm})$, in which the results of the measurements performed in the adaptation unit can be used (the dashed lines in Figure 1). Taking (1) into account and using one of the methods for the determination of the law governing the distribution of the random quantities [5], we find:

$$w(z \mid f_1, \ldots, f_n) = \tag{4}$$
$$= \int_{-\infty}^{\infty} \ldots \int \delta[\varphi(x_{11}, \ldots, x_{nm}) - z] \prod_{i=1}^{n} \prod_{j=1}^{m} w(x_{ij} \mid f_i)\, dx_{11} \ldots dx_{nm},$$

where $\delta[\cdot]$ is a delta function.

The conditional false alarm and correct detection probabilities for detectors which use a threshold rule for testing the hypotheses are:

$$F(f_1, \ldots, f_n) = \int_{z_0(f_1, \ldots, f_n)}^{\infty} w(z \mid f_1, \ldots, f_n;\ H_0)\, dz, \tag{5}$$
$$D(f_1, \ldots, f_n) = \int_{z_0(f_1, \ldots, f_n)}^{\infty} w(z \mid f_1, \ldots, f_n;\ H_1)\, dz,$$

where $z_0(f_1, \ldots, f_n)$ is the threshold which depends on the specific realization of the carrier frequencies. In the general case, the thresholds for the different realizations of the carrier frequencies do not have to coincide.

The false alarm and correct detection probabilities, averaged over the set of possible carrier frequency realizations, are:

$$F = \int_{-\infty}^{\infty} \ldots \int F(f_1, \ldots, f_n)\, w(f_1, \ldots, f_n \mid H_0)\, df_1 \ldots df_n,$$
$$D = \int_{-\infty}^{\infty} \ldots D(f_1, \ldots, f_n)\, w(f_1, \ldots, f_n \mid H_1)\, df_1 \ldots df_n,$$

or, taking (2) and the filtering property of the delta function into account,

$$F = \sum_{k_1=1}^{l} \sum_{k_n=1}^{l} R(f_1^{(k_1)}, \ldots, f_n^{(k_n)} | H_0) F(f_1^{(k_1)}, \ldots, f_n^{(k_n)}),$$
$$D = \sum_{k_1=1}^{l} \sum_{k_n=1}^{l} R(f_1^{(k_1)}, \ldots, f_n^{(k_n)} | H_1) D(f_1^{(k_1)}, \ldots, f_n^{(k_n)}). \quad (6)$$

The detection characteristics are usually plotted for $F = F_0$, where F_0 is specified. In this case, by working from this equality, the threshold is found. In our case, there is a set of thresholds $\{z_0(f_1^{(k_1)}, \ldots, f_n^{(k_n)}); k_i = \overline{1, l}; i = \overline{1, n}\}$, and for this reason, an ambiguity arises in their determination. The task of finding the set of thresholds maximizing D could be formulated, however, this case is far from practical application. In fact, the solution for the presence or the absence of a target is based on the packet processing for the specific realization of the frequencies, and not the entire set of possible realizations, and for this reason, a more natural requirement will be $F(f_1^{(k_1)}, \ldots, f_n^{(k_n)}) = F_0$ for all $k_i = \overline{1, l}$ and $i = \overline{1, n}$. In this case, taking (3) into account, and $F = F_0$, the thresholds are found from the solution of the equations:

$$\int_{z_0}^{\infty} w(z | f_1^{(k_1)}, \ldots, f_n^{(k_n)}; H_0)\, dz = F_0; \; z_0(f_1^{(k_1)}, \ldots, f_n^{(k_n)}). \quad (7)$$

The use of expressions (4), (5), (6) and (7) makes it possible to construct the detection characteristic; however, there still remained undetermined probabilities of carrier frequency realizations. To find them, it is necessary to analyze the functioning of the adaptation unit.

The operation of the quality indicator meter can be treated as the functional transformation of a multidimensional random quantity into a one-dimensional quantity. Without going into the question of measurement optimality here, we shall assume that the quality indicator meter comes up with an estimate $\hat{Q}$ for the quality indicator Q based on observations over a sample volume m, i.e., $\hat{Q}_i = \Psi_m(x_{i1}, \ldots, x_{im})$. Here, the subscript i means that the estimate is made for a sample belonging to the i-th subpacket. On analogy with (4), it is not difficult to write the expression for:

$$w(\hat{Q}_i | f_i) = \int_{-\infty}^{\infty} \cdots \int \delta[\Psi_m(x_{i1}, \ldots, x_{im}) - \hat{Q}_i] \prod_{j=1}^{m} w(x_{ij} | f_i)\, dx_{i1} \ldots dx_{im}.$$

Let $\hat{Q}$ belong to any interval, then the function of the functional converter reduces to the conversion $U_i = \Psi(\hat{Q}_i)$, where $U_i \in [0, 1]$, where U_i is a continuous, strictly monotonically increasing function of $\hat{Q}_i$. Then, designating the function which is the inverse of $\Psi(\cdot)$ as $\Psi^{-1}(\cdot)$, we have:

$$w_U(U_i|f_i) = w_Q[\Psi^{-1}(U_i)|f_i]\frac{d\Psi^{-1}(U_i)}{dU_i} =$$

$$= \frac{d\Psi^{-1}(U_i)}{dU_i}\int_{-\infty}^{\infty}\cdots\int\delta[\Psi_m(x_{i1},\ldots,x_{im}) - \Psi^{-1}(U_i)]\prod_{j=1}^{m} w(x_{ij}|f_i)\,dx_{i1}\ldots dx_{im}. \qquad (8)$$

As was noted above, the controlled random number transducer generates a discrete random quantity $V_i \in \{+1, -1\}$ with a "win" probability equal to the specific value of the random quantity U_i, i.e., V_i can be treated as a random function of the random quantity U_i. Then the conditional probability density is:

$$w(V_i|U_i) = U_i\delta(V_i - 1) + (1 - U_i)\delta(V_i + 1) \text{ и } w(V_i|f_i) = \bar{U}_i(f_i)\delta(V_i - 1) +$$
$$+ [1 - \bar{U}_i(f_i)]\delta(V_i + 1), \text{ где } \bar{U}_i(f_i) = \int_{-\infty}^{\infty} U_i w(U_i|f_i)\,dU_i.$$

The conditional "win" probability as a function of the value of the carrier frequency is $P_i(f_i) = P\{V_i \geqslant 0|f_i\} = \int_0^{\infty} w(V_i|f_i)\,dV_i = \bar{U}_i(f_i)$, or taking (8) into account:

$$P_i(f_i) = \int_{-\infty}^{\infty}\cdots\int\Psi[\Psi_m(x_{i1},\ldots,x_{im})]\prod_{j=1}^{m} w(x_{ij}|f_i)\,dx_{i1}\ldots dx_{im}. \qquad (9)$$

We shall now consider the operation of the finite automat [4]. The behavior of the finite automat is described by a complex Markov chain. Its complexity depends on the depth of memory, d, of the automat (or, in other words, on the number of internal states necessary for one action). By increasing the number of states under consideration from l (the number of actions) up to ld, the complex Markov chain is reduced to a simple one, which is completely defined by a matrix of transition probabilities over one step $\|P^{(\mu_1\mu_2)}\|$ where $\mu_1, \mu_2 = \overline{1, ld}$ are the indices of the numbers of the states. To specify the finite automat means to specify this matrix and the probabilities of the initial states $r_1^{(\mu 1)}$. In the general case of a nonsteady-state medium, the automat is specified by a system of matrices $\|P_i^{(\mu_1\mu_2)}\|$, where $i = \overline{1, n}$. The elements of the matrix depend on the structural configuration of the automat (its graph) and on the probabilities of a "win" for each action, i.e., on $P_i(f_i^{(k_i)})$, where $k_i = \overline{1, l}$, while $f_i^{(k_i)}$ is the specific value of the carrier frequency in the i-th subpacket. We shall equate the steps of the automat with a subpacket (the transition from one state to another is accomplised simultaneously with the transition from one subpacket to the other).

We shall number the states of the automat, making use of the depth of memory:

$$\mu = [1, \ldots, d]; \ldots; [d(k-1)+1, d(k-1)+2, \ldots, kd]; \ldots; [d(l-1)+1, \ldots, \ldots, ld]$$

In this case, let only one action of the automat correspond to each subset of states enclosed in the brackets, and specifically, that action which coincides with the superscript $k = \overline{1, l}$ in this expression.

The probability of the carrier frequency realization is found from an analysis of the operation of the finite automat, and it can be shown that:

$$R(f_1^{(k_1)}, \ldots, f_n^{(k_n)}) = \sum_{\mu_1}^{\xi} \ldots \sum_{\mu_n}^{\xi} r_1^{(\mu_1)} \prod_{i=1}^{n-1} p_i^{(\mu_i \mu_{(i+1)})}, \tag{10}$$

where $\mu_i = d(k_i - 1) + 1; d(k_i - 1) + 2; \ldots;$; $k_i d$ for all $k_i = \overline{1, l}$ and $i = \overline{1, n}$; $d = \text{const}$.

For a radar with an equiprobable change in the carrier frequency within the bounds of a packet, all of the realizations of the carrier frequencies are of equal value, i.e.,

$$R(f_1^{(k_1)}, \ldots, f_n^{(k_n)}) = \frac{1}{l^n} \text{ for all / для всех } k_i = \overline{1, l} \text{ \& и } i = \overline{1, n}. \tag{11}$$

For a classical radar, in the case of an equiprobable selection of the initial frequency (in the subsequent subpackets, the frequency remains unchanged):

$$R(f_1^{(k_1)}, \ldots, f_n^{(k_n)}) = \begin{cases} \frac{1}{l}, \text{ if / если } k_{i1} = k_{i2} \text{ for all / для всех } k_{i1}, k_{i2} = \overline{1, l} \\ \quad \text{\& и } i_1, i_2 = \overline{1, n}, \\ 0 \text{ в противном случае. Otherwise} \end{cases} \tag{12}$$

We shall consider the potential capabilities of the described radar using a specific example. In this case, we shall make a number of assumptions:

1) We shall assume that a random sequence is observed at the output of the linear receiver channel, the elements of which are independently normally distributed random quantities;

2) The medium is a steady-state one, i.e., the distribution functions and their parameters do not depend on time, but depend only on the values of the carrier frequency;

3) We make the set of amplitudes of the radar return $\{x_0^{(k)}; k = \overline{1, l}\}$ and the set of mean square values of the interference $\{\sigma^{(k)}; k = \overline{1, l}\}$ at the output of the linear receiver channel agree with the set of carrier frequencies $\{f^{(k)}; k = \overline{1, l}\}$, and we note that $x_0^{(k)}$ and $\sigma^{(k)}$ are unknown beforehand, and are measured with ideal accuracy only in the process of radar functioning (i.e., we assume that $m \to \infty$, while the estimate made by the quality indicator meter is asymptotically unbiased);

4) The average signal-to-noise ratio over the set of permissible frequencies is an a priori unknown:

$$\tilde{q} = \frac{1}{l}\sum_{k=1}^{l} q^{(k)}, \text{ где } q^{(k)} = \frac{x_0^{(k)}}{\sigma^{(k)}};$$

5) The spectral interference density is uniform within the passband of the linear receiver channel for every value of the carrier frequency;

6) The optimal detector is built on the basis of the statistic z, which carries out the computation of the likelihood ratio;

7) The quality indicator is chosen in the form $Q^{(k)} = q^{(k)}/\tilde{q}$;

8) The functional converter is specified by the function shown in Figures 2a. We shall limit ourselves to $l = 2$, and in this case, it can be shown that it is natural to choose $Q_0 = 2$ and $\Delta Q = 2$;

9) We shall specify the medium; let: $x_0^{(1)} = x_0^{(2)} = \tilde{x}_0$; $\sigma^{(1)} = 1{,}6\tilde{\sigma}$, $\sigma^{(2)} = 0{,}4\tilde{\sigma}$, where

$\tilde{x}_0 = = \frac{1}{l}\sum_{k=1}^{l} x_0^{(k)}$; $\tilde{\sigma} = \frac{1}{l}\sum_{k=1}^{l} \sigma^{(k)}$, , and this means that the signal-to-noise ratio with respect to voltage at the frequency $f^{(1)}$ is four times smaller than at the frequency $f^{(2)}$;

10) We shall choose a finite automat from a family of automats with "linear tactics" [4] as the adaptive device, where the number of actions is $l = 2$ (determined by the set of permissible carrier frequencies) and the depth of memory is d = 2. The graph which specifies the structure of the automat is shown in Figure 2b, where the little circles designate the internal states of the automat μ; the solid dark little circles designate the states in which the change in the actions (the carrier frequencies) occurs; the solid lines designate the transitions with the action of a "win", while the dashed lines indicate those with the action of a "loss". In the states μ = 1, 2, operation is at the frequency $f^{(1)}$, while in the states μ = 3, 4, it is at the frequency $f^{(2)}$. The probabilities of the initial states $r_1^{(\mu)} = \{0.5; 0; 0.5; 0$, where $\mu = \overline{1,4}\}$, which corresponds to the equiprobable choice of the carrier frequency $f^{(1)}$ or $f^{(2)}$ in the first step (in the first subpacket).

The use of expressions (4)-(7) and (9)-(12) taking into account the adduced presuppositions makes it possible to plot the radar detection characteristic for various algorithms for designating the frequencies: 1) corresponds to the operation of a classical radar where there is freedom in the choice of the working frequency (the frequency is chosen on an equal probability basis from a specified set of frequencies and does not change during operation); 2) corresponds to the operation of a radar with equiprobable pulse by pulse frequency tuning (the frequencies in all subpackets are chosen independently and on an equal probability basis; 3) corresponds to a radar with adaptive frequency tuning, which uses a finite automat as the learning device.

Shown in Figures 3a and b are the curves for $D(\tilde{q}^*)$ when $F = F_0 = 10^{-4}$, where $\tilde{q}^* = \tilde{q}\sqrt{mn}$, for n = 2 and n = 4 respectively. The number of the curve corresponds to the number of algorithm. Additionally: curve 4 corresponds to the operation of a radar at the best frequency, i.e., matches the case where there is complete apriori information; curve 5 corresponds to the operation of a radar at the worst carrier frequency.

We will note in conclusion that the introduction of adaptation by means of retuning the carrier frequency permits an improvement in the detection characteristic both as regards a radar which employs equiprobable tuning of the frequency and as regards a classical radar (for large values of D), which operates under conditions of apriori ambiguity with respect to the initial choice of the working frequency (the gain is greater, the greater the dependence of the effective scattering area of the target or interference on frequency).

It follows from a comparison of Figures 3a and b that increasing the number of subpackets (adaptation steps) leads to an improvement in the gain, and for this reason, when taking into account the real nature of the measurements being made and the limited observation time, the question of finding the optimal ratio between n and m comes up. It can be shown that when n, m and $d \to \infty$, the detection characteristics asymptotically tend to the potentially possible (curve 4).

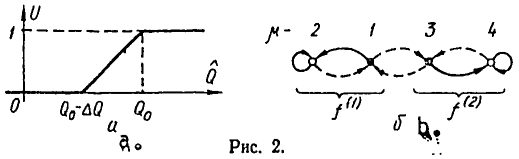

Рис. 2.

Figure 2.

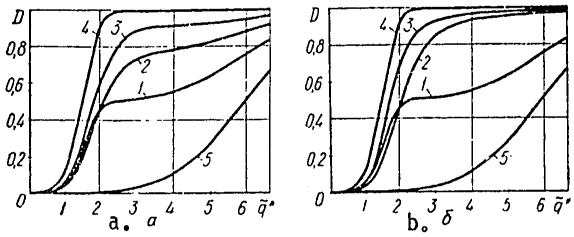

Figure 3.

BIBLIOGRAPHY

1. Gustafson, A., Es, B., "Kharakteristiki radiolokatsionnykh stantsiy s izmenyayushcheysya ot impul'sa k impul'su nesushchey chastotoy" ["The Characteristics of Radars with a Carrier Frequency which Changes from Pulse to Pulse"], ZARUBEZHNAYA RADIOELEKTRONIKA [FOREIGN RADIOELECTRONICS], 1965, No 4, pp 30-37.

2. Rey, Kh., "Povysheniye effektivnosti radiolokatsionnogo obnaruzheniya tseley po dal'nosti i uglovym koordinatam pri perestroyke chastoty" ["Improving the Efficiency of Radar Target Detection with Respect to Range and Angular Coordinates for the Case of Frequency Retfning"], ZARUBEZHNAYA RADIOELEKTRONIKA, 1967, No 6, pp 3-16.

3. Khansen, V,, "Logika posledovatel'noy raboty obzornoy radiolokatsionno stantsii s poimpul'snoy perestroykoy chastoty" ["The Logic of the Sequential Operation of a Surveillance Radar with Pulse by Pulse Frequency Retuning"], ZARUBEZHNAYA RADIOELEKTRONIKA, 1969, No 4, pp 80-98.

4. Sragovich, V.G., "Teoriya adaptivnykh sistem" ["Adaptive System Theory"], Moscow, Nauka Publishers, 1976.

5. Levin, B.R., "Teoreticheskiye osnovy statisticheskoy radiotekhniki" ["The Theoretical Principles of Statistical Radio Engineering"], Moscow, Sovetskoye Radio Publishers, 1969, Book 1.

[16-8225]

8225
CSO: 1860

Semiconductors and Dielectrics

UDC 621.382.29:539.235.3

USING PALLADIUM TO REDUCE THE REVERSE CURRENT RESTORATION TIME OF PULSE DIODES

Kiev IZV. VUZ: RADIOELEKTRONIKA in Russian Vol 22 No 8, 1979 pp 95-96
manuscript received 30 May 78; after revision 30 Dec 78

[Article by A.K. Kolebanov, A.I. Mochalov and Yu.D. Chistyakov]

[Text] Semiconductor material having a short lifetime of the charge carriers, τ, is employed in the fabrication technology for pulse diodes [1]. Gold is most frequently used to reduce τ in silicon. Because of the fact that one of the energy bands of gold falls close to the center of the forbidden band [2], the reduction in τ is accompanied by a marked increase in the reverse currents of a diode by virtue of the generation of the charge carriers in the depleted layer. Alloying silicon with platinum or palladium introduces deep and symmetrical energy levels [3]. It is well known that palladium is used in microelectronics technology to make contacts. The influence of palladium introduced into silicon during combined diffusion with phosphorous, on the parameters of pulse diodes is studied in this paper.

The experiments were performed on silicon with a crystallographic orientation of (111) and an acceptor concentration 7×10^{17} cm^{-3}. For the purpose of comparison, the combined diffusion of phosphorous with gold (a ZF batch) and phosphorous with palladium (a PF batch) was carried out. The diffusion processes for the gold and palladium were accomplished from thin films deposited on the silicon surface. The gold films were precipitated from an aqueous solution of gold chloride. The palladium films 0.02 and 0.06 μm thick were applied by the ion plasma method, and prior to the application, the surface of the silicon was subjected to ion cleaning.

The combined diffusion processes were were carried out in a quartz tube at a temperature of 1,113° K for 1,200 seconds.

The parameters of the electron-hole junctions were checked following the removal of the phosphorous silicate glass. The measurement procedure consisted in the following: a square wave DC pulse was fed to the diode being tested where the pulse had an amplitude of 100 ma (a width of 2 μm),

and then a reverse voltage pulse with an amplitude of 10 volts was applied. The pulse repetition rate was 6 KHz. In this case, a voltage drop proportional to the junction current of the diode was picked off across a load resistance inserted in series with the diode. The transient processes which occur during switching were registered on the screen of an oscilloscope. The reverse current restoration time for a pulse diode, t, is equal to the time interval between the zero crossing of the pulse diode current and the moment when the reverse current falls off to a specified readout current level.

The following diode parameters were obtained as a result of the measurements: in the PF batch, t = 30 nanoseconds, the reverse current levels were i_0 = = 0.01-0.1 μa, and the ZF group, t = 40-80 nanoseconds and i_0 = 0.01-1 μa. The forward voltage drop, U, when a current of 100 ma flowed, amounted to 4-5 volts for all samples. The subsequent production of nonrectifying contacts lead to a reduction in U down to 1.6 volts for the PF batch and down to 1.3 volts for the case of alloying with gold. When alloying with palladium, the scatter in the quantity t was insignificant, while when alloying with gold, it averaged 20%.

The reduction in the reverse current restoration time occurs because of the curtailment of the charge carrier lifetime by virtue of recombination at electrically active, deep impurity centers, created by palladium in silicon. The palladium atoms diffuse in the silicon at a temperature of 1,113° K and replace the silicon atoms at the crystal lattice cites, creating one acceptor level in the forbidden band of silicon with an energy 0.22 eV below the "bottom" of the conductivity band, and a donor level 0.33 eV above the "ceiling" of the valence band [3]. For this reason, to jointly diffuse palladium and phosphorous, a temperature of 1,113° K was chosen, since diffusion at higher temperatures leads to a reduction in the number of interstitial atoms of palladium, which introduce only acceptor levels into the forbidden band of silicon, where these levels have an energy 0.32 eV above the "ceiling" of the valence band [3], and consequently, can be the cause of a rise in the reverse currents.

Thus, it was determined that palladium, applied by the ion plasma method to the surface of silicon, reduces the restoration time following high temperature annealing, as well as the reverse current level of pulse diodes.

BIBLIOGRAPHY

1. Pasynkov, V.V., Chirkin, A.K., Shinkov, A.D., "Poluprovodnikovyye pribory" ["Semiconductor Devices"], Moscow, Vysshaya Shkola Publishers, 1973.

2. Milns, A., "Primesi s glubokimi urovnyami v poluprovodnikakh" ["Impurities with Deep Levels in Semiconductors"], Moscow, Mir Publishers, 1977.

3. Lingkon So, Sorab K., "The Energy Levels of Palladium in Silicon"
SOLID STATE ELECTRONICS, 1977, 20, p 113.
[16-8225]

USSR UDC 621.383.51

A MICROELECTRONIC POSITION PHOTODETECTOR UTILIZING THE LONGITUDINAL PHOTOGALVANIC EFFECT IN SILICON

Sofia (BULGARIA) ANNALS OF THE SOFIA UNIVERSITY'S PHYSICS DEPARTMENT in Russian No 67, 1974-75(78) pp 79-86

VASILEV, V. and VELCHEV, N.

[From REFERATIVNYY ZHURNAL, ELEKTRONIKA I YEYE PRIMENENIYE, No 1, Jan 79 Abstract No 1B386 by T. I. Olevanova]

[Text] A theoretical model of the longitudinal photogalvanic effect in one-dimensional semiconductors is proposed, and on the basis of this model there has already been developed a microelectronic position-sensitive silicon detector. In an n-Si wafer with an electrical resistivity of approximately 7.5 $\Omega \cdot$cm and a (111)-orientation one forms two strongly doped diffusion p-regions with an impurity concentration of $5 \cdot 10^{19}$ cm^{-3} which serve as resistive contact tabs. Between them runs a 1-2 mm deep high-resistance p-channel with an impurity concentration of $(1-3) \cdot 10^{16}$ cm^{-3}. The dielectric above this channel is an approximately 8000 Å thick layer of silicon dioxide. The metallic contact tabs are made of a binary tungsten-gold alloy. One standard silicon wafer 30 mm in diameter carrier four photodetectors. Such a photodetector has an exactly linear and symmetric inversion characteristic and a position sensitivity of 20 mV/mm with an interelectrode distance of 6 mm. Figures 4; references 15.

2415
CSO: 1860

ABSTRACTS FROM THE JOURNAL IZV. VUZ: RADIOELEKTRONIKA

Kiev IZV. VUZ: RADIOELEKTRONIKA in Russian No 6, 1979 pp 13, 37, 41, 57

AUTOMATIC RANGE TRACKING

[Abstract of article by Yu. M. Olyukha and S. F. Shimchik, Minsk Radiotechnical Institute]

[Text] This article considers a digital system for automatic range tracking (ASD) of a pulsed RLS [radar station]. The system is a specialized digital computer and can be made astatic both with the first, and the second and third order. The simplicity of the system in the first case is emphasized. The ASD system which was developed is based entirely on integrated circuit digital equipment parts and makes it possible to measure the distance to the target and the error in the distance measurement by means of one integrator, and the distance, velocity of target and error in distance measurement with two integrators.

Special features in making the various system units are considered, such as the distance meter, the velocity and acceleration (errors in velocity measurements) meter, the scanning unit, etc.

The system was developed to do laboratory work in the "Radiotechnical systems" course; however, the results of the work may be used successfully for designing industrial systems of automatic range tracking.

ADAPTIVE DEVICE FOR SEPARATING A SIGNAL FROM BACKGROUND NOISE

[Abstract of an article by V. B. Ferents, Moscow Electrotechnical Institute of Communication Order of Labor Red Banner]

[Text] This article considers the principles and possibilities of doppler separation of a radar signal reflected from a moving target from a background of interfering reflections from the ground.

A radar station design with an adaptive device for separating the signal was proposed which requires an additional channel for receiving the interference from the ground.

UDC 621.372.823

ANALYSIS OF HIGHER TYPE WAVES IN A MULTIWAVE WAVEGUIDE

[Abstract of an article by V. S. Vuntesmeri and V. G. Maksyutin]

[Text] A method for analyzing the structure of a multiwave waveguide field is proposed. The use of a ferrite resonator in combination with longitudinal probing of the waveguide field as a probe makes it possible to use the structure in a large range of frequencies with a relatively small volume of mathematical processing of measurement results.

UDC 621.372.834

CALCULATION OF COUPLING COEFFICIENTS BETWEEN OPEN DIELECTRIC RESONATORS AND FIELDS OF SUPERHIGH FREQUENCY CHANNELS

[Article by M. Ye. Il'chenko, S. N. Kushch]

[Text] Calculation was made of coupling coefficients between round open dielectric resonators (with basic H and E oscillations) and a field of two-wave channels. Expressions were obtained for coefficients of transmission, reflection and absorption of wave channels for the case of propagation of TE_{10} and TE_{20} waves separated by the resonators.
[247-2291]

2291
CSO: 1860

ABSTRACTS OF DEPOSITED PAPERS

Kiev IZV. VUZ: RADIOELEKTRONIKA in Russian Vol 22 No 8, 1979 pp 9, 32, 64

[Abstracts of manuscripts deposited in the Ukrainian Scientific Research Institute for Scientific and Technical Information]

UDC 621.373.5

UDC 621.373.5

V. P. Gololobov, M. G. Ishchenko, O. V. Tureyeva, G. N. Shelamov and V. I. Tsymbal

Magnetically Tuned Wideband Microwave Semiconductor Devices

Results of a study of semiconductor, magnetically tuned microwave devices are presented: filters, selective mixers, oscillators and frequency multipliers.

The results of a theoretical study of the interaction of a ferrite resonator with n-turns are given. A comparative assessment of the circuits of the devices is also given.

The devices which have been developed comprise the basis of the component base for the design of wideband, superheterodyne magnetically tuned microwave systems.

Article deposited in the UkrNIINTI [Ukrainian Scientific Research Institute for Scientific and Technical Information], Manuscript No 1118, 83-105, deposited 25 July 1978. 23 pp with illustrations, 14 bibliographic citations.

UDC 621.382

A. A. Popov

An Investigation of Microwave Power Limiters Designed Around Dynamic Nonlinear Distributed Systems

APPROVED FOR RELEASE: 2007/02/08: CIA-RDP82-00850R000200050030-1

A SHF power limiter is described, which is designed around a p-i-n structure, the per unit length parameters of the electrical model of which depend on the amplitude of the high frequency voltage or current. A chain model of the limiter is treated. Expressions are derived for the mode attenuation factor and VSWR. Concentrated and distributed type limiters are compared.

Article deposited in the UkrNIINTI, manuscript No 1118, pp 56-64, deposited 25 May 1978; 9 pp with illustrations, 6 bibliographic citations.

UDC 621.372.852.1

A. G. Fialkovskiy

A VARIATION METHOD OF RADIAL FILTER DESIGN

A coaxial waveguide with a radial resonator, formed by a double symmetrical inhomogeneity of the outer conductor, is employed in various functional microwave devices as a rejection filter. The primary mode rejection factor is represented in the form of a functional of the longitudinal electrical field at the coupling slot, where the functional is stationary with respect to small variations. The efficiency of the proposed algorithm is demonstrated even in the case of the approximation of the test field by one linear function.

Article deposited in the UkrNIINTI, manuscript No. 1118, pp 137-142, deposited 25 July 1979; 6 pp with illustrations, 8 bibliographic citations. [16-8225]

8225
CSO: 1860

- END -